

UNIVERSITY OF CALGARY

Characterizing Seedling Change Along Seismic Lines in the Boreal Forest of Alberta with
Airborne Laser Scanning

by

Yusif Sitobu Abdullai

A THESIS

SUBMITTED TO THE FACULTY OF GRADUATE STUDIES
IN PARTIAL FULFILMENT OF THE REQUIREMENTS FOR THE
DEGREE OF MASTER OF SCIENCE

GRADUATE PROGRAM IN GEOGRAPHY

CALGARY, ALBERTA

FEBRUARY, 2026

© Yusif Sitobu Abdullai 2026

Abstract

Seismic lines – linear disturbance corridors constructed for petroleum exploration – contribute to shifts in wildlife populations, species interactions, and other ecosystem functions in Alberta’s boreal forest. As a result, characterization of post-disturbance vegetation growth along these lines is important for forest management. However, peer-reviewed work aimed at mapping vegetation growth along seismic lines with Airborne Laser Scanning (ALS) is limited. Here, I demonstrate how ALS data employed to map conifer seedling growth along seismic lines is influenced by choice of remote-sensing unit of analysis and ecosite type. I compared point-cloud-based and raster-based approaches to estimate height-change for 194 field-measured seedlings located in upland and wetland ecosite types in a 7 km² study area over a five-year monitoring period. Results show that point-cloud models produced more accurate estimates of seedling height change than raster models, with a point-cloud 60th percentile metric model performing best (RMSE = 25.70 cm, MAE = 15.05 cm). Upland sites produced more accurate results (RMSE = 20.55 cm, MAE = 11.27 cm, MEDAE = 7.03 cm) than wetland sites. Mapping seedling growth across the study area revealed that 33.24 km of seismic lines were in a state of minimal or no growth, while 4.21 km and 3.65 km were in a state of moderate and high growth, respectively. I found that factors such as overhanging trees or adjacent forest noise influenced the accuracy of height-change estimates. Overall, this study demonstrates the applicability of ALS technologies for mapping seedling growth across large areas and supports further research using these approaches.

Preface

This thesis was prepared with the combined effect of my skills and generative artificial intelligence (GenAI) tools. Specifically, ChatGPT and Google AI were employed to find relevant material, fix algorithm errors I encountered, refine wording and improve clarity. The final text, analyses, interpretations and conclusions contained in this document are mine, and all GenAI-assisted content was comprehensively reviewed and edited by me. Also, grammatical editing and phrasing were carried out with the help of Grammarly. The use of GenAI in this manner is consistent with the guidelines and recommendations of the University of Calgary Faculty of Graduate Studies guideline for Generative AI use in Graduate Studies. Its purpose and extent were also reviewed and authorized by my supervisor.

Acknowledgements

I would like to express my profound gratitude and appreciation to my supervisor Dr. Greg McDermid and Dr. Julia Linke for offering me the opportunity to pursue a thesis-based master's degree in Geography in Canada. I was very lucky to have been selected from a large pool of applicants at a time when I had a dream of pursuing my master's study but had nowhere to start. Despite the immigration hurdles in getting to Canada in spite of COVID-19, they were patient and understanding and never relented in offering me the utmost support to make sure I had all the right information and access to get here. I would also like to thank them for their help and advice on my research and journey here in Canada.

Also, I am very grateful to those who offered me the opportunity to use their data for this research, including BERA collaborators and the Alberta Biodiversity Monitoring Institute (ABMI). Without your hard work and assistance, this research would not have been conducted successfully. I offer my thanks to Colette Shellian for offering her field data and guidance for this research. I also offer my thanks to Irina Terenteva for offering her AI-generated seedling data to be used for this study.

I would also like to thank all members of the Applied Geospatial Research Group for their mentorship and kindness. Thank you to Tanya Yeomans for being a wonderful and supportive course mate and friend throughout my journey in this program. Also, to Xue Yan Chan, Nicole Byford and Jiaao Guo for being patient and ever ready to help when I found myself wanting. I want to thank Maverick Fong and Qing Ye Richard for their tremendous technical support in processing my data and producing other GIS data products. I would like to extend my gratitude to the Department of Geography at the University of Calgary.

Finally, I would like to thank my wife, Hawa Ibrahim, my mother and my entire family back in Ghana for their endless love, support and encouragement.

Dedication

I dedicate this thesis to my brother Zibblim Sitobu Abdullai, who has always wished the best for me but is not here to see how far I have come. Rest in Peace.

Table of Contents

Abstract.....	i
Preface.....	ii
Acknowledgements.....	iii
Dedication.....	v
Table of Contents.....	vi
List of Tables.....	viii
List of Figures and Illustrations.....	ix
List of Symbols, Abbreviations, and Nomenclature.....	xi
1 Chapter One: Introduction.....	1
1.1 Background and Motivation.....	1
1.2 Seismic Lines in Alberta: Extent and Impact.....	3
1.3 Tracking Vegetation Growth for Seismic Line Restoration.....	7
1.4 Previous Studies.....	10
1.5 Research Objectives.....	14
1.6 Organization of Thesis.....	15
2 Chapter Two: Background: ALS Data for Characterizing Vegetation Change or Recovery, a Literature Review.....	17
2.1 ALS Point Cloud.....	18
2.1.1 Processing ALS Point Cloud Data.....	19
2.2 Change Detection.....	22
2.2.1 Unit of Analysis.....	25
2.2.2 Comparison Method.....	28
2.3 Comparison of Units of Analysis and Comparison Method for ALS Vegetation Change Detection Studies.....	30
3 Chapter Three: Methods.....	36
3.1 Study Area.....	36
3.2 Sampling and Field Data.....	39
3.3 Airborne Laser Scanning (ALS) Data.....	43
3.4 ALS Preprocessing.....	44
3.5 Change Detection Workflow.....	45
3.5.1 Raster (DSM) Image Differencing.....	46
3.5.2 Point Cloud (Cloud Compare) Image Differencing (PC _{CC}).....	47

3.5.3	Point Cloud (Point Metrics) Image Differencing (PC _{PM})	49
3.6	Regression-Based Bias Adjustments.....	50
3.7	Assessing Ecosite Influence on Change Detection Accuracy.....	50
3.8	Non-Parametric Accuracy Assessment and Tests of Difference.....	51
3.9	Assessing Seedling Height Change Across the Study Site.....	53
4	Chapter Four: Results.....	57
4.1	Accuracy of ALS Point Cloud and Raster-Based Predictions of Seedling Height Change Between 2017 and 2022.....	57
4.2	Ecosite Influence on the Accuracy of the Best-Performing Change Detection Approach 58	
4.3	Conifer Seedling Height Change Across the Study Area.....	59
5	Chapter Five: Discussion.....	62
5.1	Point Clouds Provide Better Estimates of Seedling Height Change.....	62
5.1.1	Sources of Errors in ALS Seedling Height Change Estimates.....	65
5.1.2	Comparison with Other Studies.....	71
5.2	Seedling Height Change Detection Works Better in Upland Ecosite Types.....	73
5.3	Patterns of Seedling Height Change Across the Study Area.....	74
5.4	Assumptions and Limitations.....	75
5.5	Contributions and Study Significance.....	79
5.6	Implications for Operational Restoration.....	80
5.7	Future Outlook.....	81
6	Chapter Six: Conclusion.....	84
	References.....	87
	APPENDIX A: Relative Shift Between Bitemporal Point Cloud.....	104
	APPENDIX B: Accuracy Statistics for all ALS-Detected Change Results for All Point Cloud Point Metrics and Raster Threshold Metrics.....	106
	APPENDIX C: Change Results for All Seedlings Across the Three Approaches.....	107
	APPENDIX D: Quantile Regression and Test of Difference.....	120

List of Tables

Table 1.1: This table summarizes the various types of seismic lines, and their corresponding construction period, width, shape, pattern or construction method.....	5
Table 2.1: This table summarizes and categorizes ALS-based vegetation change detection studies based on the location of the study, change detection method, and unit of analysis applied.	31
Table 3.1: Seedling height statistics for the 194 reference seedlings measured across 9 field plots within the study area for the two study periods (2017 and 2022).....	43
Table 4.1: RMSE, MAE, MEDAE, bias, and ranks of ALS predicted seedling height change for the three change detection approaches after systematic bias correction is applied. An asterisk by the MEDAE indicates that, according to the Wilcoxon paired or signed rank test, the MEDAE results from that approach is significantly different from the PC _{PM} approach at a confidence level of 95%.....	58
Table 4.2: RMSE, MAE, MEDAE, and bias of predicted seedling height change by ecosite type. An asterisk by the MEDAE indicates that, according to the Wilcoxon independent or rank sum test, the MEDAE results from that ecosite type is significantly greater at a confidence level of 95%	59
Table 4.3: Length (km) of seismic lines in different recovery classes (No/Minimal, Moderate, High) across upland and wetland/transitional ecosite types within the study area.....	60
Table 5.1: Field-measured and ALS-detected mean seedling heights for both study years (2017 and 2022) by ecosite type.....	74

List of Figures and Illustrations

- Figure 1.1:** Aerial views of LIS lines in lattice pattern (A) and mechanically straight conventional seismic lines (B) (Source: Xue Yan Chan)..... 6
- Figure 2.1:** Visualization of an ALS pulse from an airborne platform capturing multiple returns from a tree and ground. The first return is the earliest return detected and usually represents the highest object the pulse encounters followed by the second and third returns respectively..... 21
- Figure 3.1:** Map of the study site in northeastern Alberta, Canada (left), including a detailed map highlighting linear footprint and field plots where ground measurements were taken (upper right). Below the detailed map is an inset photo giving a visual example of a seismic line on ground. . 37
- Figure 3.2:** Illustration of a 100-meter square plot with 10-meter square subplots positioned along a seismic line..... 40
- Figure 3.3:** Illustration of seedling height measurements taken in the field during the summer of 2021. This diagram shows how seedling height growth was determined using visible bud scars along the seedling stem, each representing the end of the growing season. The leader height is the vertical growth of the terminal bud from the previous year's bud scar to the current year's bud scar. The total height is the cumulative height of the seedling measured from the base to the current year's terminal bud. The spring height of a given year is estimated based on the cumulative height from the base to the position of the bud scar from the previous year, reflecting the seedling's height at the beginning of that year's growing season..... 42
- Figure 3.4:** Change detection workflow illustrating the steps involved in assessing changes across both units of analysis and accuracy evaluation. "PC" denotes point cloud, and "DSM" stands for digital surface model..... 46
- Figure 4.1:** Conifer seedling height changes along seismic lines within the study area between 2017 and 2022. The top panel: (i) displays 50-meter seismic line segments classified by mean

conifer seedling height change. The insets below the main map show zoomed-in areas highlighting: (ii) a closer view of the 50-meter square mean conifer seedling height change segments within the seismic line ground footprints (middle row); and (iii) individual conifer seedlings' height change values extracted within the seismic lines (bottom row). These illustrations present both aggregated and localized patterns of conifer seedling height change along seismic lines within the study area.

..... 61

Figure 5.1: An illustration of a seedling and its corresponding point cloud return profile highlighting upper percentiles which are usually missed or represented by few returns and the mid section which comparatively is represented by more points making it more stable for seedling change detection across my study area. 64

Figure 5.2: Scatterplots showing ALS-detected seedling height change (Top Row) and predicted seedling height change (Bottom Row) against Field-Observed seedling height change for all three approaches. (a) ALS-Detected PC_{PM} Change (b) ALS-Detected PC_{CC} Change (c) ALS-Detected Raster Change (d) Predicted PC_{PM} Change (e) Predicted PC_{CC} Change (f) Predicted Raster Change. Outlier errors are highlighted in orange (Data Loss), yellow (Overhanging Canopies and Adjacent Forest), and green (Other Errors), while seedlings with non-extreme errors are shown in blue. . 69

Figure 5.3: Observed versus ALS detected seedling heights for i) 2017 dataset and ii) 2022 dataset 77

List of Symbols, Abbreviations, and Nomenclature

ABMI - Alberta Biodiversity Monitoring Institute

ALS - Airborne Laser Scanning

ASPRS - American Society for Photogrammetry and Remote Sensing

BERA - Boreal Ecosystem Recovery and Assessment

CHM- Canopy Height Models

DEM - Digital Elevation Model

DIPCs - Drone-Based Image Point Clouds

DSM- Digital Surface Model

DTM - Digital Terrain Model

GEOBIA - Geographic Object-Based Image Analysis

GSD - Ground Sampling Distances

IoU - Intersection over Union

LDTRF - Lake Duparquet Teaching and Research Forest

LiDAR - Light Detection and Ranging

LIS – Low Impact Seismic Line

MAE - Mean Absolute Error

MEDAE - Median Absolute Error

nDSM- Normalized Digital Surface Model

NGA - National Geospatial Agency

PC_{PM} - Point Cloud Percentile Metrics

PC_{CC} - Point Cloud Image Differencing carried out in Cloud Compare

RGB-NIR - Red-Green-Blue Near Infrared

RMSE - Root-Mean-Square-Error

RPAS - Remotely Piloted Aircraft System

RT-DETR - Real-Time Detection Transformer

RTK GNSS - Real-Time Kinematic Global Navigation Satellite System

SfM - Structure-from-Motion

TIN - Triangular Irregular Network

TLS - Terrestrial Laser Scanning

UAV - Unmanned Aerial Vehicle

USA - United States of America

Chapter One: Introduction

1.1 Background and Motivation

Linear footprint features associated with oil and gas exploration in Alberta, Canada, have altered landscapes in the boreal forest, leading to a variety of ecological consequences. For example, linear disturbances have contributed to the decline of woodland caribou (*Rangifer tarandus caribou*) in western Canada (Dabros et al., 2018; Finnegan et al., 2019). In Alberta, woodland caribou have been declared a threatened species under the Alberta Wildlife Act (Cichowski & Dzus, 2010). Unsustainable predation has been identified as the primary link between linear industrial footprint and caribou population decline (Finnegan et al., 2019). Wolves (*Canis lupus*), which are the main predators of caribou, use linear-disturbance features as movement corridors. This increases their hunting efficiency (Dickie et al., 2017) and reduces their spatial separation from caribou (Latham et al., 2011). Also, other ungulate species such as moose, elk, and deer are attracted to industrial disturbances due to the abundance of early seral vegetation on them (Dickie et al., 2017; Finnegan et al., 2018). This increases ungulate numbers in caribou ranges, which attracts more predators and leads to incidental kills (Finnegan et al., 2019).

In addition to the effects on wildlife, linear industrial disturbances significantly alter soil structure and hydrological processes, especially during the construction of seismic lines. Seismic lines are narrow linear clearings created for the purpose of emitting and receiving seismic waves for locating underground petroleum deposits. The use of heavy machinery such as bulldozers during the creation of seismic lines leads to the removal of vegetation and compaction of the topsoil. This compaction affects the soil hydrological balance and cycle (Davidson et al., 2020; Weiland et al., 2024). The compaction of topsoil reduces infiltration of water into the soil, thereby creating water pools at the soil surface (Arnup, 2000). Davidson et al. (2020) reported that seismic lines significantly alter soil properties, with soil bulk density and volumetric water content

increasing relative to the undisturbed surroundings. This pattern affects carbon cycling and can lead to carbon loss from the soil (Davidson et al., 2020). These findings have been further supported by Davies et al. (2025), who found that seismic lines lower the dry bulk density of soil due to reduced soil organic matter and disruptions to the carbon cycle. The clearing of vegetation associated with seismic line construction also leads to a reduction in soil water uptake and reduced evapotranspiration, which leads to high soil moisture conditions on seismic lines as compared to adjacent forest (Dabros et al., 2017). This hydrological imbalance affects the soil conditions necessary for plant growth, which can lead to slow or no recovery along linear features (Dabros et al., 2018; Weiland et al., 2024). Permafrost layers, which remain frozen all year-round, are also sensitive to these effects, including high soil moisture conditions and hydrological imbalance (Dabros et al., 2018). Permafrost has been reported by Quinton et al., (2011) to control the hydrological interactions between deep ground water and near surface water. The destruction or exposure of this layer due to the creation of seismic lines could lead to it thawing for most part of the year and in some extreme cases, its complete disappearance (Dabros et al., 2018). Linear features can also act as snow basins where snow lasts for longer than usual periods. This shortens the growing season, thereby delaying plant growth and succession (Dabros, 2009; Dabros et al., 2018).

Linear footprint features can affect the ability of peatlands to store carbon, thereby contributing to greenhouse gas emissions (Strack et al., 2019). Peatlands, including those found in permafrost regions, have stored and accumulated carbon stocks for millennia (Loisel et al., 2014). Per the United Nations Environment Programme (2022), peatlands store up to 550 billion tonnes of carbon globally. The slow decomposition and anoxic environments within these soils enable it to store carbon for long periods (Harris et al., 2023). The thawing and degradation of permafrost

and peatland along linear footprint due to their exposure when vegetation is cleared causes the methane and carbon they store to be released into the atmosphere which further contributes to global warming (Braverman & Quinton, 2016; Christensen et al., 2004; Kurz et al., 2013).

Vegetation-community composition along linear footprint features has been shown to shift towards disturbance-tolerant and non-native species, which impedes the recovery of native pre-disturbance species (Dabros et al., 2018). Finnegan et al. (2018) found that disturbance-tolerant species are more abundant on linear footprints and line edges as compared to interior forests in the lower and upper foothills and subalpine regions of Alberta. The growth of non-native plants along linear footprint can inhibit the growth and succession of native species (Dabros et al., 2018). In northeastern Alberta, Revel et al. (1984) found the presence of invasive or non-native vegetation species to be a factor contributing to the slow growth of native species along linear footprint.

1.2 Seismic Lines in Alberta: Extent and Impact

The most abundant linear industrial footprint features in northern Alberta are seismic lines which are constructed for the transportation and deployment of the geophysical equipment needed to locate subsurface oil and gas resources (Dabros et al., 2018). Seismic survey programs are made up of four components: (i) an energy source that generates the acoustic energy released into the ground, (ii) a sensor or receiver that detects the returning seismic energy, (iii) a recording device that collects and stores the resulting data, and (iv) a geophysicist who interprets the data (Page, 2025). Based on the positioning of the energy and the source line, seismic lines can be categorized as combination, source, and receiver lines. Combination lines are defined as seismic lines where the energy source and the receiver are all located on the same line. Source lines are used

exclusively as energy source for emitting energy into the subsurface, while the receiver lines are exclusively used for recording seismic waves returning from the subsurface (Page, 2025).

The construction practices used to create seismic lines has been progressively modified over time, with the aim of reducing their effect on the environment. As a result, there are several types of seismic lines found in northern Alberta. In general, seismic lines can be constructed through either hand cutting or mechanical means. Hand-cut lines are low-impact lines approximately 1.75 meters in width, constructed with chainsaws in environmentally sensitive areas or in very wet terrain where mechanical equipment cannot access (Page, 2025). Mechanical lines, on the other hand, are relatively wider linear clearings mostly constructed with bulldozers and mulchers (Page, 2025). The environmental effect of seismic lines was described as early as the 1960s when it was reported that seismic operations in the summer affected the top layer of soil than winter (Bliss & Wein, 1972). However, even winter operations have a significant effect on the soil, causing attention to be shifted to the elevation of machinery blades and the addition of more rounded edges known as mushroom heads (Bliss & Wein, 1972).

Table 1.1 summarizes the various types of seismic lines based on the period within which they began to be constructed, their widths as well as their shape, pattern or construction method. Historically, seismic lines have had widths that range from 5-10 meters. These are referred to as legacy or conventional seismic lines (Page, 2025). Before the 1980s, conventional seismic lines were constructed with bulldozers and averaged 8 to 10 meters wide. Starting in the 1980s, seismic line widths were reduced to 5 to 8 meters to reduce their effect on the environment (Dabros et al., 2018; Page, 2025) to use equipment with less environmental footprint. The late 1980s also saw the development of early low-impact seismic (LIS) or ‘avoidance’ lines, which were constructed with avoidance techniques that involved meandering around large merchantable trees using smaller

bulldozers. These LIS construction techniques were mainly introduced to reduce timber damage but were also seen to be beneficial in reducing line of sight related to wildlife (Page, 2025).

Table 1.1: This table summarizes the various types of seismic lines, and their corresponding construction period, width, shape, pattern or construction method

Name	Construction Period	Width	Shape or Pattern / Construction Method
Legacy or Conventional Seismic Lines	Early 1940s to late 1980s	8-10 meters	Straight lines constructed with bulldozers
Avoidance/Early Low Impact Seismic Lines (LIS)	Late 1980s to early 2000s	5-8 meters	Meandering lines to avoid large merchantable trees using equipment that has less effect on the environment
Modern LIS	Early 2000s to date	2-4 meters	Lattice pattern. Made up of source and receiver lines perpendicular to each other
Modern Conventional Seismic Lines	2000s to date	6 meters	Straight lines with meander every 200 meters
Zero Impact Lines	Since 1970s to date	-	Hardly noticeable. Only lower branches, shrubs and hazardous trees may be removed through hand cutting

The early 2000s saw the emergence of modern LIS lines with widths of 2-4 meters (Finnegan et al., 2019). According to Page (2025), modern LIS lines are composed of separate source and receiver lines, which are mostly laid out perpendicular to each other in a lattice pattern (Figure 1.1 (A)). Source lines are approximately 2.75 meters wide, while receiver lines are approximately 1.75 meters wide and commonly constructed with mulchers or hand cutting. The term modern-conventional lines is applied to mechanical straight combination lines (Figure 1.1 (B)) still constructed within this period (2000 to date). Unlike old conventional lines, these lines are constructed with mulchers instead of bulldozers and are narrower, with an average width of 6 meters. In order to introduce a line-of-sight break, a meander is constructed at 200-meter intervals. Modern conventional lines are intended to reduce linear footprint because meandering lines in

dense timber forests, where avoidance is not possible, would lead to more timber loss than a straight line.

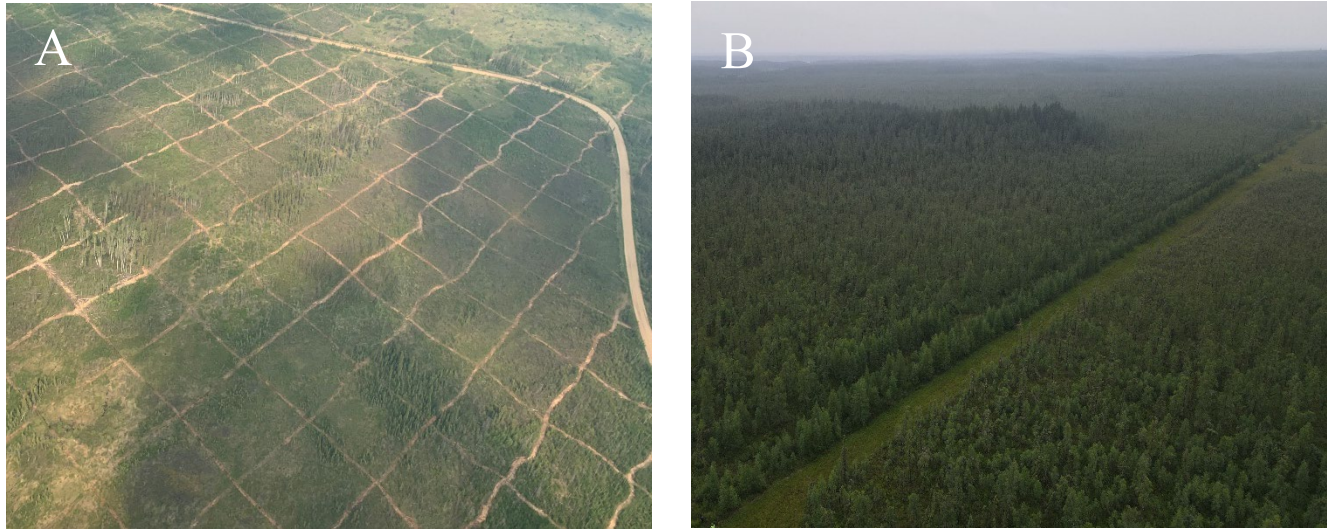


Figure 1.1: Aerial views of LIS lines in lattice pattern (A) and mechanically straight conventional seismic lines (B) (Source: Xue Yan Chan).

Other seismic line types exist, namely line-of-sight lines and zero-impact lines. Line-of-sight lines are about 1.5 meters or less in width and are constructed to maintain temporary visibility down a line using detours or sharp bends. Zero-impact seismic lines on the other hand require very little to no clearing, where in forested areas, only lower branches, shrubs and hazardous trees may be removed through hand cutting for seismic programs. In this instance, the forest canopy stays intact, thereby making it difficult to see the footprint from aerial imagery (Page, 2025).

Millions of kilometers of seismic lines occur across Alberta, with most of them going unnoticed across the landscape due to their occurrence in open fields (Page, 2025). However, when they are constructed in forested areas, seismic lines leave behind a distinct, detectable footprint (Page, 2025). In 1999, it was estimated that the total length of seismic lines in Alberta was about 1.5-1.8 million kilometres (Timoney & Lee, 2001). A more recent study also suggested that seismic lines accounted for 46% of all linear footprints across Canada's boreal forest (Pasher et al., 2013).

Even though the construction of legacy seismic lines were discontinued in the 2000s, about 582,000 kilometers of those footprints remain across the landscape of Alberta (Page, 2025).

Many seismic lines remain in early successional stages for long periods, not following the usual successional trajectory (Sutheimer et al., 2024; van Rensen et al., 2015). As a result, seismic lines continue to have long-term ecological effects. Sutheimer et al. (2024) found that vegetation recovery along seismic lines in transitional and peatland forests of Alberta can take over 30 years due to regeneration lag of tree species. The creation of seismic lines using heavy equipment together with continuous human use of these lines leave behind compacted soils and altered environmental conditions causing many conventional seismic lines not to recover naturally (Finnegan et al., 2019; Dabros et al., 2018).

1.3 Tracking Vegetation Growth for Seismic Line Restoration

Forest managers are adopting active restoration efforts on seismic lines to mitigate their long-term ecological impact and to support caribou recovery in the boreal forest, especially in areas that are not naturally recovering. Also, the extensive network of seismic lines in the boreal forest presents a management challenge that would require prioritization of restoration efforts (Finnegan et al., 2019; Ray, 2014) to areas that are not naturally recovering or are recovering at very slow rates.

In Alberta, the Provincial Restoration and Establishment Framework (hereafter ‘the framework’) was developed to guide government and voluntary industry-led active restoration programs on requirements and recommendations towards restoring habitat ranges of caribou across Alberta (Government of Alberta, 2017). These guiding steps include distinguishing targets that classify areas that require active restoration from those that are recovering naturally. Those lines

that are recovering naturally are referred to as advanced regeneration sites and are currently identified by static targets of vegetation height and density. Survival assessments and establishment surveys, on the other hand, are post-treatment monitoring exercises designed to evaluate whether seedlings have successfully established on the restored lines at a sufficient density and height (Government of Alberta, 2017). Manually assessing these targets through traditional field mensuration techniques would be difficult to scale across large expanses and might lead to further destruction of regenerating seedlings. These static targets (height and density) are important in assessing the recovery status of seismic lines. However, they do not fully inform on the recovery trajectory of these lines.

Tracking seedling height change along seismic lines offers insights into ecosystem recovery dynamics and the effectiveness of restoration efforts, which can be helpful in informing land management decisions. A key indicator of seedling recovery is height, with taller seedlings signifying a return to pre-disturbance forest structure, improved soil stability and habitat suitability for wildlife species such as the woodland caribou. However, measuring seedling height only provides information about the current state of the seedling, but does not indicate if growth is stagnated or slow. Monitoring seedling growth on the other hand, provides an indication of the change in height occurring over a particular time period as well as the direction of this change. This thereby suggests that measuring or tracking seedling height change over time would allow forest managers and researchers to assess recovery progress by identifying areas that are naturally recovering and areas that require active restoration efforts. This information also goes further to help determine active intervention efforts that are producing good results and those that are not in order to guide future restoration decisions.

While there are traditional forest mensuration strategies for obtaining seedling heights using handheld instruments (Kershaw et al., 2016), these procedures are time-consuming and difficult to scale (Lovell et al., 2005; Magnussen et al., 2012; White et al., 2016). Over the past 40 years, remote sensing technologies such as airborne laser scanning (ALS) and photogrammetric point clouds have been used to measure forest structural attributes (Aldred & Bonnor, 1985; Arp et al., 1982; Maclean & Krabill, 1986). ALS is an active remote sensing technology based on the pulse-ranging principle of light (Lim et al., 2003) while photogrammetry involves the extraction of 3D information from overlapping digital images of real-world scenes or objects (Wolf et al., 2014). Both technologies have revolutionized forest inventorying and vegetation monitoring due to their ability to describe 3D forest structural attributes such as volume (An & Froese, 2023; Cao et al., 2019) and height (Peng et al., 2021; Zhou et al., 2020) quickly and repeatedly across large areas. Routinely acquired from drones and piloted aircraft platforms, ALS and photogrammetric point clouds have great potential for vegetation monitoring (Castilla et al., 2020; Chen et al., 2017; Madsen et al., 2020; Zieba-Kulawik & Wezyk, 2022). In addition to providing efficient observations of vegetation and seedling structural attributes, ALS is also less restricted by illumination and atmospheric effects (Qin et al., 2016), making them attractive data sources for change detection and time-series analyses. With such acquisitions becoming more commonplace, applications that measure changes in forest structure through time using ALS and photogrammetric point clouds are starting to appear in the literature (e.g., Fisher et al., 2015; Madsen et al., 2020). However, this is an emerging field (Ferraz et al., 2018; Zieba-Kulawik & Wezyk, 2022), and standard processing strategies have not yet been fully articulated.

1.4 Previous Studies

Several previous studies have applied 3D point cloud data in several forms and methods in detecting tree or seedling height as well as characterizing vegetation growth (e.g., Stepper et al., 2015; Szostak & Pająk, 2023). However, fewer studies have applied point clouds in specifically detecting seedling height and characterizing height change along seismic lines in the boreal forest of Alberta.

Detecting vegetation change with ALS point clouds can be categorized based on the unit of analysis and the comparison method applied (Tewkesbury et al., 2015). Common units of analysis for detecting change using ALS point cloud data include pixels (e.g., Jones et al., 2024; Szostak & Pająk, 2023), objects (e.g., Angelidis et al., 2017; Hanssen et al., 2021) and the point cloud itself (e.g., Arumäe et al., 2020). The most-used comparison methods are image differencing (e.g., Stepper et al., 2015; Szostak & Pająk, 2023) and post-classification (e.g., Angelidis et al., 2017; Madsen et al., 2020) change detection. Most studies that have utilized ALS data in detecting change in vegetated areas have converted point cloud into raster canopy height models (CHM) for analysis (e.g., Boehm et al., 2013; Song et al., 2016; Szostak & Pająk, 2023).

Szostak and Pająk (2023) applied ALS point cloud to assess the ecological succession process by extracting vegetation height and canopy cover as well as change in vegetation height and volume in the repository of the Fryderyk mine in southern Poland. While the static height (95th percentile) and canopy cover parameters were extracted from the raw point cloud using the FUSION procedures (McGaughey et al., 2004), a rasterized product was produced to extract vegetation height and volume change parameters. Statistical comparisons were also applied to compare vegetation classes (low, medium and high) for the study years (2011 and 2019). Even though the accuracy of the methodology applied in this study was not assessed, it confirmed the

capacity to apply ALS data for assessing vegetation structure, especially for monitoring vegetation growth.

Stepper et al. (2015) applied digital aerial imagery obtained in 2009 and 2012 as well as field measurements recorded in 2008 and 2013 as reference data to assess the periodic annual stand height increments across 199 terrestrial inventory plots in a forest near Traunstein, Germany. This study adopted the max height CHMs of both study years and assigned three height classes based on forest successional stages, namely youth, vigour and old age, to the various inventory plots. The height percentiles as well as the periodic annual stand height increments obtained from the CHMs were compared to those obtained from the field data to assess their correlation across the various height classes. Results revealed that the max height percentile was closely correlated to field measurements for both study years as compared to other height percentiles (25th, 50th, 75th, 90th, and 95th). Also, the overall periodic annual stand height increment obtained for the field data was 0.22 meters, while that of the CHM-based measurements, was computed to be 0.30 meters.

Studies that have specifically applied unmanned aerial vehicle (UAV) and ALS point cloud data along linear disturbances or seismic lines in the boreal forest have done so in estimating seedling heights (Castilla et al., 2020; Chen et al., 2017) as well as tracking vegetation change (Chasmer et al., 2021; Finnegan et al., 2019). These studies have demonstrated the effectiveness of 3D point cloud data in capturing fine-scale forest structural attributes, which allows for reliable assessment of vegetation recovery along seismic lines.

Castilla et al. (2020) investigated the effect of ground sampling distances (GSD), phenological states (leaf-on and leaf-off), and ground-determination methods in determining conifer seedling heights along linear disturbances using drone-based image point clouds (DIPCs). With point cloud as the unit of analysis, they found that the GSD had the most effect in determining

conifer seedling heights using DIPCs, with finer GSDs producing the best results, especially for taller seedlings (>30 cm). In relation to phenology (leaf-on and leaf-off), Castilla et al. (2020) reported that the best result was obtained for leaf-off conditions, even though the differences were not statistically significant. This was attributed to the presence and interference of taller adjacent deciduous forest, which might have led to an overestimation of height during the leaf-on period. In terms of ground determination method, it was realized that ground determination derived from DIPC data provided more accurate height estimates than those from ALS DTM.

Similarly, Chen et al. (2017) surveyed the height of vegetation along seismic lines in Alberta's boreal forest using a point-intercept method sampling strategy to validate height estimates derived from unmanned aerial vehicles (UAVs) at the point and site level. Using the 99th percentile of UAV point cloud heights within 20cm buffer of precise seedling locations and three ground determination methods (UAV, RTK, and LiDAR) they found that the UAV_RTK method provided the lowest RMSE (28cm) at the point level. Based on two-tailed z-tests, the study found significant differences between field-measured vegetation heights and remote sensing estimates for all three methods at the point level. The three methods demonstrated better accuracies in low (0–0.5 m) to medium (0.5–2 m) vegetation height strata than in high (>2m) vegetation height strata. At the site level, no significant differences were observed between field measurements and remote sensing estimates from all three methods with the UAV ground determination method having the lowest RMSE (8 cm). Since the three methods performed similarly in terms of accuracy and RTK or LiDAR ground measurements did not significantly improve accuracy under the conditions of this study at the point and site levels, the study concluded that UAV alone can be used to estimate vegetation height.

Chasmer et al. (2021) demonstrated how bitemporal ALS data collected around 2008 and 2018 could be used to identify relationships between the density of linear disturbances, changes in vegetation height, and wetland shape complexity within wetlands in Alberta. Vegetation height change was determined based on the 95th percentile height differences of point cloud within 2-meter cell resolution over the 10-year study period. Of the over 1800 wetlands within the study area, this study found that 50% of wetlands in some regions were disturbed by anthropogenic disturbances with most of these disturbances occurring in fens. Their study also reported that bogs with dense anthropogenic disturbance resulted in increased growth and spread of shrubs, with the opposite occurring in fens and swamps during the 10-year study period. Although this study aimed to determine vegetation height change using ALS data, it was carried out on wetlands within which linear disturbances occurred rather than directly along linear disturbances.

Despite these advancements in utilizing point cloud in determining seedlings and vegetation height and height change, there remain gaps in understanding which vegetation height and change detection method – particularly the unit of analysis – best models or predicts field-measured change. Also, most previous studies using point cloud data to assess vegetation on seismic lines in the boreal forest of Alberta have focused on single-time assessments which are limited in assessing change or growth of seedlings. Fewer have employed multitemporal point cloud data to track vegetation height change along linear disturbances. No previous studies, that I am aware of, have compared the accuracies of unit of analysis derived when utilizing pixel and point cloud product of point cloud data when determining change along linear disturbances in the boreal forest of Alberta. Furthermore, none of these studies have assessed the effects of overhanging canopy and ecosite type on the accuracy of detecting seedling change and height along seismic lines in the boreal forest. My research seeks to address these gaps by revealing the

workflows needed to reliably map seedling height change on seismic lines in the boreal forest using bi-temporal ALS data.

1.5 Research Objectives

The overarching goal of this thesis is to develop a methodological workflow for reliably mapping seedling height change along linear disturbances in the boreal forest of Alberta. To make progress towards achieving this goal, I addressed the following three research objectives:

1. To determine whether ALS point cloud data provides a more accurate means of detecting seedling height change along seismic lines than ALS raster products. I expect that ALS point cloud data will be significantly more accurate in detecting seedling height change than an alternative raster-based approach, since derived raster products interpolate point cloud values over grids. This interpolation involves some modification and generalization of the raw point cloud information and could cause the introduction of some uncertainty in the change results obtained (Mitasova et al., 2005; Vepakomma et al., 2008). Point clouds, on the other hand, maintain the precise structural measurements obtained from the sensor with less modification to the data and, subsequently, the derived change results.
2. To evaluate whether ecosite type (upland and wetland/transitional) affects the accuracy of the best performing change detection approach on seismic lines. I expect that seedling height-change estimates in upland ecosites will be significantly less accurate than those in wetlands, due to variable canopy cover in upland sites which might block ALS pulse from penetrating to capture seedlings in the understory compared to wetland which are mostly characterized by more open canopies.

3. To apply the most accurate change detection approach for mapping height change of conifer seedlings across all seismic lines across a study area to demonstrate the application of my approach and to provide insight into seedling recovery patterns to support restoration and conservation efforts.

I carried out change detection by applying an image-differencing approach on both point-cloud and raster-based ALS products. Height change estimates derived from each approach were compared to a reference dataset of 194 conifer-seedling growth measurements obtained in the field. My research was performed in a 7 km² study area in northern Alberta.

1.6 Organization of Thesis

In Chapter One, I introduced the background and motivation for mapping vegetation height change or recovery along seismic lines in the boreal forest of Alberta and the objectives of this study. Chapter Two introduces ALS point cloud and how it is obtained and processed for use in vegetation change detection. It also touches on different change detection methods adopted in literature as well as a literature review of studies that have utilized ALS data in characterizing vegetation recovery. Point cloud, raster, and object-based approaches to utilizing ALS data in studying vegetation recovery are introduced and compared. Chapter Three introduces and describes the study area, data, and methodology of this research. Chapter Four covers the results which includes a non-parametric comparison of the accuracies of change obtained from point cloud and rasterized ALS data. Chapter Five delves into discussing the important findings of this study, comparing this study to other studies as well as the limitations and errors of this study as well as a future outlook. Finally, Chapter Six concludes this study by reporting its significance and contributions as well as any direction for future research.

This study forms part of the Boreal Ecosystem Recovery and Assessment (BERA) project which is a collaborative alliance that brings together researchers, government, and industry partners with a shared focus on ecosystem restoration within the boreal natural region of Canada.

Chapter Two: Background: ALS Data for Characterizing Vegetation Change or Recovery, a Literature Review

Light Detection and Ranging (LiDAR) is an active remote sensing technology based on the pulse-ranging principle used to derive ranges or distances using the product of the speed of light and the time it took for the emitted light pulse to hit the object (Lim et al., 2003). Airborne laser scanning (ALS) data is a kind of LiDAR data that is obtained by mounting a laser scanner on airborne platforms such as airplanes or drones (Maltamo et al., 2014). ALS systems acquire vertical and horizontal information about the area under study and distribute it as geospatial data. This data has great capacity for vegetation monitoring (Madsen et al., 2020; Zieba-Kulawik & Wezyk, 2022), as it offers the opportunity to measure vegetation structural changes directly. ALS data captures structural attributes such as the height of vegetation, which, when measured over the same area across different time periods, can help understand forest dynamics and track vegetation recovery. Qin et al. (2016) suggested that the introduction of an extra dimension (i.e., height of entities) in this data type presents an opportunity to take advantage of the physical geometry of objects, as well as obtaining vegetation structural properties. ALS also overcomes some of the limitations of traditional optical data types such as Landsat as it is less restrictive to seasonal or atmospheric effects (Qin et al., 2016). Recent advancements in image-based photogrammetry also offer the opportunity to generate 3D point clouds for vegetation analysis or applications through structure-from-motion (SfM) techniques. However, this study does not consider this data type because, unlike photogrammetry, ALS data is able to directly measure the distance to objects and penetrate vegetation or canopy cover to capture ground data. This is essential to characterize the height of vegetation as well as obtaining vegetation height change over time.

ALS data is mostly delivered in point cloud format, which are data points containing X, Y and Z position of returns derived from sensor pulse interaction with objects (Dong & Chen, 2018). Point-cloud information, however, is mostly processed and analyzed in pixel format such as digital surface models (DSMs), digital terrain models (DTMs), and canopy height models (CHMs) (Dong & Chen, 2018). There are two approaches by which ALS point cloud data can be utilized in monitoring forest or vegetation parameters. These include area-based and individual tree-detection methods (Hanssen et al., 2021; Nurminen et al., 2013). The area-based method uses a plot-based approach to represent and estimate vegetation metrics at the plot level while the individual tree-detection method uses the individual tree crown to represent or estimate vegetation metrics of each tree. This chapter begins by describing ALS and how it is acquired and processed. I will go further to describe change detection in remote sensing as well as various change detection methods and units of analysis that have been utilized in remote sensing literature. I will also compare the various units of analysis and change detection methods that have been adopted and utilized in characterizing vegetation change with ALS data.

2.1 ALS Point Cloud

ALS point clouds are generated from active sensors mounted on airborne platforms that use electromagnetic waves in optical and infrared wavelengths to send and receive signals (McManamon, 2019). The fundamental principle behind ALS is that the signals or waves emitted from the sensor reflects off objects such as vegetation and terrain. The reflected waves are recorded and translated into the objects' precise horizontal and vertical positions.

LiDAR sensors can be mounted on space-borne, ground, or airborne platforms. Airborne LiDAR is often referred to as Airborne Laser Scanning while Ground-based LiDAR is referred to as Terrestrial Laser Scanning. The choice of platform adopted is usually dependent on the size of the study area, the resolution of data required, and the frequency at which data needs to be collected (McManamon, 2019).

ALS data is mostly collected by mounting sensors on platforms such as piloted aircraft, helicopters, and Remotely Piloted Aircraft System (RPAS). Piloted aircraft are mostly adopted for large or regional-scale surveys while UAVs which are comparatively less expensive with higher flexibility, are adopted for smaller surveys. An ALS system mostly consists of a laser range finder for detecting ranges and a positioning and orientation system that is used to measure the orientation and location of the sensor (McManamon, 2019). It is based on this position and orientation system, that the x, y and z coordinates of the objects being scanned are obtained. Point cloud data may also contain information on the class of each point, as well as the intensity of the return pulse (Szostak & Pająk, 2023). ALS platform can perform scans in a zig zag, parallel, or elliptical format (Dong & Chen, 2018).

2.1.1 Processing ALS Point Cloud Data

ALS point cloud data is usually distributed in 'las' format. The American Society for Photogrammetry and Remote Sensing (ASPRS) defines 'las' as a public file format developed primarily for interchanging 3-dimensional (x, y, z) point cloud data between users. Processing ALS point cloud is usually an application-specific task. Many new workflows to process ALS point clouds have been proposed; hence there is no definite single approach to processing and analyzing this data (Dong & Chen, 2018).

Dong & Chen, (2018) describe two basic steps to processing ALS data: (i) classification of laser points and (ii) interpolation of the discrete points into a continuous surface such as Digital Elevation Models (DEMs). Classifying these points involves the characterization of laser pulse returns from objects such as trees, buildings and the ground. Interpolation, on the other hand, involves transforming these ALS data points into pixels. The attributes which are usually assigned to these pixels are based on interpolated height values of points falling within each pixel. Interpolation methods include Triangular Irregular Networks (TIN) and grid-based interpolation methods such as kriging.

McManamon (2019) describes ALS data processing to involve six levels based on the National Geospatial Agency (N.G.A) in the United States of America (U.S.A). These processing levels include (i) Level 0 (L0) which describes the raw ALS data in the form which was collected directly from the mapping platform; (ii) Level 1 (L1) which is the unfiltered raw point cloud obtained after applying algorithms on Level 0 to project it into a 3D representation of measurements taken; (iii) Level 2 (L2) is the filtered 3D point cloud where noise within L1 is taken out and relative registration or extrinsic calibration has been applied (D'Adamo et al., 2018); (iv) Level 3 (L3) which is the data derived after registering the L2 data to a known geodetic datum system; (v) Level 4 (L4) are the ALS products produced from the point cloud including Digital Elevation Models (DEMs); and (vi) Level 5 (L5) are specialized products produced from L4 using specialized tools.

ALS point-cloud data is mostly converted to pixel format such as digital surface models (DSMs), digital terrain models (DTMs), and canopy height models (CHMs) (Dong & Chen, 2018). In vegetated terrain, pulses from ALS sensors are able to penetrate gaps in the vegetation canopy

to interact with the ground underneath the canopy. As a result, multiple returns can be derived for a single pulse (Figure 2.1).

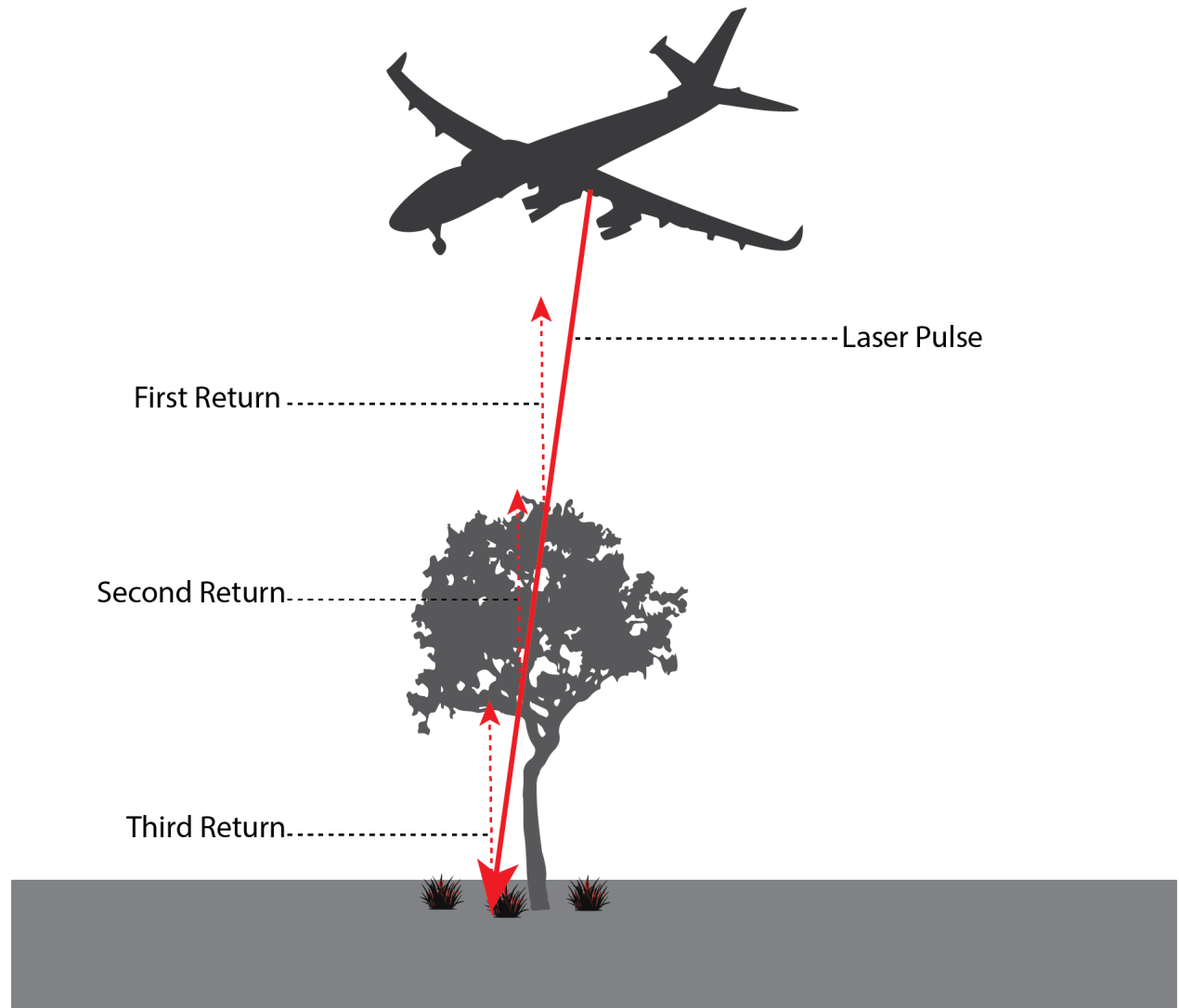


Figure 2.1: Visualization of an ALS pulse from an airborne platform capturing multiple returns from a tree and ground. The first return is the earliest return detected and usually represents the highest object the pulse encounters followed by the second and third returns respectively.

ALS returns can be classified to represent ground and non-ground objects. DSMs are models produced from point cloud of the top of the canopy while DTMs are produced from ground points (Koch et al., 2013). It is from the difference between DSMs and DTMs that CHMs are

obtained. CHM are also referred to as normalized DSMs (nDSM) which can simply be defined as the difference between the DSM and DTM, which represents vegetation height models within a given area (Koch et al., 2013). CHMs have been applied in most forest applications of ALS data (Boehm et al., 2013; Spadavecchia et al., 2022; Su et al., 2016).

As noted by Dong & Chen (2018), ALS data collection is a sampling approach rather than a complete representation of ground conditions. This limitation may result in missing ground or canopy points, potentially leading to an underestimation of forest canopy height. Also, the production of these models from point cloud data introduces a certain amount of error based on the transformation method adopted (Vepakomma et al., 2008). This can subsequently degrade the results that are obtained from these data types.

ALS data offers valuable vegetation structural data and presents an even higher benefit when collected at multiple time periods across the same area. This allows for detecting changes in vegetation height and volumes necessary to inform ecological management activities such as forest monitoring.

2.2 Change Detection

Change detection in remote sensing can be defined as the process of extracting information from two or more images within the same area, acquired at different time periods, about changes in the spatial, spectral, and thematic properties of objects of interest (Fatemi, 2019). Remote sensing has become a major source of data for change detection applications over the past several decades due to the advantages of its synoptic view, repetitive data and digital format for computer processing (Lu et al., 2004; Singh, 1989).

To achieve a good change detection, Lu et al. (2004) suggested that information on area of change, change rate, spatial distribution of change types, change trajectories of landcover types, and accuracy assessment of change detection results need to be provided. Image preprocessing to correct images geometrically, atmospherically, and topographically; selection of suitable change detection technique; accuracy assessment are considered the three major steps when implementing a change detection project (Hussain et al., 2013; Lu et al., 2004).

The first preprocessing stage is very important as it helps to ensure that the occurrence of errors such as misregistration which is usually as a result of geometric misalignment are drastically reduced. Geometric misalignment alone could affect change detection results by up to 5% for medium resolution images (Townshend et al., 1992). Atmospheric conditions such as wind and duct could also affect imaging conditions of the remote sensing data being studied, subsequently affecting change detection results hence the importance of atmospheric correction (Fatemi, 2019). Also, using data with similar or the same spectral and spatial resolution is important to avoid errors (Fatemi, 2019; Hussain et al., 2013).

There is no single best change detection technique in approaching a change detection project, hence, choosing an appropriate change detection method can be a very strenuous test which affect the final results (Lu et al., 2004). The context of the change detection project, what is expected, and the result expectation at the end of it is very important in determining the method to be used. For instance, certain change detection methods provide change, and no change (binary) results, while others provide directional change (Hussain et al., 2013). The unit of analysis is also crucial to the change detection approach employed (Hussain et al., 2013). Due to this, some change

detection works within the literature have resorted to a combination of more than one approach (Huang et al., 2009; Wang et al., 2018) to obtain the maximum accuracy possible.

There exists in literature an ever-growing list of approaches to carrying out change detection. This makes it a very difficult and complicated task to uniformly categorize change detection techniques and approaches universally. Efforts have been made to try and categorize change detection approaches or techniques within groups (Afaq & Manocha, 2021; Hussain et al., 2013; Lu et al., 2004; Qin et al., 2016; Tewkesbury et al., 2015). However, there is no uniformity in categorization across board. Lu et al. (2004) presented a very comprehensive categorization of change detection approaches by placing them in seven groups namely algebra, transformation, classification, advanced models, GIS, visual analysis, and other approaches to include those approaches that do not suitably fit into the other categories. A similar categorization can be realized in the review by Afaq & Manocha (2021). Hussain et al. (2013) categorized change detection approaches into main groups of pixel-based and object-based approaches. Tewkesbury et al. (2015) categorized these techniques based on the unit of analysis and comparison method to provide a clear and synoptic view of the field. Qin et al. (2016) also went further to support this by providing a description of change detection methods based on 3D information used, that is geometric comparison and geometric-spectral analysis.

Another aspect of change detection that makes it a difficult and complicated task is the accuracy assessment of change results. Accuracy assessment in change detection is a daunting task due to complications in collecting reliable temporal field-based data for various change classes of interest (Fatemi, 2019). Also, the reliability of several factors including complexity of the landscape, analyst's skills and experience, the change detection technique employed and how well

preprocessing, such as geometric correction and normalization is done (Lu et al., 2004) adds to making change detection a daunting task.

2.2.1 Unit of Analysis

The unit of analysis in a remote-sensing change-detection project specifies the data entity upon which a change comparison method is applied (Tewkesbury et al., 2015). Most change-detection studies use image pixels as their units of analysis (Tewkesbury et al., 2015). As the name suggests, these pixel-based change analysis approaches involve working with the pixels, the basic unit of raster images, for change detection. Pixel values in such analysis are representative of the intensity, height or reflectance of landcover features on the ground. Tewkesbury et al. (2015) suggested pixel and kernel as unit of analysis of change detection that entails analysis being applied on individual pixels of an image or a group of neighbouring pixels respectively. Using pixels as units of analysis has been criticized because it does not capture contextual information of imagery, like shape and texture. Hence, kernel processing has been considered as an upgrade that addresses this issue. Kernel processing, also referred to as moving-window analysis, reduces spurious errors by incorporating contextual information into change decisions not just spectral intensity, tone, or radiance (Tewkesbury et al., 2015). ALS data pixel forms include DSMs, DTMs, and CHMs (Dong & Chen, 2018). While ALS is normally delivered in a point-cloud format, these discrete point cloud data are commonly gridded based on a transformation process including inverse distance weighted, inverse quadratic, local polynomial, krigging, and TIN (Vepakomma et al., 2008). The derived transformation value of the points that fall within a user-defined pixel size is then applied to each pixel or grid cell.

Unfortunately, the rasterization of the point clouds introduces a certain amount of error based on the transformation method adopted (Vepakomma et al., 2008), which can subsequently degrade the change-detection results. This is due to the modification and in some cases generalization of the attributes of the raw point cloud into a single pixel value. For instance, Hodgson & Bresnahan (2004) evaluated the interpolation-induced elevation error of different land cover categories by comparing field-surveyed elevations to interpolated ALS elevation values. Their results showed that interpolation accounted for errors ranging between -12.9 cm to +12.8 cm for the various land cover categories.

Over the last two decades, object-based image analysis has become more widespread. Advancements in high-performance computing software coupled with efficient software algorithms as well as the success of commercial package software such as eCognition are attributed as the reasons why object-based image analysis is becoming more widespread (Blaschke, 2005; Chen et al., 2012; Hall & Hay, 2003). The recent advent of high-resolution satellite imagery and airborne imagery has resulted in a need to reconsider traditional pixel-based change detection approaches (Chen et al., 2012). Geographic Object-Based Image Analysis (GEOBIA) is the paradigm, not in the sense of it replacing traditional pixel-based approaches, but as a new way of understanding the world (Blaschke et al., 2014). The authors describe segmentation as the only means of delineating an image object of interest based on a lesser heterogeneity among constituents or basic units of a segment as compared to heterogeneity in conjunction with its neighbours. This approach is often applied to very high-resolution satellite or aerial imagery, where a group of similar pixels make up an object, instead of the traditional low and medium-resolution imagery, where an object is usually contained in a single pixel. Tewkesbury et al. (2015) subdivided objects as units of analysis into image object overlay, image object comparison, multi-

temporal image object and vector polygon. A hybrid option was also mentioned, which entails detecting change using pixels and segmenting the change results into image objects.

With ground entities being represented by several pixels in high spatial resolution images instead of the coarser representation of entities in medium to low-resolution images, objects are delineated more accurately. Image objects were defined by Chen et al. (2012) as a group of pixels that represent a meaningful object in an image scene. Object-oriented processing techniques are adopted to segment multispectral images into homogenous regions based on spectral and spatial properties of neighbouring pixels (Blaschke, 2005). Spurious changes can be introduced when using traditional pixel-based change detection or classification approach on very high-resolution images due to high spectral variability among pixels. Object-based approaches tackle this by smoothing out this high variability within an object and treating it as a single entity (Chen et al., 2012). Also, the issue of misregistration, which can lead to errors, is also easily identified and mitigated. Object-based change detection adopts change detection approaches applied on pixels by creating objects out of entities on the map for change assessment rather than directly using pixels.

Object-based approaches to change detection come with their own challenges including the creation of slivers as a result of misregistration and inconsistent segmentation when comparing image objects from different time periods (Chen et al., 2012). Segmentation of image objects independently from different temporal scales almost never produces the same results or boundaries. Linke et al. (2009) recognized these object mismatches as boundary overshoots and undershoots that could lead to the creation of sliver objects, spurious stretches, spurious encroachment, and spurious gaps. These kinds of errors were tackled through the development of

a spatio-temporal disturbance-inventory database and boundary matching procedures for map updating and backdating. It is worth mentioning that the appropriate unit of analysis for a change detection procedure is dependent on the resolution of imagery being considered and its ability to deliver the comparison features of interest (Tewkesbury et al., 2015).

2.2.2 Comparison Method

Comparison method in a change-detection study can be defined as the processing technique used to detect changes in a variable or target of interest. These techniques include image differencing, post-classification analysis, regression, and machine learning (Hussain et al., 2013). There is no universal best method for performing change detection, and the selection strategy is an increasingly confusing task (Ehlers et al., 2014; Hussain et al., 2013; Tewkesbury et al., 2015). However, the most commonly used change detection methods adopted in the literature include the image differencing and post-classification change detection methods.

Image differencing change detection method involves co-registering of images precisely and subtracting the first date image from the second date image pixel by pixel, to produce a residual image that is representative of change (Hussain et al., 2013; Lu et al., 2004). This is a simple and straightforward technique that is easy to interpret. However, it does not provide detailed from-to information. Change is absolute in image differencing, and the same value may have a different meaning (Hussain et al., 2013; Lu et al., 2004). Image differencing also requires the selection of a threshold which could lead to mis or over-detection.

Post-classification comparison involves classifying multi-temporal images independently to create thematic map products that are compared pixel by pixel to produce change maps showing

a complex matrix of changes or class transitions (Lu et al., 2004; Singh, 1989; Tewkesbury et al., 2015). Qin et al. (2016) defined post-classification comparison approach as a method that involves classifying the multi-temporal dataset and then comparing the classification labels of these datasets to detect change. Since the classified maps are produced independently, there is no need to carry out any atmospheric corrections before carrying out the change detection approach (Tewkesbury et al., 2015). This method also avoids the direct comparison of height and spectral properties of the 3D data and has the potential of improving the accuracy of the change detection (Qin et al., 2016). This approach is more robust to temporal changes; however, it highly depends on the accuracies of classification (Qin et al., 2016). Even though much information about change is provided when using the post-classification comparison approach, there is a tendency to spend a lot of time in creating a classified image with fewer errors as these errors could be introduced into the change product if not tackled (Lu et al., 2004; Tewkesbury et al., 2015).

Other comparison methods include Change Vector Analysis (CVA), which is a technique that can handle multiple bands and offers both magnitude and direction of change in its products by determining the spectral difference and Euclidean distance between end points through the n-dimensional change space respectively (Afaq & Manocha, 2021; Lu et al., 2004; Tewkesbury et al., 2015). It is, however, complex to identify direction of land cover change with this approach (Afaq & Manocha, 2021; Hussain et al., 2013; Lu et al., 2004). Multi-date direct comparison, also referred to as Spectral-temporal combined analysis, involves stacking multi-temporal data into a single file and classifying it to directly identify static and dynamic land covers (Lu et al., 2004; Tewkesbury et al., 2015). This technique is simple because it requires just one classification stage. However, it is difficult to identify and label change as a complete change matrix information is not provided (Hussain et al., 2013; Lu et al., 2004; Tewkesbury et al., 2015).

2.3 Comparison of Units of Analysis and Comparison Method for ALS Vegetation Change Detection Studies

This section will consider literature that has utilized ALS data in vegetation change detection. I searched the Web of Science with keywords ‘LiDAR’ or ‘ALS’ and ‘change detection’ and ‘vegetation’ or ‘forest’ and ‘remote sensing’ to identify peer-reviewed articles published in the past 15 years (2010 to date). Other articles deemed relevant from other sources such as Google Scholar as well as a few relevant studies from before 2010 were also included. I was only interested in change detection studies that used ALS data for vegetation or forest change detection, and so excluded studies using Terrestrial Laser Scanning (TLS) data and others that utilized ALS in conjunction with other multispectral image data sets except aerial images. Studies that used ALS for purposes other than vegetation change detection are also excluded. I ended up with 24 articles that fit these criteria, which are summarized in Table 2.1. The studies were categorized by change-detection method (e.g., post-classification, image differencing, etc.) and unit of analysis (i.e., pixel, object, or hybrid).

Table 2.1: This table summarizes and categorizes ALS-based vegetation change detection studies based on the location of the study, change detection method, and unit of analysis applied.

Publication	Location	Change Detection Method	Unit of Analysis
Mielcarek et al. (2025)	European Białowieża Forest, Poland	Post Classification/ Statistical Comparison	Hybrid (Pixel and Object)
Jones et al. (2024)	Utikuma Region Study Area (URSA), Alberta, Canada	Image Differencing	Pixel
Szostak & Pająk, (2023)	Poland	Image Differencing and Statistical Comparison	Hybrid (Pixel and Point Cloud)
Spadavecchia et al. (2022)	Slovenia	Post Classification	Hybrid (Object and Point Cloud)
Poorazimy et al. (2022)	Finland	Image Differencing	Object
Marinelli et al. (2022)	British Columbia, Canada	Image Differencing and Change Vector Analysis	Pixel
Tymińska-Czabańska et al. (2022)	Katowice Region, Southern Poland	Image Differencing	Pixel
Przewoźna et al. (2021)	Poland	Post Classification	Object
Hanssen et al. (2021)	Oslo, Norway	Post Classification/ Statistical Comparison	Object
Arumäe et al. (2020)	Estonia	Statistical Comparison	Point Cloud
Madsen et al. (2020)	Mols Bjerge, Denmark	Post Classification	Pixel
Marinelli et al. (2019)	Trento, Southern Italian Alps	Statistical Comparison	Pixel
Zhao et al. (2018)	Scotland, UK	Image Differencing/ Statistical Comparison	Hybrid (Pixel and Object)
Angelidis et al. (2017)	Southern Jutland, Denmark	Post Classification	Object
Song et al. (2016)	Osaka, Japan	Image Differencing	Pixel
Su et al. (2016)	California, USA	Post Classification/Image differencing	Hybrid (Pixel and Point Cloud)
Stepper et al. (2015)	Traunstein in Bavaria, Germany	Image Differencing	Pixel
Fisher et al. (2015)	Bushbuckridge Municipality and Sabi Sand Wildtuin, South Africa	Post Classification and Statistical Comparison	Object
Frew et al. (2016)	Oregon, USA	Image Differencing	Object
Boehm et al. (2013)	Central Kalimantan, Indonesia	Image Differencing/Statistical Comparisons	Pixel
Dolan et al. (2011)	Southeastern USA	Post Classification and Statistical Comparison	Pixel
Wang & Glenn, (2009)	Clark County, Idaho, USA	Image Differencing	Pixel
Vepakomma et al. (2008)	Lake Duparquet Teaching and Research Forest, LDTRF, Canada	Post Classification (Binary-Presence of gaps or not and further gap dynamics)	Object
Yu et al. (2004)	Kalkkinen, Helsinki, Finland	Image Differencing	Hybrid (Pixel and Object)

Of the 24 studies cited in this literature review, 23 of them have characterized vegetation change using ALS data based on pixels or objects, being at least one of the units of analysis. Only two studies were carried out with point cloud being at least one of the units of analysis (Arumäe et al., 2020; Spadavecchia et al., 2022). The most common pixel data utilized are CHMs or nDSMs with 18 of the 24 studies adopting this data type. CHMs and nDSMs are produced by subtracting DTM from DSM. DTM is representative of bare ground elevation which is obtained as a result of ALS data being able to penetrate forest canopy. Studies that utilized objects as the unit of analysis converted point cloud into CHM raster pixels before segmenting raster canopies into objects for change detection. Using objects for change detection has also involved converting ALS point cloud into raster, after which individual tree crowns or forest stands are segmented to produce objects. Segmentation methods commonly used include watershed segmentation (Hanssen et al., 2021; Poorazimy et al., 2022; Yu et al., 2004; Zhao et al., 2018), inverse watershed (Przewoźna et al., 2021) and manual boundary delineation (Angelidis et al., 2017).

Image differencing is the most used change detection comparison method, with 12 of the 24 cited studies applying this comparison method on ALS data. This method has been mostly applied with pixel data to determine change in vegetation. Image differencing is the simple task of subtracting the reference data image from the compared date image. It is also widely used as it is simple, straight forward, easy to use and implement (Lu et al., 2004). The user is however, faced with a daunting task of selecting a suitable threshold of change as well as the right image band to depict change (Lu et al., 2004). Image differencing change results cannot be used to produce matrices of change as can be done with post-classification comparison. Hussain et al. 2013 also suggest that this approach produces absolute difference or change values hence a single value may have different meanings in different scenarios.

Post-classification comparison method has also been leveraged in 10 out of the 24 studies cited in Table 2.1, with this comparison method being commonly applied in object-based analysis. Hussain et al. (2013) identified post-classification analysis as the most common comparison method adopted in change detection studies that involve pixels and objects.

Arumäe et al. (2020) used point clouds as unit of analysis and statistical comparison (T-tests and linear regression models) to assess change in canopy cover and height percentiles of forest stands in a hemi-boreal forest in Estonia where tree thinning had been carried out before, after and during ALS surveys. Stand height was extracted by clipping each stand point cloud and extracting point cloud metrics including the 25th, 50th, 80th, and 95th percentiles based on the stand polygons. Canopy cover was also assessed based on the ratio of count of returns from stand canopy against the count of returns in stand point cloud. Change was then assessed statistically based on t-tests and linear regression models.

Marinelli et al. (2022) used image differencing to detect horizontal and vertical changes in the forest. They calculated the 95th percentile height of all point clouds within each pixel and determined canopy cover by dividing the number of first returns above a specific height threshold by the total number of first returns per pixel. Both change metrics were then converted from Cartesian to polar coordinates to obtain the magnitude and direction of change. After applying a majority filter to reduce noise and outliers, their method identified changes, including forest growth, regeneration, and harvesting, with an overall accuracy of 98.07%.

Hanssen et al. (2021) mapped changes in urban tree canopy cover in Oslo, Norway, using ALS data from 2011, 2014, and 2017. They detected changes through an object-based post-classification approach by first segmenting various CHM pixels into tree canopy cover. After

segmentation, they compared the total tree canopy area and canopy volume to assess changes in the urban canopy. They also statistically compared the number of trees in different height categories across the three years.

Madsen et al. (2020) reported the challenge of sampling training data while using post-classification method in change detection analysis in detecting biomass and structural change in *Cytisus scoparius* shrubs in seminatural grasslands. They adopted pixels as the unit of analysis after extracting height values from point cloud to quantify the biomass volume for 2017 and 2018.

Zhao et al. (2018) used ALS data to measure forest changes over time at both individual tree and grid levels, including tree growth in Aberfoyle village in Scotland, UK. While this study used both pixels and objects as the units of analysis, the individual tree growth was extracted by first segmenting individual tree crowns from a derived CHM and using these objects to clip out the point cloud of each tree from which the max height of the tree was extracted and subtracted for growth metrics.

Vepakomma et al. (2008) also carried out an object-based approach to evaluate the feasibility of canopy gap change in the Lake Duparquet Teaching and Research Forest (LDTRF), Canada, using 5-year interval ALS data. They did this by comparing and selecting the optimal resolution and optimal interpolation method for rasterizing ALS data. Out of the eight interpolation methods tested, Inverse Distance Weighted was adopted as the optimal while the optimal resolution was selected based on the number of returns per grid and the resolution that mapped the new forest gaps the most.

Several studies have successfully detected change in vegetation using ALS data. For example, Vepakomma et al. (2008) estimated canopy gap change using an object-based method at

an accuracy of 96%. Angelidis et al. (2017) assessed changes in non-forest woody vegetation at accuracies of 81.74% (new vegetation), 99.07% (unchanged vegetation), and 90.07% (removed). Marinelli et al. (2022) detected horizontal and vertical changes in the forest using a pixel-based approach at an accuracy of 98.07%. Spadavecchia et al. (2022) applied a hybrid object and point cloud-based approach to automatically detect change in forests at an individual tree level. Their proposed change detection algorithm achieved an F1 score of 63% demonstrating its effectiveness in identifying change. While these studies detected change in vegetation at significant accuracies, none of the studies considered in this literature review compared the accuracy of change detection using point cloud and any other unit of analysis.

This chapter reviewed ALS data studies as well as the common units of analysis and comparison methods that have been adopted in the literature to characterize vegetation change. Also, I made a comparison of literature that utilized objects, pixels and point cloud as units of analysis, as well as post-classification and image differencing as comparison methods. While the literature emphasizes the growing interest in using ALS data for vegetation monitoring, only a few studies have analyzed and compared raster (pixels) and point cloud-based approaches in detecting seedling height changes, especially in structurally complex environments like seismic lines. Also, the influence of ecosite types on assessing this kind of change is largely overlooked. These gaps emphasize the need for this study, which directly addresses these issues by evaluating and comparing the accuracies of ALS point cloud and raster (pixels) seedling height change detection approaches, assessing how ecosite type influences these accuracies, and applying the most accurate approach to support restoration planning.

Chapter Three: Methods

3.1 Study Area

My research was conducted in the lower Athabasca region of northeastern Alberta, Canada, approximately 150 km south of Fort McMurray near the town of Conklin (Figure 3.1). The study area, about 7 km² in size, is located within the Central Mixedwood subregion of the Boreal Forest and is characterized by a mixture of upland, transitional, and wetland treed ecosite types. Upland ecosite types have unsaturated soils for extended periods with tree canopy present, while wetland sites have their soils saturated for all or part of the year with sparser tree canopies due to elevated water table levels (Beckingham & Archibald, 1996). The most common conifer species in this study area include white spruce (*Picea glauca*), black spruce (*Picea mariana*), tamarack (*Larix laricina*), and jack pine (*Pinus banksiana*). Aspen (*Populus tremuloides*) and balsam poplar (*Populus balsamifera*) are the most common deciduous species (Alberta Parks, 2015). Annually, this area experiences temperatures above 15°C for one to two months, and rainfall of 475 mm with peak rainfall occurring in July. 60 to 70% of the annual rainfall is received between April and August (Alberta Parks, 2015; Natural Regions Committee, 2006).

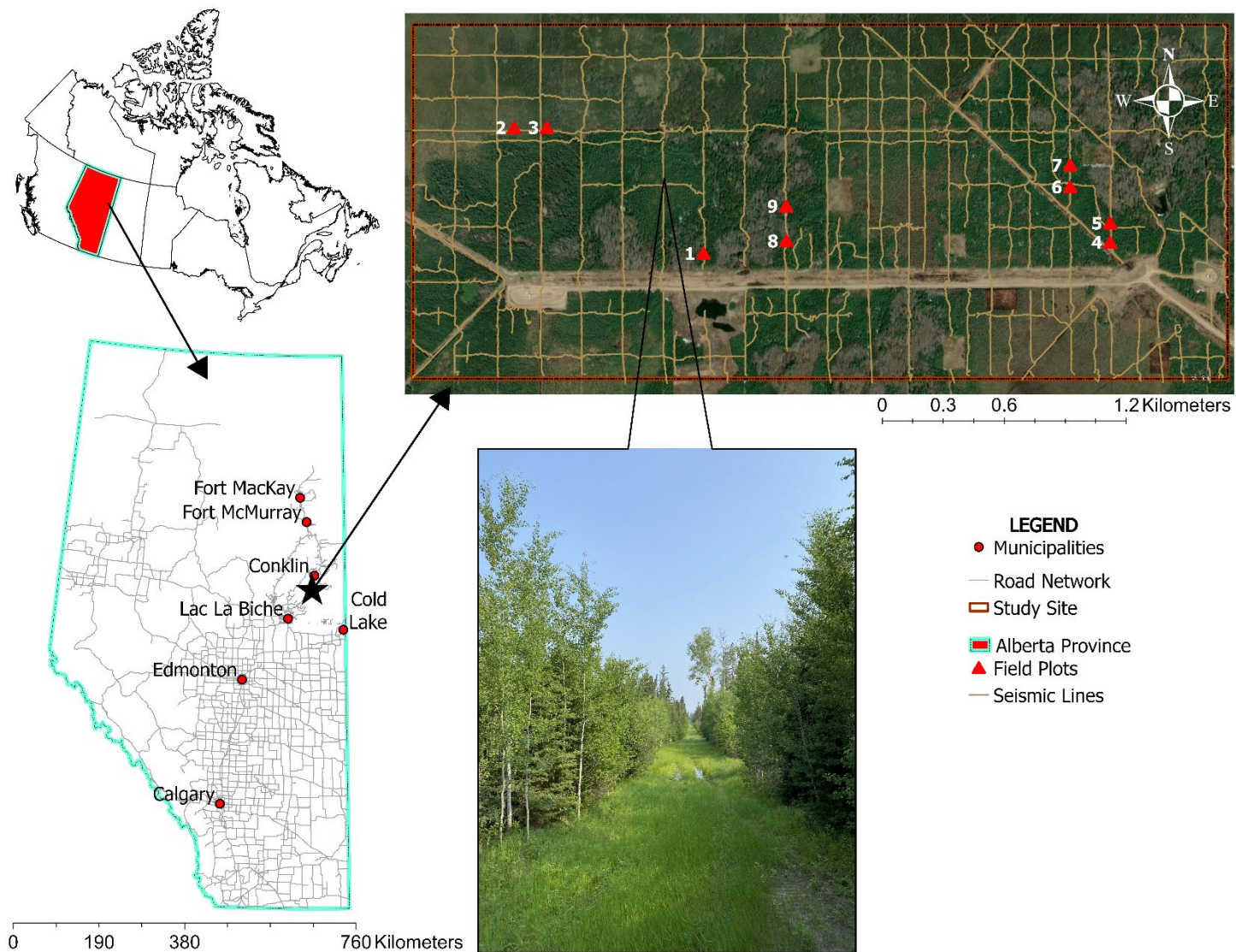


Figure 3.1: Map of the study site in northeastern Alberta, Canada (left), including a detailed map highlighting linear footprint and field plots where ground measurements were taken (upper right). Below the detailed map is an inset photo giving a visual example of a seismic line on ground.

The study area contains a dense network of linear industrial features totaling 41.1 kilometers, most of which are seismic lines. The linear features are a mixture of conventional and low-impact seismic lines, trails, and roads. The width of seismic lines within this study site ranges between 3 and 8 meters. Most were constructed between 1989 and 2005, with the initial disturbance years provided by the Alberta Biodiversity Monitoring Institute (ABMI) Human Footprint Inventory and the Regional Industry Caribou Collaboration (unpublished data). A visual assessment of aerial ALS data also revealed that some lines were constructed after 2017.

In 2015, 8.7 kilometers of seismic lines within the study area underwent silvicultural treatment (mounding and tree planting) to restore forest cover. Inverted mounding, which involves the overturning of the upper organic layer of the soil with an excavator, was applied, after which two-year nursery-grown black spruce and tamarack seedlings were planted on these treated lines to mimic the species composition of the adjacent forest. Shellian et. al (2024) assessed the growth rates of coniferous seedlings in this study area by comparing height growth between naturally recovering and actively restored seismic lines. These height-growth measurements serve as the foundation for my own research. I used Shellian's field data to construct field-measured seedling growth over a five-year time period (2017 to 2022) for a sample of 194 seedlings spread across my study area. I compared this ground-measured growth to Light Detection and Ranging (LiDAR) derived growth over the same time period to address the objectives of my thesis. My sample design, data sets, processing strategies, and statistical analyses are outlined in the following sections.

3.2 Sampling and Field Data

The 100 square-meter sample plots adopted for this study are a subset of some permanent Boreal Ecosystem Recovery and Assessment (BERA) research plots established in the summers of 2017 and 2021 (Shellian et al., 2024). Shellian et al. (2024) adopted a subset of these permanent research plots to include sites where the ecosite was a treed fen, the site had been treated with mounding and planting, or the site had been left to naturally regenerate. I used a total of nine of these sample plots distributed across upland and wetland ecosite types: seven from treated lines and two from untreated lines (Figure 3.1). These field plots are a subset of the Shellian et al. (2024) sample plots, found within my study site, where real-time kinematic global navigation satellite system (RTK GNSS) locations of measured seedlings had been taken. The field plots were located at least 15 meters from seismic line intersections or well pads to avoid the edge effects and to ensure that the plot was at a point where the adjacent forest was undisturbed. Each 100 square-meter plot contained ten 10 square-meter subplots (Figure 3.2). The length and width of the plots varied as a function of the width of the seismic line they are set up on, but the area was always 100 square meters (Linke et al., 2022).

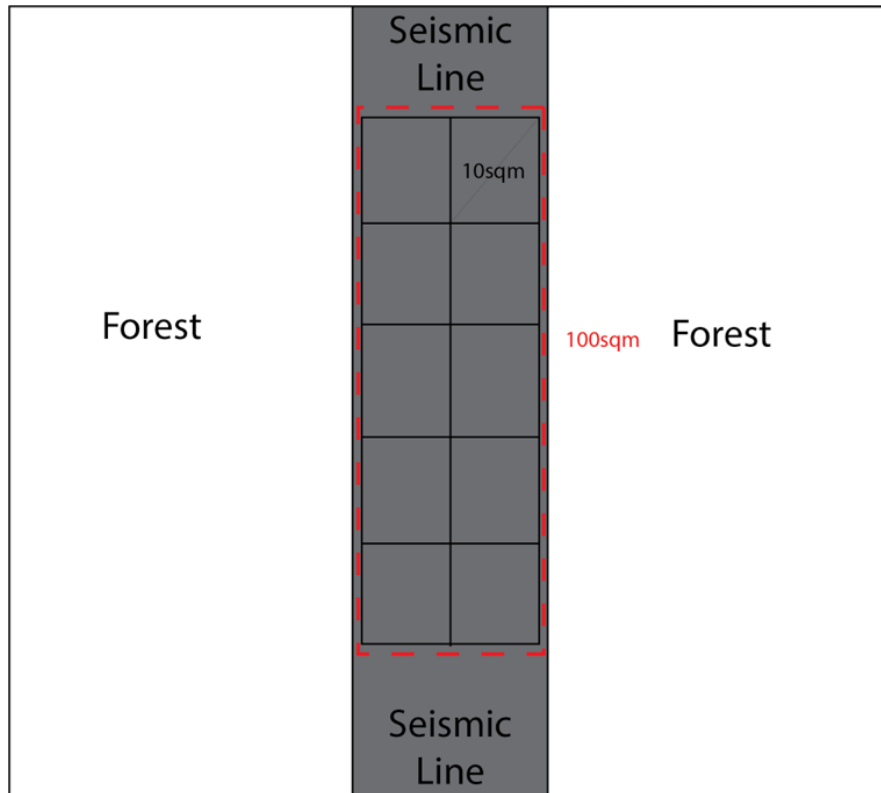


Figure 3.2: Illustration of a 100-meter square plot with 10-meter square subplots positioned along a seismic line.

Measurements of all the seedlings occurring within the nine sample plots were collected by field crews in the summer of 2021 in support of Shellian et al.’s (2024) research comparing seedling growth rates on treated and untreated seismic lines. For that study – and this one – seedlings were defined as regenerating trees below 3m height. The field protocol involved selecting and measuring the three tallest black spruce and the three tallest tamarack seedlings occurring within each 10m² subplot, if they were available. The number of seedlings measured per subplot varied, as the densities and distribution of species were variable across the plots sampled. Seedlings in the treated plots were comprised of both seedlings, planted in 2015, and naturally occurring seedlings. Untreated plots contained only naturally occurring seedlings.

Field crews in the Shellian et al. (2024) study measured growth of each sampled seedling between 2016 to 2021 by counting the number of whorls or bud scars on the main stems (Figure 3.3). The 2016 spring height was determined by measuring from the base of the seedling stem to the 2016 bud scar. The 2021 spring height was determined by measuring from the base of the seedling stem to the 2021 bud scar. Since my monitoring horizon (2017 to 2022) varied slightly from Shellian et al.'s (2016 to 2021), some adjustments were required. I calculated the 2017 spring height as the 2016 spring height plus the growth increment before the 2017 bud scar: in other words, the 2016 leader growth (Equation 1). The 2022 spring height was calculated as the 2021 spring height plus the 2021 leader growth (Equation 2). In these instances, I assumed that all the 2021 leader growth had been completed when measurements were taken in the summer of 2021.

$$2017 \text{ Spring Height} = 2016 \text{ Spring Height} + 2016 \text{ Leader Height} \quad (1)$$

$$2022 \text{ Spring Height} = 2021 \text{ Spring Height} + 2021 \text{ Leader Height} \quad (2)$$

By subtracting the 2017 seedling spring heights from the 2022 seedling spring heights, the approximate field change within the 5-year study period (2017 to 2022) of this study was extracted (Equation (3)).

$$\text{Field Height Change} = 2022 \text{ Spring Height} - 2017 \text{ Spring Height} \quad (3)$$

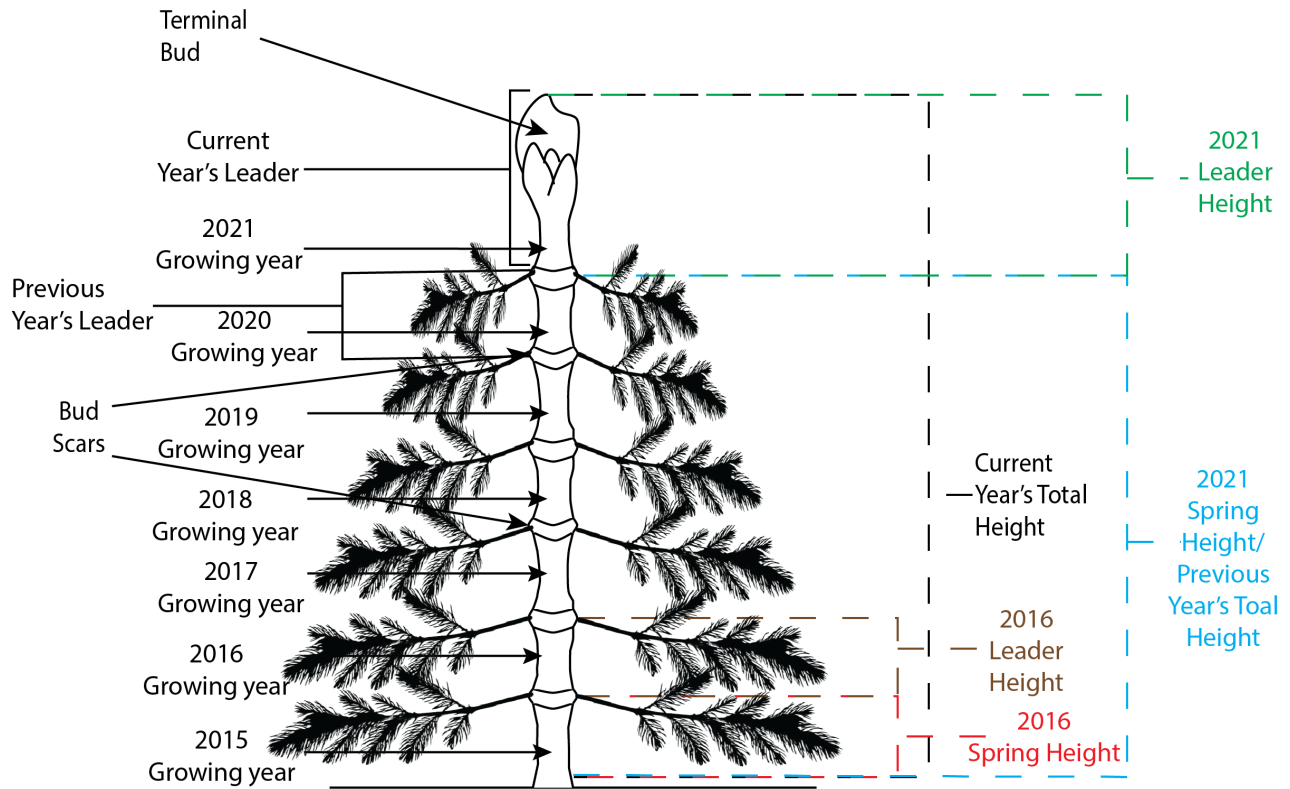


Figure 3.3: Illustration of seedling height measurements taken in the field during the summer of 2021. This diagram shows how seedling height growth was determined using visible bud scars along the seedling stem, each representing the end of the growing season. The leader height is the vertical growth of the terminal bud from the previous year's bud scar to the current year's bud scar. The total height is the cumulative height of the seedling measured from the base to the current year's terminal bud. The spring height of a given year is estimated based on the cumulative height from the base to the position of the bud scar from the previous year, reflecting the seedling's height at the beginning of that year's growing season.

A total of 206 seedling measurements were extracted from the 9 field plots within the study area. Seedlings that showed a reduction in height were assumed to be caused by data collection errors and were excluded from further analysis. This brought the number of reference seedlings included in this study down to 194 (Table 3.1). The seedlings' precise locations were collected by Shellian et al. (2024) in the summer of 2021 while height measurements were being taken. The coordinates of each seedling were recorded with a RTK GNSS survey method, which can provide centimeter-level accuracy. It was assumed that these seedling locations captured the precise center

of the seedlings, which were required in subsequent processing steps to match and extract the LiDAR-measured change values for each individual seedling.

Table 3.1: Seedling height statistics for the 194 reference seedlings measured across 9 field plots within the study area for the two study periods (2017 and 2022). An asterisk by field plot indicates that it is a wetland site.

Field Plot	Sample Size	2017 Mean Height (cm)	2017 Height Range (cm)	2022 Mean Height (cm)	2022 Height Range (cm)
1	31	29.2	11 - 85	55.7	23 - 182
2*	20	28.6	16 - 55	52.9	31 - 76
3*	34	111.0	18 - 230	194.0	48 - 410
4	32	33.6	8 - 74	62.1	20 - 121
5	22	13.7	8 - 32	33.8	23 - 61
6	12	18.2	10 - 30	35.8	21 - 57
7	11	19.4	9 - 42	37.4	25 - 63
8	5	69.2	23 - 110	103.0	34 - 155
9	27	43.9	10 - 125	69.9	24 - 176
Total = 194					

3.3 Airborne Laser Scanning (ALS) Data

Bi-temporal ALS data were used to estimate height change for the 194 seedlings that were surveyed in the field. Once again, the monitoring horizon stretched across five growing seasons between 2017 and 2022, corresponding with the time period over which seedling growth was measured in the field. The first ALS dataset was acquired between July and August of 2017 with a Leica RCD 30 sensor flown at an altitude of 850 m. The second was acquired between June and August of 2022 with the Riegl VQ-1560ii sensor flown at an altitude of 1800 m. The 2017 and 2022 datasets featured point densities of 37.2 points/m² and 29.2 points/m², respectively. The vendor-supplied horizontal root-mean-square-error (RMSE) of both point clouds was 30 cm and 35 cm for the 2017 and 2022 datasets, respectively.

The relative vertical shift between both datasets was approximately 6.1 cm, while the relative horizontal X and Y shifts were 8.5 cm and 21.2 cm, respectively (Appendix A). The relative horizontal and vertical geometric alignment or shift between both point clouds was calculated by identifying static points in both datasets. These static points included locations on all-weather roads, constructed surfaces, and bare land that remained the same between both study years. By assessing the vertical and horizontal (X and Y) differences between those points, I was able to derive the relative vertical and horizontal shift between both datasets. This vertical shift value was used as the basis for setting a threshold of actual change in the change results. Based on the relative horizontal shift between both datasets falling below the vendor-provided horizontal RMSE, I assume there is minimal misalignment or systematic errors between the datasets that could significantly alter the seedling height change results.

3.4 ALS Preprocessing

Pre-processing was carried out with LASTools to produce clean point clouds and digital surface models (DSMs) to minimize errors in the change detection process. Noise in the ALS data, including duplicate points, points representing unwanted objects, and points that were picked up by more than one flightline, were identified, marked, and removed using the LASnoise, LASduplicate, and LASoverage tools. The z-values of the point cloud data were retained for the seedling change detection. However, the point cloud was also height-normalized and stored as an extra byte or field in order to set vegetation height thresholds in subsequent steps.

Further processing was also applied to the original point cloud after removal of noise to produce a rasterized DSM (60cm resolution) for both years. This was carried out using the

LAS2dem tool from the LASTools package for the purpose of carrying out the rasterized change detection. I also ensured that the horizontal and vertical coordinate reference systems (Horizontal: NAD_1983_CSRS_UTM_Zone_12N, Vertical: Canadian Geodetic Vertical Datum of 2013) were the same to align the bi-temporal datasets and minimize any shifts to the barest minimum.

3.5 Change Detection Workflow

I estimated the ALS changes in seedling height between 2017 and 2022 using three change-detection workflows: (i) based on image differencing carried out on pixels (Raster), (ii) based on point cloud image differencing carried out in Cloud Compare (PC_{CC}), and (iii) based on differencing of point cloud percentile metrics (PC_{PM}). A summary of the methodological workflow of this study is provided in Figure 3.4. A height-differencing change-detection strategy was applied for all approaches in this study. This involved simple subtraction arithmetic on the bitemporal datasets to produce residual height change maps, which are indicative of change in seedling height within the study area between 2017 and 2022. According to Qin et al. (2016), this is an easy-to-implement approach that can be carried out over large areas, as was the case in this study.

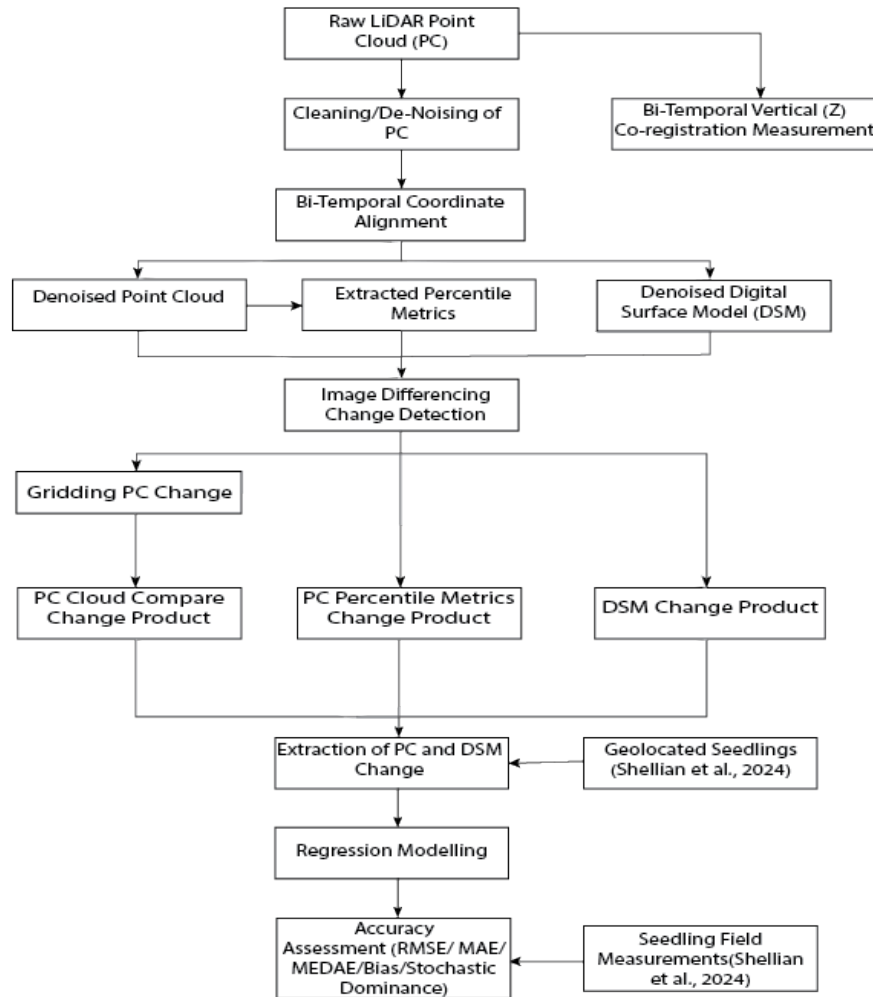


Figure 3.4: Change detection workflow illustrating the steps involved in assessing changes across both units of analysis and accuracy evaluation. "PC" denotes point cloud, and "DSM" stands for digital surface model.

3.5.1 Raster (DSM) Image Differencing

Image-differencing change detection using the Raster Calculator tool in ArcGIS Pro was applied on the rasterized DSMs for 2017 and 2022. The change detection was carried out based on the difference in the input band. The input band to be assessed was the interpolated unnormalized elevation (z) values for each pixel in the DSM. Each pixel band value of the older year (2017) was subtracted from the corresponding latest year (2022) pixel value to come up with a change residual

map across the study area. In this case, it was assumed that the minimal relative shifts accounted for between both datasets and the pixel size of 60 cm would be enough to ensure that the same seedlings from each year align with each other for change to be determined between them. In order to minimize the effect of overhanging canopy and branches of adjacent forest or taller trees on seedling change results for this approach, percentile cutoffs (40th, 50th, 60th, 70th, 80th, 90th) were applied to the raw point clouds before interpolating to produce rasterized DSM products. These percentile cutoffs were applied and tested, and the most accurate was adopted as the raster-based approach for the study. I assumed that the most accurate percentile cutoff would minimize the influence of overhanging canopy as much as possible while maintaining seedlings along the seismic lines for accurate seedling height change to be detected.

Individual seedling raster change was then extracted from the residual height change raster product using the seedling geolocated points and the Extract Multi Values to Point tool in ArcGIS Pro. This tool extracts the height change value at each pixel where a seedling point falls within and populates a field that has those change values representing height change for each seedling for the study period (2017 to 2022).

3.5.2 *Point Cloud (Cloud Compare) Image Differencing (PC_{CC})*

This point cloud-based change detection was carried out in Cloud Compare using the cloud-to-cloud distance tool. This is a robust distance computation tool based on nearest neighbor distance that computes the distance between each point in a “reference” point cloud and its closest points in a “compared” point cloud dataset. The “reference” point cloud are the points upon which distances would be calculated relative to. The “compared” point cloud on the other hand are the points upon which distances are calculated, and the height change values would be hosted on. The

technique is based on the Hausdorff distance equation (Equation 4), which can be defined as the common distance between two sets of points that comprises computing for each point p of a cloud S , the distance to the nearest point in the other cloud S' (Girardeau-Montaut et al., 2005). In order to ensure that the true nearest neighbour of a point is found, the distances of all points close to the reference point are checked until no other point is closer than the true closest point (Girardeau-Montaut et al. 2005). This suggests that there is no point without a neighbour, regardless of how far the distance between the points. For this reason, a maximum distance parameter can be set to stop the tool from calculating distances farther than the set max distance. The cloud-to-cloud distance tool allows for signed (negative and positive) distances, only when horizontal (x and y) and vertical (z) distances are split. This tool works well with dense point clouds, hence, it is advisable to have the densest point cloud as the reference point cloud.

$$d(p, S') = \min_{p' \in S'} \|p - p'\|_2 \quad (4)$$

For the PCcc approach, the first returns of the point clouds were retained and all other returns were dropped. This was done to minimize computational requirements and noise that might be introduced by other returns, which often represent hits on other seedling parts other than the apex, such as branches and other lower surfaces. The 2017-point cloud served as the reference dataset while the 2022-point cloud served as the compared dataset.

The products produced by the cloud-to-cloud tool included x , y , and z cloud distances (change or differences) which were output as a scalar factor on the compared point cloud i.e. the 2022-point cloud for this study. The z -change or height change scalar field were then isolated and converted into a gridded product of 60 cm pixel size using the LASgrid tool in LAStools. LASgrid

was adopted for this approach to ensure that the actual point cloud height change values were maintained, instead of the LAS2dem tool, which would distort these values by triangulating them to produce a raster. The geolocated seedling points, assuming they fall right on top of the seedling apex, were then applied to extract the individual seedling change using the Extract Multi Values to Point tool in ArcGIS Pro. No cutoff or threshold was applied to this approach to minimize the effect of overhanging canopy or adjacent forest branches due to its reliance on the principle of nearest neighbour. The assumption is that understory seedlings' apexes would match between both study years since they are closer, rather than matching with the overhanging canopy or branches of larger trees, which in most instances would be further away.

3.5.3 *Point Cloud (Point Metrics) Image Differencing (PC_{PM})*

A 60 cm buffer was created around each geolocated seedling point to create a cylindrical buffer around each seedling. Following the approach of Chen et al. (2017), point cloud change detection was also carried out by extracting the max, average, 40th, 50th, 60th, 70th, 80th, 90th, and 99th percentiles of each seedling using the LAScanopy tool in LAStools. Since the highest field-measured seedling height over the five-year monitoring horizon was 410 cm and the documented relative Z shift between the two LiDAR datasets was 6.1 cm, a height threshold of 450 cm was applied to the PC_{PM} approach to seedling change detection. My assumption was that this threshold would be capable of capturing the full height of the seedlings of interest while excluding most overhanging canopies and branches of the adjacent forest and larger trees. The percentile metrics were extracted for both study years (2017 and 2022) for each unique seedling. For each metric and for each unique seedling, R statistical software was used to subtract the derived height metric (z value) for each seedling between both study years in order to obtain seedling height changes

between 2017 and 2022. Preliminary analysis is carried out on all the metrics to test and determine the most accurate, which is then adopted as the PC_{PM} approach for this study.

3.6 Regression-Based Bias Adjustments

In order to minimize the systematic bias that could arise between ALS-detected seedling height change and the observed field change, I constructed regression models to predict seedling height change from ALS height change. I used the quantile regression model equation (Equation 5) to derive predicted seedling height change, within which systematic bias would be significantly reduced.

$$Q_Y(\tau | X) = \beta_0(\tau) + \beta_1(\tau)X \quad (5)$$

Where $Q_Y(\tau | X)$ represents the predicted seedling height change at the median quantile ($\tau = 0.5$), X is the ALS-detected seedling height change between 2017 and 2022, Y is the observed field change, and β_0 and β_1 are the estimated intercept and slope for the quantile regression model. The quantile regression models was also adopted because it is capable of making predictions without assuming the normality or constant of variance (Cade & Noon, 2003). Since the main goal of this regression model was to reduce systematic underestimation bias, this justifies the adoption of this model to predict seedling height change.

3.7 Assessing Ecosite Influence on Change Detection Accuracy

Of the 9 field plots adopted in this study, 2 were found within wetland/transitional ecosite types, comprising 54 reference seedlings, while 7 were found within upland ecosite types, comprising 140 reference seedlings. The predicted seedling height change results of the best

approach are separated based on ecosite type and accuracy statistics are derived to determine how ecosite type influences the accuracy of seedling height change results between 2017 and 2022. This objective assumes that the comparatively higher presence of overhanging canopy and adjacent forest branches across seismic lines in upland sites would negatively impact the accuracy of predicted seedling height change results obtained from these sites as compared to wetland sites.

3.8 Non-Parametric Accuracy Assessment and Tests of Difference

For all 194 seedlings employed in this study, I compared the field-derived seedling height changes to the LiDAR-predicted seedling height change results between 2017 and 2022 using three approaches: (i) Raster, (ii) PC_{CC}, and (iii) PC_{PM}. Four accuracy metrics were used to measure the differences in each pair of data sets: (i) root mean square error (RMSE), (ii) median absolute error (MEDAE), (iii) mean absolute error (MAE), and (iv) bias. MEDAE was selected to assess how effectively the change detection approaches are predicting seedling height change between 2017 and 2022 while accounting for the presence of outliers. MEDAE is robust to outliers (Castilla et al., 2020) which justifies its inclusion in this study. In order to determine the approach that performs best considering all the metrics considered, the total ranking of accuracy metrics of each approach was deduced.

RMSE was obtained by summing the individual squared differences between observed (y_i) and predicted (\hat{y}_i) seedling height change values and dividing this by n which is the total number of seedlings for which change was assessed. The square root of this yields the RMSE as shown in Equation (6) below:

$$\text{RMSE} = \sqrt{\frac{\sum_{i=1}^n (y_i - \hat{y}_i)^2}{n}} \quad (6)$$

MEDAE was calculated by finding the median of the sum of the absolute differences between observed (y_i) and predicted (\hat{y}_i) seedling height change values for a total n number of seedlings (Equation (7))

$$\text{MEDAE} = \text{median} (\sum_{i=1}^n |y_i - \hat{y}_i|) \quad (7)$$

MAE was derived from summing the absolute differences between observed (y_i) and predicted (\hat{y}_i) seedling height change values to obtain the total error and then dividing the total error by n (total number of seedlings) (Equation (8)).

$$\text{MAE} = \frac{\sum_{i=1}^n |y_i - \hat{y}_i|}{n} \quad (8)$$

Bias was defined as the average error or deviation of the predicted seedling change (\hat{y}_i) from the observed seedling change (y_i) (Equation (9)). It is the measure that portrays whether predictions from a model are underestimating or overestimating the observed values.

$$\text{Bias} = \frac{\sum_{i=1}^n y_i - \hat{y}_i}{n} \quad (9)$$

Non-parametric test of difference was carried out to determine if there was a significant difference between the MEDAE of the best change detection approach and other approaches. Even though several accuracy metrics were considered, the test of difference was applied only to MEDAE since it is robust to outliers and can be tested for significance. This was also applied to test if there was a statistically significant difference between MEDAE of predicted ALS seedling height change between 2017 and 2022 in upland and wetland ecosite types. A Wilcoxon signed rank or paired test is carried out to test if the MEDAE of the best change detection approach is significantly different (lesser or greater) than the MEDAE of other approaches. Since the validation

seedlings being compared are independent of each other within ecosite types, the two-sampled Wilcoxon rank-sum test (Wilcoxon, 1992) is carried out to test if the MEDAE of the best approach is significantly smaller or different from the MEDAE of other approaches:

$$H_0: \text{MEDAE}_{\text{best}} = \text{MEDAE}_{\text{others}}$$

$$H_A: \text{MEDAE}_{\text{best}} < \text{MEDAE}_{\text{others}}$$

These accuracy metrics are calculated and derived in R Studio. The two-sample Wilcoxon rank-sum test is carried out with the `Wilcox.Test` Function of the Stats R Package (R Core Team, 2019). The test was carried out at a confidence level of 95% (alpha value = 0.05).

3.9 Assessing Seedling Height Change Across the Study Site

Prior to mapping seedling height change across my study site, I evaluated how ecosite type (upland and wetland) affected the accuracy of the best-performing seedling height change detection approach on seismic lines. In order to map the change in height of conifer seedlings along seismic lines within my study area between the years 2017 and 2022, I needed the accurate location of the seismic lines in my study area, as well as the location of the conifer seedlings growing on seismic lines. I used the Forest Line Mapper (FLM): a tool developed by the Applied Geospatial Research Group for the purpose of mapping and attributing linear footprints in forests (Queiroz et al., 2020) to create line and polygon-based representations of all the seismic lines in my study area. Input for the FLM tool includes linear footprint information, obtained from the ABMI, and rasterized CHMs derived from the 2022 ALS point cloud. The footprints and centerlines were then divided into 50-meter or less segments using the `Generate Points Along Lines` and `Split Line at`

Point tools in ArcGIS Pro. I did this to depict the mean conifer seedling height change between 2017 and 2022 at 50-meter or less increments.

Each individual conifer seedling growing on seismic lines across the study area was detected using a RT-DETR (Real-Time Detection Transformer) deep learning model from Ultralytics. The model was trained on 4-band red-green-blue near infrared (RGB-NIR) orthophotos with a spatial resolution of 4–6 cm, acquired over a large region within the Cold Lake area which is about 120 km south-east of the study area in 2024. Validation of results against geolocated conifer seedlings in the field from the same area yielded a mean average precision of 0.865, indicating strong detection performance. The trained model was then applied to my study area using RGB-NIR optical imagery from 2017. To refine results, overlapping predictions were filtered using an Intersection over Union (IoU) threshold of 50%, ensuring spatially distinct seedling detections. The IoU threshold is defined as the threshold within a precision bounding box used to determine if a prediction is correct. A 5-meter seedling height threshold was applied to predicted conifer seedlings across linear footprints within the study area. This threshold was applied with the intention of excluding larger saplings or trees. The deep learning detections also had a confidence field ranging between 0 and 1, which defines how reliably they can be classified as true seedlings, with 1 being the most reliable. A threshold of 0.5 was applied which brought the total conifer seedlings identified along seismic lines within the study area to 8,489. Since the approach in identifying these seedlings relied heavily on high-resolution airborne orthophotos, I assumed that this approach would not be able to capture all seedlings, especially those falling below overhanging canopy.

The best change detection approach was applied to map conifer seedling height change between 2017 and 2022 for all 8,489 seedlings detected on all of the seismic lines within the study

area. A unique ID was assigned to each individual conifer seedling to be able to apply the best change detection method on each unique seedling for both study years. The predicted change represents the height change of each unique seedling between 2017 and 2022, which was then applied to the seedling polygons and colour-coded into a change map. The mean predicted height changes of conifer seedlings between 2017 and 2022 within each 50-meter segment was calculated, attributed to that segment, and colour-coded. Growth thresholds or cutoffs were selected based on the relative vertical (z) shift between the ALS datasets adopted for this study, the field validation data adopted for this study from Shellian et al. (2024), as well as the findings reported in that study. Height changes equal to and below 0.06 meters representing the relative vertical (z) shift between both datasets, including areas of vegetation loss (negative change), were classified as Minimal or No Growth areas. To further classify height changes into moderate and high growth classes, the growth rates reported by Shellian et al. (2024) were consulted. Over the studied 5-year growth period, Shellian et al. (2024) reported that black spruce seedlings of average initial height (i.e. 50 cm) exhibited growth rates of 20.2 cm (± 1.4) and 25.4 cm (± 3.8) in poor and rich fens, respectively. The rates, however, could reach on average 28.4 cm (± 1.5) and 46.3 cm (± 3.7) in poor and rich fens respectively across areas where growth was higher due to restoration site-preparation treatments (i.e. on artificially created mounds). Tamarack seedlings on the other hand showed average growth rates of 34.7 cm (± 4.2) and 51.6 cm (± 6.3) in poor and rich fens, respectively. These rates were able to reach an average of 45.7 cm (± 3.8) and 67.2 cm (± 7.7) in poor and rich fens respectively, across sites that were equally treated with site preparation (i.e. on artificially created mounds). Poor fens and black spruce were both reported to be more common across the project area from which validation data were collected (Shellian et al., 2024) and were therefore used to guide the growth threshold between moderate and high change, as guided by the

comparison between untreated and treated sites. However, since Shellian et al (2024) only focused on wetlands, I assessed the growth rate of black spruce seedlings within upland sites in my study area across treated and untreated sites. Growth rates of black spruce within upland sites in my study area recorded an average growth of 23.84 cm (± 1.71) in treated sites and 18.0 cm (± 1.72) in untreated sites. Although slightly lower, the average growth for black spruce in upland sites were still close to the black spruce growth rates reported by Shellian et al. (2024), which were 20.2 cm (± 1.4) and 25.4 cm (± 3.8) in poor and rich fens, respectively in untreated sites. An approximate threshold of 30 cm was adopted to classify change falling above 0.06 meters but below and equal to 30 cm as Moderate Growth areas the study site. All change values above 30 cm were classified as High Growth areas or seedlings. The change results were created to provide forest managers or stakeholders with information describing how different stretches of seismic lines are recovering and identifying those areas that might require additional restoration efforts.

Chapter Four: Results

4.1 Accuracy of ALS Point Cloud and Raster-Based Predictions of Seedling Height Change Between 2017 and 2022

Table 4.1 summarizes the mean changes and accuracy statistics of ALS-predicted seedling height change between 2017 and 2022, as estimated by the three change detection approaches across all 194 sample seedlings. The ranked sum of all the accuracy metrics considered suggests that the PC_{PM} was the best-performing strategy. PC_{PM} recorded the lowest RMSE (25.70 cm), MAE (15.05 cm), and Bias (5.60 cm) while recording the second lowest MEDAE (8.53 cm) after the Raster approach (8.35 cm). The RMSEs for PC_{CC} and Raster approaches were 31.33 cm and 35.24 cm, respectively; the MAEs were 17.42 cm and 18.04 cm, respectively; and MEDAEs were 8.87 cm and 8.35 cm, respectively. Based on the Wilcoxon paired or signed rank test, it was determined that the p-value derived for the best approach (PC_{PM}) against the PC_{CC} approach was higher than the alpha value of 0.05, while that of the Raster approach was lower than the alpha value (Appendix D). This suggested that the MEDAE of PC_{PM} was significantly different from the MEDAE of the Raster approach but was no significantly different from the PC_{CC} approach.

Between 2017 and 2022, the mean field-measured height change across all seedlings was 34.92 cm, while the mean ALS-predicted change for all three approaches, PC_{CC}, PC_{PM}, and Raster, was 26.38 cm, 29.32 cm and 23.73 cm, respectively.

Of all the metrics considered, the 60th percentile point metric produced the most accurate change results for the PC_{PM} approach. The raster approach on the other hand, performed best when the 40th percentile cutoff threshold was applied to minimize errors caused by overhanging canopy.

My results suggest that using point clouds as the unit of analysis provides a more accurate seedling height change than rasters. In addition, ALS point cloud change detection carried out with ALS point cloud height metrics (PC_{PM}) detects seedling height change better than ALS point cloud change detection carried out in Cloud Compare for the study period between 2017 and 2022.

Table 4.1: RMSE, MAE, MEDAE, bias, and ranks of ALS predicted seedling height change for the three change detection approaches after systematic bias correction is applied. An asterisk by the MEDAE indicates that, according to the Wilcoxon paired or signed rank test, the MEDAE results from that approach is significantly different from the PC_{PM} approach at a confidence level of 95%

Rank	Change Detection Approach	N	Mean Field Height Change (cm)	Mean Predicted Height Change (cm)	RMSE (cm)	MAE (cm)	MEDAE (cm)	Bias (cm)
2	PC _{CC}	194	34.92	26.38	31.33	17.42	8.87	-8.53
1	PC _{PM}	194	34.92	29.32	25.70	15.05	8.53	5.60
3	Raster	194	34.92	23.73	35.24	18.04	8.35*	11.19

4.2 Ecosite Influence on the Accuracy of the Best-Performing Change Detection

Approach

Table 4.2 summarizes the accuracy statistics, including mean observed and predicted seedling height changes, for the best change detection approach (PC_{PM}) applied in both wetland and upland sites within the study area. The PC_{PM} approach, which is the best-performing change detection approach in this study, predicted seedling height change more accurately in upland sites than in wetland sites. All the accuracy statistics within wetland sites were higher than upland sites, suggesting lower model performance within wetland sites in predicting seedling height change for the study period. The RMSEs for seedlings across upland and wetland ecosite types were 20.55

cm and 35.74 cm, respectively; the MAEs were 11.27 cm and 24.83 cm, respectively; and MEDAEs were 7.03 cm and 16.37 cm, respectively. The MEDAE of the upland site was statistically lower than that of the wetland site per the two-sample Wilcoxon rank-sum test (Appendix D, $p < 0.05$).

Across both site types, seedling height change was underpredicted by a bias of 0.07 cm across upland sites and 19.93 cm across wetland sites. The mean field or observed height change across upland and wetland sites was 24.71 cm and 61.37 cm, respectively, suggesting higher seedling height change observed in wetland sites as compared to upland sites. The mean predicted seedling height change for the best approach (PC_{PM}) within upland sites was 24.65 cm, and 41.44 cm for wetland sites for the study period between 2017 and 2022.

Table 4.2: RMSE, MAE, MEDAE, and bias of predicted seedling height change by ecosite type. An asterisk by the MEDAE indicates that, according to the Wilcoxon independent or rank sum test, the MEDAE results from that ecosite type is significantly greater at a confidence level of 95%

Ecosite Type	N	Mean Field Height Change (cm)	Mean Predicted Height Change (cm)	RMSE (cm)	MAE (cm)	MEDAE (cm)	Bias (cm)
Upland	140	24.71	24.65	20.55	11.27	7.03	0.07
Wetland	54	61.37	41.44	35.74	24.83	16.37*	19.93

4.3 Conifer Seedling Height Change Across the Study Area

A map of ALS-predicted conifer seedling height change across all seismic lines within the study area between 2017 and 2022 is presented in Figure 4.1. This map showcases the aggregated ALS-predicted conifer seedling height change pattern within the 50-meter seismic line segments classified by the mean of individual ALS-predicted conifer seedling height changes within those segments between 2017 and 2022 (Figure 4.1.i). The localized ALS-predicted conifer seedling

change pattern within the insets also highlights the zoomed-in 50-meter seismic line segment mean ALS-predicted conifer seedling height change (Figure 4.1.ii) and the corresponding ALS-predicted conifer seedling height change of individual seedlings extracted within the seismic lines between 2017 and 2022 (Figure 4.1.iii).

Table 4.4 summarises the approximate length (km) of seismic lines within each growth or conifer seedling height change classification, continuous change ranges, and ecosite type. The 5-year study period revealed that 33.24 kilometres of the seismic lines present across the entire study site, were in a state of Minimal or No Growth for conifer seedlings. 4.21 kilometres of these lines were in a state of Moderate Growth, while 3.65 kilometres were in a state of High Growth for conifer seedlings. Most of the seismic lines classified as being in Minimal or No growth state were found within wetland ecosite type (18.18 km) as compared to upland sites (15.06 km). Moderate growth state mostly occurred in wetland sites (3.20 km) as compared to upland sites (1.01 km). 1.55 km of high growth seismic lines were found within upland sites as compared to 2.10 km found within the wetland ecosite types.

Table 4.3: Length (km) of seismic lines in different recovery classes (No/Minimal, Moderate, High) across upland and wetland/transitional ecosite types within the study area.

Change Classification	Continuous Change Range (m)	Upland	Wetland	Total
Minimal or No Growth	≤ 0.06 m	15.06 km	18.18 km	33.24 km
Moderate Growth	0.06 m > and ≤ 0.30 m	1.01 km	3.20 km	4.21 km
High Growth	> 0.30 m	1.55 km	2.10 km	3.65 km
Total		17.62 km	23.48 km	

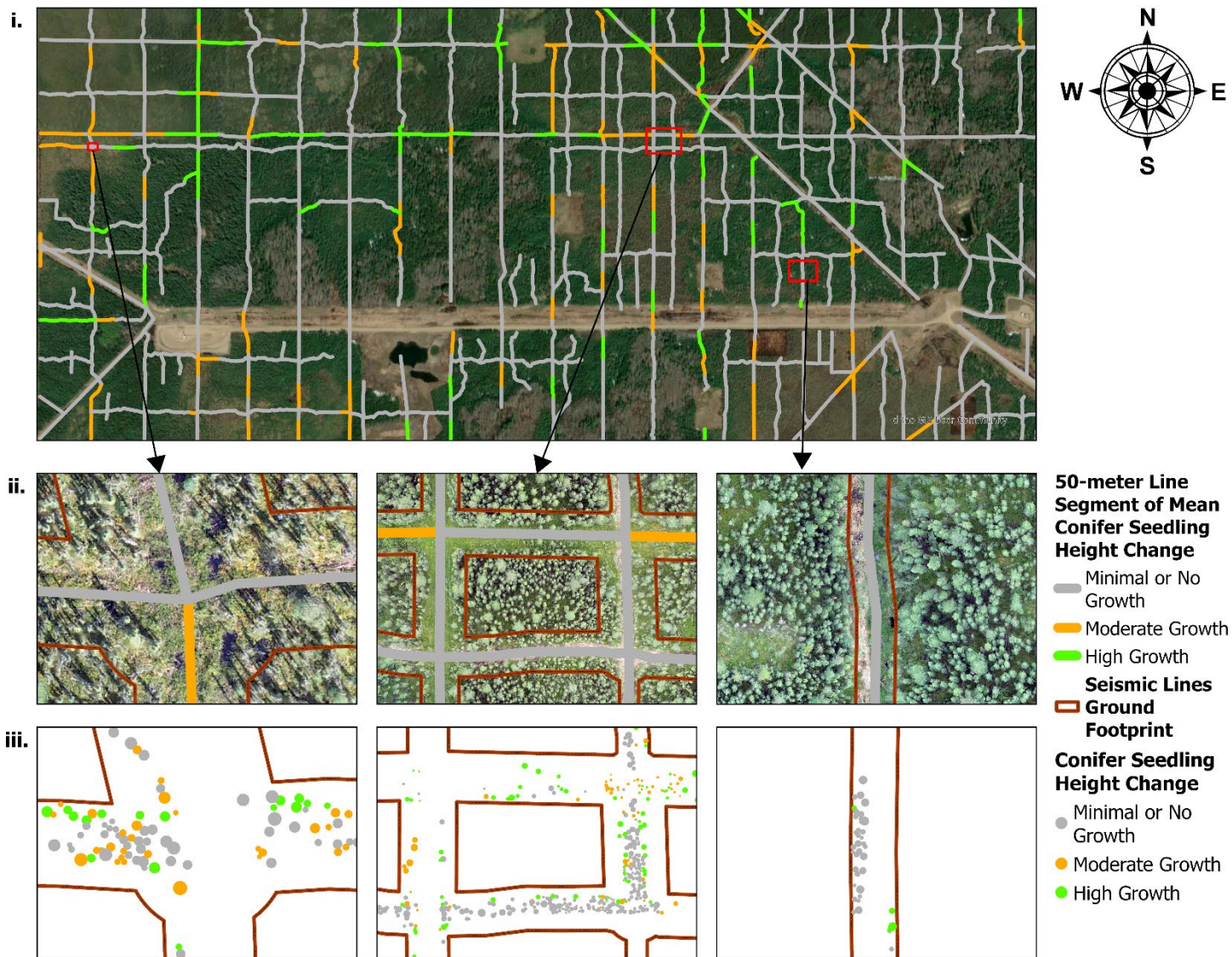


Figure 4.1: Conifer seedling height changes along seismic lines within the study area between 2017 and 2022. The top panel: (i) displays 50-meter seismic line segments classified by mean conifer seedling height change. The insets below the main map show zoomed-in areas highlighting: (ii) a closer view of the 50-meter square mean conifer seedling height change segments within the seismic line ground footprints (middle row); and (iii) individual conifer seedlings' height change values extracted within the seismic lines (bottom row). These illustrations present both aggregated and localized patterns of conifer seedling height change along seismic lines within the study area.

Chapter Five: Discussion

5.1 Point Clouds Provide Better Estimates of Seedling Height Change

My results suggested that the ALS point cloud approaches produced better predicted seedling height change results than the raster approach. This can be attributed to the point cloud model working directly on point cloud data, which preserves the full and actual vertical height profile of the seedling. In contrast, the raster-based approach interpolates these measurements, where actual seedling height metrics could be distorted or generalized. Of the two point-cloud-based approaches, PC_{PM} obtained the highest ranking per the accuracy parameters considered, with the lowest RMSE (25.70 cm), MAE (15.05 cm), and bias (5.60 cm) while recording the second lowest MEDAE (8.53 cm). The robustness of the PC_{PM} approach in smoothing out and excluding noise, such as overhanging canopies and branches of taller trees, when mid-percentile metrics were adopted, contributed to it performing better than other approaches. Also, the isolation of each seedling point cloud in a 60 cm cylindrical buffer ensured that much of the surrounding noise that could have negatively impacted change results was excluded, as compared to the other methods, where change was applied on the entire dataset. This is consistent with the findings of Castilla et al. (2020) who reported that the adoption of a narrow cylinder design in extracting point cloud information helps reduce the effect of neighbouring tall shrubs and adjacent mature trees which could lead to overestimation errors.

The 60th percentile performed best with the PC_{PM} approach. This was not expected, as I assumed the maximum or higher percentiles (90th and 99th) seedling height readings should have accounted for the most accurate seedling height change. The superior performance of the 60th percentile as compared to other metrics is because, apart from being able to minimize noise from

overhanging canopy, adjacent forest and vegetation, it mostly fell within or represented the mid-section of the seedling. The mid-section is where most of the ALS returns within the individual seedlings' point cloud profile occurred as is highlighted in Figure 5.1. ALS pulses can miss the apex of seedlings as reported by Castilla et al. (2020). As a result of this, higher percentiles are typically represented by few or in some cases no returns within the seedlings point cloud, as these percentiles most likely occur around the apex. The mid-range percentiles, including the 60th percentile, on the other hand, are mostly captured by several returns within the seedling point cloud profile (Figure 5.1). For this reason, the 60th percentile was more robust in capturing seedling height change, particularly in cases where seedlings' apexes were missed in one study year and captured in the other or vice versa. Such conditions suggested that seedling height was either overestimated or underestimated in one or both study years, which also subsequently led to the underestimation or overestimation of seedling height change in higher percentiles. Mid-percentiles (60th percentile), on the other hand, which were mostly represented by several returns within the seedling profile, meant they could reliably compare seedling mid-heights for both years, resulting in improved seedling height change detection within my study area. The adoption of the 60th percentile as the best percentile for reporting seedling height change along seismic lines is a unique finding of this study. Most earlier studies that reported on ALS vegetation change detection and extracting static vegetation height have adopted the maximum height or upper percentiles to characterize vegetation height. Based on the literature reviewed for this study, studies that have applied ALS data to report seedling height change along seismic lines or linear disturbances are limited. This suggests limited guidance or information on the optimal percentile for reporting seedling height change along linear disturbances such as seismic lines while accounting for the complexities of such environments, including overhanging canopy and adjacent forest.

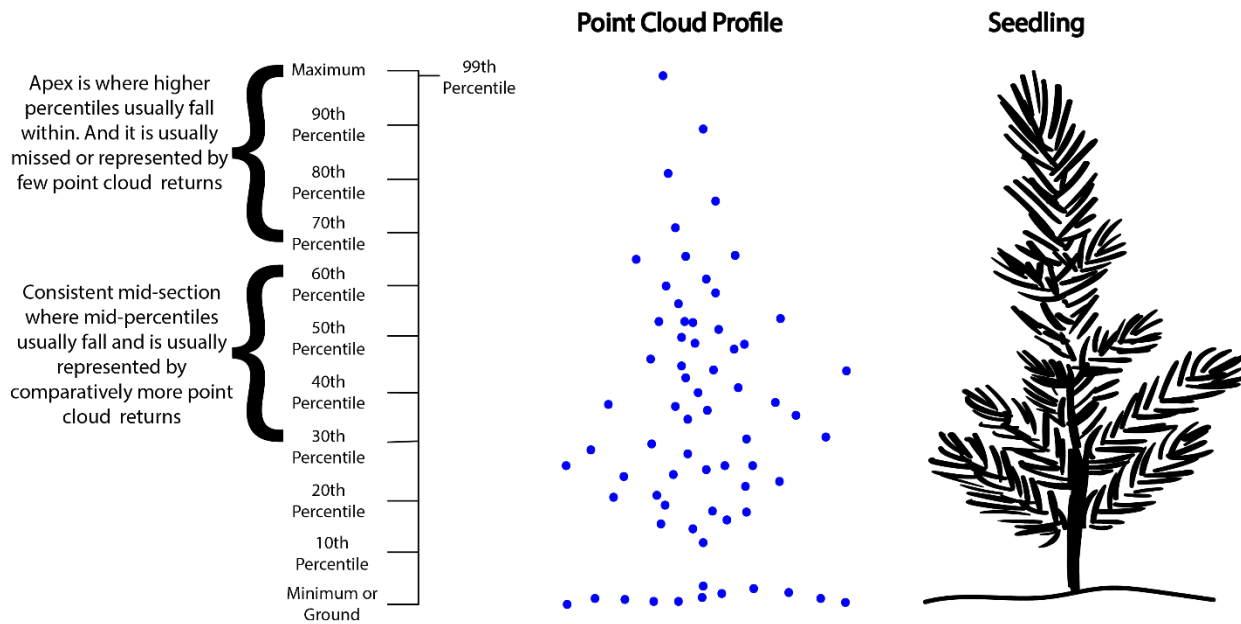


Figure 5.1: An illustration of a seedling and its corresponding point cloud return profile highlighting upper percentiles which are usually missed or represented by few returns and the mid section which comparatively is represented by more points making it more stable for seedling change detection across my study area.

The PC_{CC} approach had the second-best RMSE (31.33 cm), MAE (17.42 cm) and bias (-8.53 cm) while recording the highest MEDAE (8.87 cm) recorded among all approaches adopted. Overall, the PC_{CC} approach performed less accurately than the PC_{PM} approach due to the absence of the isolation of seedlings from the surrounding noise, as is present in the PC_{PM} approach. This made this approach more susceptible to noise as compared to the PC_{PM} approach.

The raster-based approach demonstrated the lowest performance, primarily due to the smoothing or interpolation effect in the rasterization process as compared to other approaches which relied directly on the point cloud. This can be attributed to the conversion of point cloud into two-dimensional raster pixels, which reduces the structural complexity contained in the actual point cloud vertical profile that can be leveraged to capture the seedlings that usually fall in the understory. This aligns with findings by Vepakomma et al. (2008), who reported that the

rasterization of point clouds introduces a certain amount of error based on the transformation method adopted, primarily due to the modification and in some cases generalization of the attributes of the raw point cloud into a single pixel value. By comparing field-surveyed elevations to interpolated ALS elevation values, Hodgson & Bresnahan (2004) also reported that interpolation accounted for errors ranging between -12.9 cm to +12.8 cm.

5.1.1 Sources of Errors in ALS Seedling Height Change Estimates

I constructed scatterplots comparing ALS-detected seedling height change prior to systematic bias correction and field-measured height change across my five-year monitoring horizon for each of the three processing approaches I tested to explore the various types of errors that each method is subject to. For comparative purposes, I also presented scatterplots of ALS-predicted seedling height change after systematic bias correction and field-measured height change across my study area. Figure 5.1 summarizes the ALS-detected and predicted seedling height change results for the three approaches adopted in this study and highlights the distinct error patterns that occur across the ALS-detected seedling height changes. Seedlings that exhibited these types of errors are colour-coded, including overhanging canopy or adjacent forest errors highlighted as yellow data points, data loss errors due to thresholds set represented by orange data points as well as other sources of errors represented by green data points. Regular or non-outlier observations are also presented as blue data points.

All three approaches that I tested overestimated and underestimated change at varying degrees, primarily due to the errors that had varying influence on the accuracy metrics. The presence of overhanging canopy or adjacent forest noise in one or both years of study, despite the thresholds set to minimize their effect on the change results, accounted for the very high negative

and positive outliers highlighted as yellow data points in Figure 5.1 (Top Row). Despite the occurrence of high negative and positive outliers, an underestimation bias was recorded in instances where the positive residuals outweighed the negative residuals and vice versa, when an overestimation bias was recorded. Even though the overhanging canopy and adjacent forest thresholds were generally effective across the entire study site, they failed to adequately tackle this issue in certain areas, highlighting the need for a relative or ecosite-specific threshold being applied to tackle it. The PC_{CC} approach recorded the lowest number of errors of this kind (Figure 5.1(b)) as compared to other approaches, primarily due to its reliance on the nearest neighbour principle rather than a threshold applied across the entire study area. The nearest neighbour principle ensured that despite the presence of overhanging canopy, the seedling apexes of the two study years were compared because they were closer to each other rather than the overhanging canopy, which was in most cases, further away. However, this was not always effective as in some instances, overhanging canopy change was recorded over the understory seedling change due to the gridding applied to the PC_{CC} change product during the extraction of seedling height change results for this approach. Also, other instances had the seedling apex visibly present in 2017; however, not present in 2022, possibly due to the overhanging canopy restricting returns from the understory. Hence, change was applied based on the 2017 seedling apex and the 2022 overhanging canopy.

Even though the adoption of a lower percentile height metric (60th percentile) across all seedlings and the canopy thresholds might have contributed to the overall performance of the PC_{PM} approach, it also contributed to the loss of some seedling height data. Seedlings that recorded this type of error are represented by orange data points across the ALS-predicted against field seedling height change scatter plots for the various approaches (Figure 5.1 (Top Row)). All seedlings that passed as this error type either underestimated or overestimated change as can be seen in Figure

5.1 (Top Row). This error can be especially realized with some seedlings that performed better in some percentile metrics or thresholds, and worse in others, subsequently leading to the underestimation of change among those seedlings. This also led to some negative change recordings among some of the seedlings because height data loss caused the 2022 seedling height reading to fall below the 2017 height reading. Also, the PC_{CC} approach relied on just the first returns of the seedling point cloud in order to reduce noise and computational time. This implied that some seedlings were not represented by the first returns or were represented by fewer first returns. This meant that there were instances where seedlings were not included or their heights were underestimated in the analysis. These specifically contributed to the loss of some seedling data or height profile, and in some cases, the entire returns of understory seedlings.

Other sources of errors represented by green data points in Figure 5.1 (Top Row) existed, which included unexplained disturbances in the field that affected the point cloud returns within the study period, clustered seedlings that influenced how well seedling apexes matched each other, among others. Clustered seedlings included small seedlings as well as large seedlings that were very close to each other and impacted the change results of at least one of the seedlings. Also, the nearest neighbour principle negatively impacted the accuracy of seedling height change in some cases for the PC_{CC} approach. This occurred with seedlings that had their 2017 apex closer to the lower parts of the 2022 seedling point cloud than to the 2022 actual seedling apex. The orientation of the seedling point cloud between datasets of both study years caused seedling apexes from one study year to appear closer to other points, other than the seedling apex of the corresponding study year. These errors accounted for some negative changes recorded, thereby impacting the accuracy of seedling height change recorded. Also, the gridding instead of interpolation of the change point cloud into a raster format for the purpose of preserving, integrating and extracting height change

result for each individual seedling led to some no data points (represented by 0) for the PC_{CC} approach. This was because the gridding approach did not adopt the normal point cloud interpolating approach that avoided “pits” as suggested by Khosravipour et al. (2014). These errors also included unexplained factors that led to the reduction in seedling heights or, in some cases, the complete loss of seedlings after field data collection and before ALS surveys.

In order to minimize the effects of the extreme errors of outliers as well as systematic bias in our change model, the median quantile regression model was adopted. This is presented in Figure 5.1 (Bottom Row) as the corresponding ALS-predicted seedling height change scatter plots for each approach. The reduction of the bias, together with the improvements in the other accuracy metrics, is reflected in the shift in data points closer to the 1:1 line. The median quantile regression provides a robust representation of the central tendency of my data, especially due to the presence of large errors where median has proven superior to the mean (Koenker, 2005), and offers predicted seedling height change that aligns closely with observed field change.

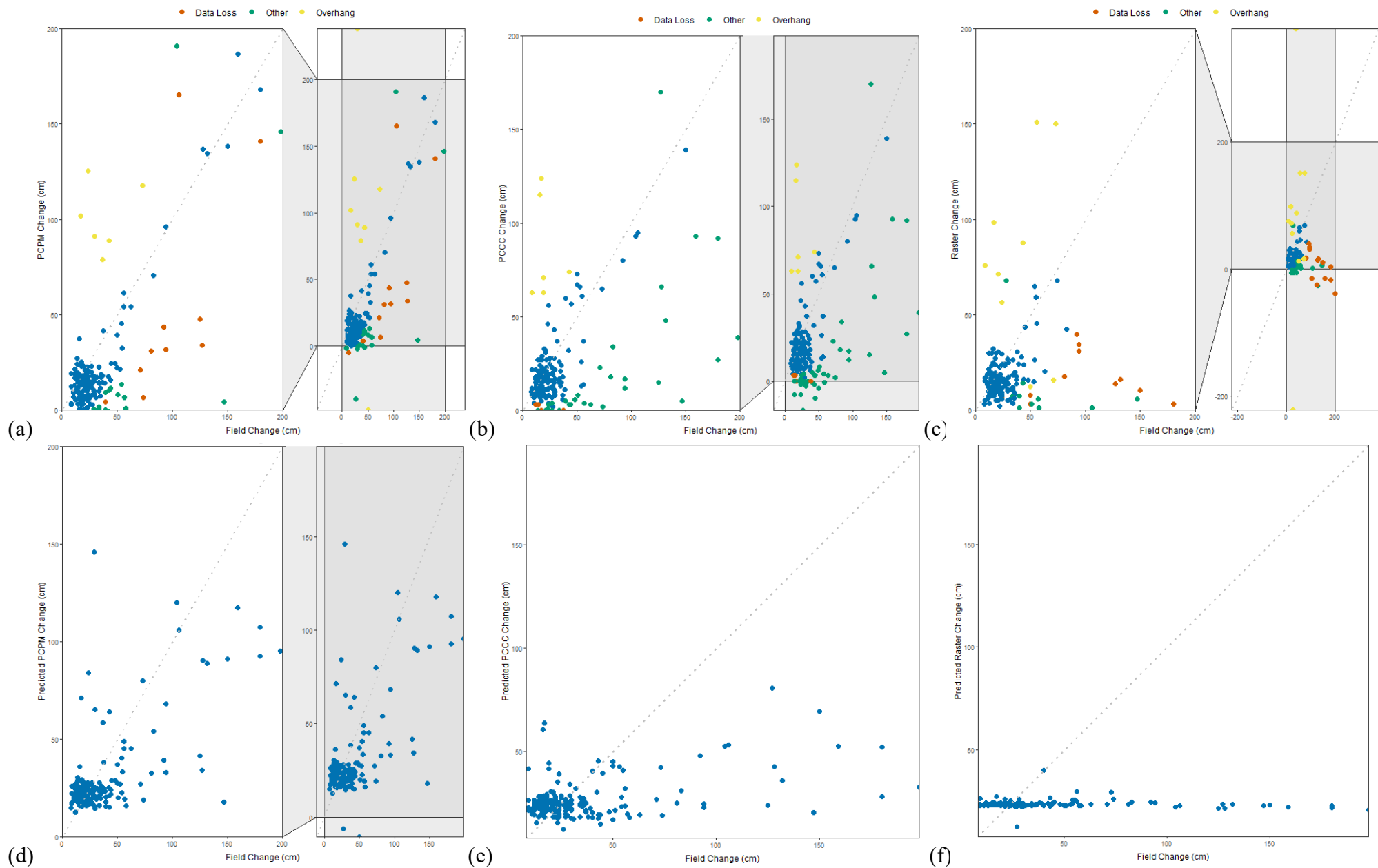


Figure 5.2: Scatterplots showing ALS-detected seedling height change (Top Row) and predicted seedling height change (Bottom Row) against Field-Observed seedling height change for all three approaches. (a) ALS-Detected PC_{PM} Change (b) ALS-Detected PC_{CC} Change (c) ALS-Detected Raster Change (d) Predicted PC_{PM} Change (e) Predicted PC_{CC} Change (f) Predicted Raster Change. Outlier errors are highlighted in orange (Data Loss), yellow (Overhanging Canopies and Adjacent Forest), and green (Other Errors), while seedlings with non-extreme errors are shown in blue.

Several other factors also contributed to the reduced accuracy observed across all three seedling-height change detection approaches applied over the study period between 2017 and 2022. These errors include those that arose from ALS acquisition and processing workflow approaches that overall influenced how well the seedling height change was captured and estimated.

The relatively low or moderate point density (29.2 – 37.2 points/m²) of ALS point cloud data for both study years (2017 and 2022) likely contributed to the low accuracy in predicting vegetation height change, even with the best-performing PC_{PM} approach. The relatively low or moderate point density suggests a moderate chance of the seedling apex being hit and captured by laser pulses at the time of surveys. This is likely translated into seedling apices being missed by the laser sensor, especially those of small, clustered or understory seedlings, which may have resulted in an underestimation of change. This aligns with findings by Castilla et al. (2020), who noted that the apex of low-lying or small vegetation may sometimes fail to generate an ALS data point, which translates into an underestimation of seedling height.

Horizontal and vertical mismatches between datasets from both time periods and seedling locations introduced some overestimation and underestimation errors. Misalignment between some seedling apices which represent the highest height of the seedling between both study years in the DSMs and point clouds datasets led to some underestimation or overestimation of change. To add to this, a misalignment between the various height change products of the three approaches and the seedling point shapefile accounted for the capturing of underestimated or overestimated change signals rather than the actual change signal at the seedling apex. This further reduced the

relationship between observed and predicted seedling height change for the study period between 2017 and 2022.

5.1.2 Comparison with Other Studies

In this study, I applied two point-cloud-based and one raster-based method to estimate conifer seedling height change along seismic lines within my study area between 2017 and 2022. Most previous studies that have utilized ALS data to characterize vegetation change have done so using raster pixels as the unit of analysis (Boehm et al., 2013; Chasmer et al., 2021; Madsen et al., 2020; Marinelli et al., 2022; Song et al., 2016; Szostak & Pająk, 2023; Yu et al., 2024). These studies have tended to estimate vegetation change at the plot or stand level or in close proximity to linear disturbances like seismic lines (Chasmer et al. 2021). Chasmer et al. (2021) found that variability in the rates of vegetation change within wetlands in close proximity to seismic lines or other linear disturbances is affected by a variety of cumulative and proximal environmental drivers. Yu et al. (2024) applied rasterized CHM products of bi-temporal ALS data to monitor forest growth in the boreal forest and recorded an RMSE of 0.86 meters, which was higher than all the RMSEs recorded for all approaches in my study, including the raster-based approach which performed the poorest. Only one study (Finnegan et al., 2019) was found to have examined vegetation growth or change along linear disturbances using ALS data. My models outperformed Finnegan et al. (2019), who detected change with lesser accuracy, with detected changes deviating by ± 2.32 meters from field measurements. In this study, I applied point clouds and raster pixels as units of analysis for detecting seedling height change along seismic lines while conducting a comparison of ALS seedling height change estimates and field height change measurements of both approaches. To my knowledge, my study is the first demonstration of mapping and testing how the unit of analysis impacts conifer seedling height changes along seismic lines in the boreal forest using ALS data.

In this respect, this current study is unique. Despite my study focusing specifically on seedling height change along seismic lines, seedling height provides an important context for situating my findings since it directly underpins how seedling height change is detected in this study. Many earlier studies have employed ALS data to characterize vegetation height in forests (Castilla et al., 2020; Chen et al., 2017; Sparks et al., 2022). My findings concur with Sparks et al. (2022) that non-raster-based individual tree detection methods that operate directly on the ALS point cloud may be better suited for detecting vegetation height in denser forest conditions as compared to raster-based methods, especially for seedlings obscured by overhanging vegetation. Castilla et al. (2020) also highlighted how the heights of small seedlings (≤ 30 cm) could be unreliable in point clouds due to the presence of adjacent low vegetation, which might affect how well the seedling height is captured. They also emphasized how location error was expected in some cases to shift coordinates from their true geographic location because of complexities within the point cloud acquisition processes.

Despite the overall effectiveness of thresholds set to minimize the effect of overhanging canopy or occlusion across the entire study site, future research would do well to investigate how thresholds can be set in relation to microsite conditions in order to minimize their effect and avoid data loss. These findings also suggest the need for higher point density ALS data that appropriately capture seedling apices, and more accurate data alignment approaches that minimize the errors introduced in the change detection process.

5.2 Seedling Height Change Detection Works Better in Upland Ecosite Types

The results of this study revealed that seedling height change predicted within upland areas yielded more accurate results with lower bias (0.07 cm), RMSE (20.55 cm), MEDAE (7.03 cm), and MAE (11.27 cm) as compared to wetland sites which recorded bias (19.93 cm), RMSE (35.74 cm), MEDAE (16.37 cm), and MAE (24.83 cm).

This was not expected, as upland areas have higher canopy cover present as compared to wetland areas (Harper et al., 2021) which was expected to introduce more errors. However, the poorer performance in wetland sites could be attributed to the blanket threshold applied across the entire study area. An assessment of each individual seedling occurring across both ecosite types revealed that seedlings in wetland sites recorded most of the data loss outlier errors (8 out of 54 seedlings) as compared to upland sites (3 out of 140 seedlings). Other outlier errors, such as overhanging canopy and adjacent forest branches, were few in wetland sites. This suggests that with overhanging canopy not being prominent in wetland sites, the adoption of a lower percentile across the entire study site had an adverse impact on seedlings within wetland sites, leading to data loss while having a positive impact in upland sites, where it helped to minimize the effect of overhanging canopy and adjacent forest branches. This is depicted in the relatively higher underestimation bias in wetland sites (19.93 cm) as compared to upland sites (0.07 cm).

Additionally, one of the two wetland plots was identified to be in an advanced stage of regeneration with most of the seedlings being close to each other. This led to seedling clusters and overlapping of the 60 cm cylindrical buffers for these seedlings, subsequently introducing noise in the change detected across this plot.

Also, seedlings sampled within my study area were taller in wetland sites as compared to upland sites, as is depicted in Table 5.1. The 2017 mean seedling heights recorded in the field were 30.3 cm in upland sites and 80.5 cm in wetland sites. In 2022, the mean seedling heights recorded in the field were 55.01 cm in upland sites and 141.87 cm in wetland sites. This suggested that the adoption of lower percentiles might have had a more adverse effect on the taller seedlings in wetland sites as compared to upland sites. These findings suggest the need for ecosite-specific seedling height growth assessment strategies

Table 5.1: Field-measured and ALS-detected mean seedling heights for both study years (2017 and 2022) by ecosite type.

Ecosite Type	2017 Field Mean Seedling Height	2017 ALS Mean Seedling Height	2022 Field Mean Seedling Height	2022 ALS Mean Seedling Height
Upland	30.3 cm	23.34 cm	55.01 cm	38.25 cm
Wetland	80.5 cm	58.67 cm	141.87 cm	129.69 cm

5.3 Patterns of Seedling Height Change Across the Study Area

The total length of seismic lines with no or minimal mean conifer seedling height change or growth within my study site between 2017 and 2022 was 33.24 kilometers. This was followed by moderate and high mean conifer seedling height change occurring across 4.21 and 3.65 kilometers of seismic lines, respectively. These estimates suggest that close to 80% of the total seismic lines in my study area (41.1 km) were in a state of minimal or no growth based on conifer seedlings accessed across these lines between 2017 and 2022.

Previous studies have reported on how most seismic lines remain in a state of arrested succession or slow growth several years after they were initially created (Lee and Boutin, 2006; van Rensen et al. 2015). My study complements these studies by illustrating how a larger

proportion of seismic lines within my study area remain in a state of minimal or no recovery, assessing conifer seedling height change between 2017 and 2022.

The framework characterizes the current state of seismic lines by assessing indicators, including seedling density, height and survival. While these indicators are important for informing whether recovery targets are being met, they only provide a static snapshot of the state of the line. This means that lines that might be naturally and rapidly recovering could be classified as not meeting establishment targets. This could suggest a management decision being applied on the site that could cause further disturbance to the site that is on its way to meeting targets. Assessing growth as has been demonstrated in this study provides an extra and dynamic indicator that could support forest managers in applying the framework to also distinguish between lines that are below static targets but actively improving as well as those that meet targets but are growing unusually slow. This extra information including annual growth rates would assist forest managers to make more informed decisions about active restoration efforts and prioritizing management actions.

5.4 Assumptions and Limitations

I assumed that the ALS datasets from both study years as well as seedling location measurements, were spatially accurate and adequately coregistered with my ground observations. Both point cloud datasets for both study years recorded horizontal RMSEs ranging from 30 cm to 35 cm. This could have affected the spatial alignment between the same seedlings across the two study years. Additionally, ALS data collection occurred during two different periods under varying conditions, which may have introduced further discrepancies. Differences in acquisition platforms, parameters, and collection times could have resulted in slight shifts or inconsistencies between the

two datasets, which could affect the accuracy of change detected. The average relative vertical shift between both datasets was recorded to be 6.1 cm while the average relative horizontal shifts were recorded to be 8.5 cm (X) and 21.2 cm (Y). This suggested some degree of vertical and horizontal misalignment which could have contributed to errors that affected change results. Collectively, these vertical and horizontal shifts between both datasets as well as between both datasets and seedling location measurements, could have contributed to some misalignments which subsequently impacted seedling change detection results recorded.

I also assumed that the location of seedlings in my reference dataset was correct. While RTK measurements of seedling locations were taken at relatively high accuracies (1.5 cm vertical accuracy and 0.8 cm horizontal accuracy), the presence of overhanging canopy may have introduced significant errors by blocking the RTK's communication with satellites. RTK GNSS survey relies on good communication between base station, the rover and satellites, which is best achieved with clear sky conditions and fewer obstacles blocking signals. This implies that signal blockage could have caused seedling positional inaccuracies or location errors.

I assumed the seedling height measurements obtained in the field by counting and measuring seedling whorls accurately represented actual seedling heights used for validating change results from this study. However, several factors may have contributed to errors in these field measurements. These could include human errors introduced during the reading and recording of these measurements in the field, as well as errors emanating from the limited accuracy of measuring instruments. Since field measurements from which the observed change was derived for this study were taken in the summer of 2021, this meant that seedling growth that occurred from the spring to the summer of 2022, when the ALS survey was carried out, was excluded from

the final observed seedling height change results. This possibly contributed to the overestimated change recorded among some of the predicted seedling height change results.

I also assumed that ALS-detected seedling heights accurately captured the true heights of seedlings standing up from the ground. However, an assessment of the correlation between observed seedling heights and predicted seedling height revealed that ALS data underpredicted and overpredicted seedling heights for both study years (Figure 5.3). There is an obvious spread of taller seedlings which suggests high variability in predicting taller seedling height but a more general underestimation of predicting smaller seedling heights. This could possibly be attributed to inadequacy of the point cloud in capturing the seedling leader or apex especially for smaller seedlings, thereby leading to an underestimation of seedling height. This translates into how well seedling height change was predicted in the study area between 2017 and 2022.

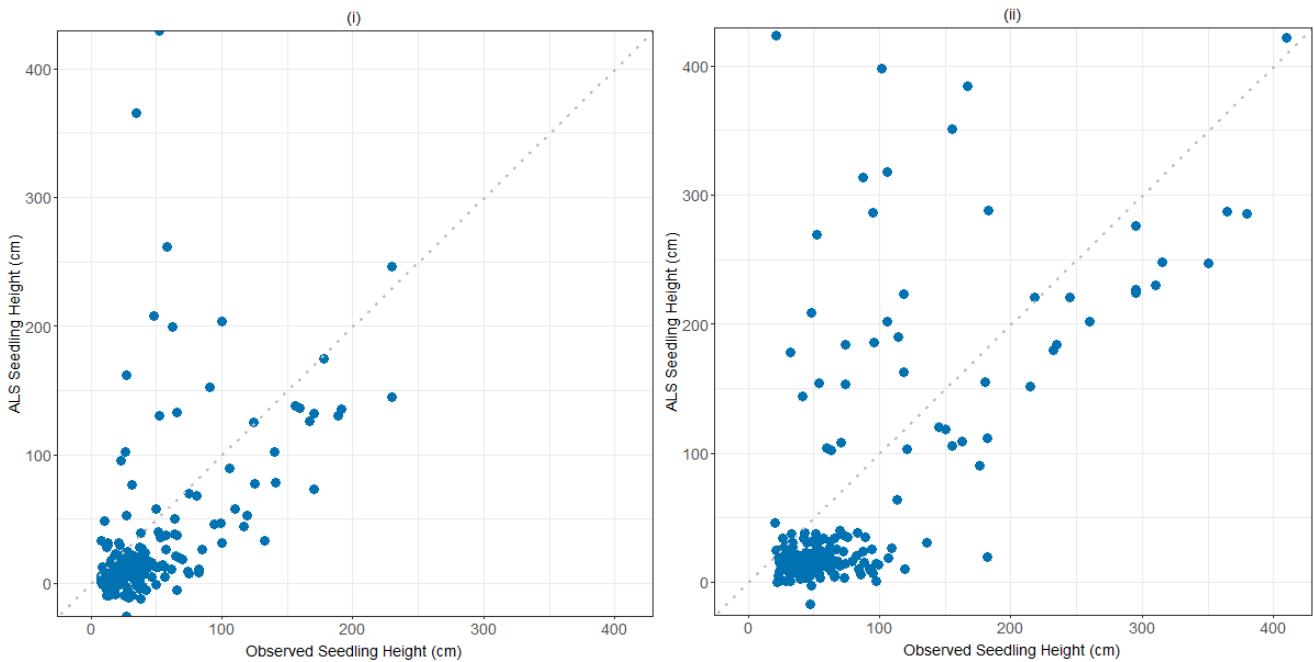


Figure 5.3: Observed versus ALS detected seedling heights for i) 2017 dataset and ii) 2022 dataset

Also, I assumed that the three change detection approaches (PC_{CC} , PC_{PM} , Raster) were capable of accurately predicting seedling change. All three approaches are based on image differencing change detection, hence requiring that seedlings correspond and are subtracted across both study years. This suggests that all three approaches were prone to positional inaccuracies discussed earlier as well as other limitations that may influence the accuracy of results obtained. The PC_{CC} approach adopted only point cloud first returns and the nearest neighbour principle to identify and compare seedling apexes for change detection. Only the first returns were used in order to minimize noise and compare the true seedling apexes only as much as possible and reduce computational time. However, this might have led to loss of data or underestimation of seedling heights. For instance, areas where an overhanging canopy was prominent and understory seedlings were represented by second or subsequent returns meant that such understory seedlings were excluded from the dataset when they had to be included. Also, in relation to the nearest neighbour principle, this could have introduced some errors due to the presence of the lower part of the ‘compared’ seedling other than the apex, which were closer than the apex of actual or ‘reference’ seedlings in the compared dataset. PC_{PM} , on the other hand relies on metrics extracted directly from point cloud within a 60 cm buffer of seedling point coordinates or location to capture seedling metrics as much as possible. However, this could have led to overestimation or underestimation errors in instances where small seedlings occur in clusters leading to the inclusion of multiple seedlings under one seedling buffer. The interpolation of the highest return and maximum seedling height only for the raster-based approach suggests the failure to include height metrics of seedling falling under canopy present despite the threshold set. Collectively, all these suggest that all three approaches are prone to errors due to the structural complexity of the boreal forest canopy, which

potentially reduces the accuracy of seedling height change detected for the study period between 2017 and 2022.

5.5 Contributions and Study Significance

This study contributes to the field of ALS data, vegetation change detection, and ecological conservation in the boreal forest. The methods, results, and recommendations presented in this study offer valuable insights for ALS data users, highlighting the importance of considering important parameters such as the unit of analysis, point density, and canopy penetration when applying this data type for vegetation change detection. Furthermore, this study also depicts the potential of ALS data in capturing changes in vegetation across large areas of interest.

This study also contributes to seismic line restoration and habitat conservation efforts within the boreal forests of Canada. Monitoring the growth, recovery or regeneration status of vegetation or seedlings along these seismic lines is an important component of wildlife conservation, particularly for the woodland caribou whose habitat is significantly affected by seismic lines. Considering the extensive network of these seismic lines across the boreal forest of Canada and the challenges of traditional field assessment especially in remote and inaccessible areas, this research demonstrates the potential of ALS data as a reliable and cost-effective tool for mapping seedling height change or growth along linear disturbance over large areas.

Finally, this research contributes to the BERA (Boreal Ecosystem Recovery and Assessment) collaborative research project which has strategic priorities of assessing and monitoring recovery along linear disturbances in the boreal forest of Alberta. Building upon this study would prove the utility of ALS point cloud in detecting change across large areas.

Preliminary results of this study were presented at the Canadian Symposium on Remote Sensing (CSRS) entitled Exploring Past, Present, and Future, June 2024, in Halifax, Nova Scotia.

5.6 Implications for Operational Restoration

This study offers several important insights on how seedling recovery could be monitored and managed along seismic lines in the boreal forest of Alberta by forest managers, government agencies, policy makers, and other relevant stakeholders.

The PC_{PM}, being the most accurate approach in predicting seedling height change along seismic lines within my study site, highlights the value of adopting point cloud-based methods in predicting more accurate change in seedling height as compared to other methods, especially the raster-based method. The raster-based method, which is commonly used in most vegetation change detection studies, involves the interpolation of elevation values over a fixed grid, which may underreport or omit understory vegetation height metrics or seedling height changes. Point cloud approaches, on the other hand, utilize structural information from all canopy strata, making them more effective in detecting height changes in seedlings, which are mostly found understory. This finding is critical to restoration efforts as functional recovery along seismic lines is usually assessed based on understory recovery and not the overhanging canopy.

Furthermore, the finding that upland ecosite types produce more accurate seedling height change results as compared to wetland sites, despite greater canopy complexity, highlights the importance of site-specific seedling height growth assessment strategies. Forest and restoration managers could benefit from applying site-specific monitoring protocols to guide restoration decisions, planning, and evaluation.

This study also highlights the importance of improving ALS data acquisition and its utilization for effective restoration monitoring programs. There is a need for enhancing ALS data acquisition standards, such as point density and consistent flight parameters. It also highlights the need for consistent inter-year acquisition of ALS data alongside robust surveying strategies that would help align these datasets together. These are essential to minimize horizontal and vertical mismatches between datasets from different periods and improve periodic and long-term change monitoring.

Although all approaches underestimated and overestimated observed seedling height change, this study offers a scalable approach to mapping and identifying areas undergoing recovery and those undergoing arrested succession across large expanses. This makes it easier to prioritize restoration efforts and target resources to areas where active restoration efforts are actually needed. Also, it offers insights that would guide efforts to control human access to lines that are naturally recovering in order to avoid further disturbance.

Finally, this study offers an approach to monitor how active restoration treatments, including silvicultural treatments such as mounding and planting, are performing periodically to test their success rates across several site types. This would help inform future restoration decisions and needs to improve restoration outcomes.

5.7 Future Outlook

This study has successfully addressed its three main objectives and has also made contributions to the fields of remote sensing and ecological monitoring, and conservation.

However, several issues that are important but beyond the scope of this study require further research in the future, which I would address and recommend in this section.

To begin with, future research should explore how flight parameters such as point density, scan angle, flight altitude, and season of acquisition affect the accuracy of seedling change detection along seismic lines. It would be beneficial to analyze how these factors affect the accuracy of predicted seedling height change, and also how to minimize the errors they might be contributing. This study highlighted the need for higher point density, which would suggest a higher chance of capturing seedling apices, subsequently improving the accuracy in detecting seedling height change. Other factors which were not captured within this study but might have an effect on point density as well as the probability of capturing seedling apices, are the season of acquisition and flight altitude. It is expected that with more seedling foliage present in the summer as compared to the winter seasons, the chances of capturing seedling apices would be higher. On the other hand, a lower flight altitude would suggest higher point density. Future research should assess how these parameters could affect the accuracy of seedling height change detection along seismic lines.

Secondly, further research should also address multi-temporal ALS data alignment techniques. It would be valuable to assess ways of improving the vertical and horizontal alignment of ALS data acquired at different periods. This could include more robust ground control strategies, especially in dense canopy environments such as the boreal forest as well as advanced data coregistration algorithms.

Furthermore, future research should analyze how uncertainties or errors in individual factors such as ALS misalignment, RTK positions, and overhanging canopy, contribute to errors

in predicting seedling height change along seismic lines. It is important to assess how each of these factors individually propagates errors into the final results and also how to minimize each of them.

Chapter Six: Conclusion

The prevalence of seismic lines among other linear disturbances has fragmented the boreal forest of Alberta, thereby altering functional and ecological balance. These include the slow recovery or arrested tree regeneration along seismic lines (Dabros et al., 2018; Filicetti & Nielsen, 2020; van Rensen et al., 2015), the decline in the population of threatened species such as the woodland caribou (Environment and Climate Change Canada, 2020), among several other effects. To minimize these effects, forest managers and stakeholders require information to monitor regeneration along these seismic lines and to determine areas where resources need to be targeted for active restoration, as well as how well active restoration efforts are performing. Recent studies have highlighted the effectiveness of ALS data in characterizing vegetation change quickly and extensively than traditional field-based approaches by mostly adopting the approach of converting raw ALS point cloud into raster-based products, including Canopy Height Models (CHMs) and Digital Surface Models (DSMs). However, very little research has been done to test how the accuracy of seedling change detection results derived from raster-based data format vary from those obtained from point-cloud format. Similarly, very few studies have evaluated how well ALS can effectively map seedling change along seismic lines, considering the canopy and adjacent forest dynamics in different ecosites within the boreal forest.

The main goal of this study was to determine the best technical workflow for characterizing conifer seedling height change along seismic lines using ALS data. I wanted to know: could ALS point cloud data provide a more accurate means of detecting seedling height change along seismic lines than ALS raster products? Does ecosite type (upland and wetland) influence the accuracy of the best-performing change detection approach on seismic lines? Finally, to apply the best-performing change detection approach for mapping height change of conifer

seedlings across all seismic lines within the study area between 2017 and 2022. This was to provide a large-scale insight into seedling recovery patterns to support restoration and conservation efforts.

To address the first research question, I applied the image-differencing change-detection technique on two-point cloud-based approaches and one raster-based approach using ALS datasets obtained over the study area in 2017 and 2022. Percentile metrics (40th, 50th, 60th, 70th, 80th, 90th, 99th) were tested to minimize noise from overhanging canopy and branches of adjacent forest and larger trees as much as possible and determine the best percentile to capture understory change for the PC_{PM} approach. The PC_{CC} approach leveraged the nearest neighbour principle to help reduce the effect of overhanging canopy and adjacent forests on seedling height change results. Percentile thresholds (40th, 50th, 60th, 70th, 80th, 90th) were also tested to minimize noise from overhanging canopy and branches of adjacent forest and larger trees as much as possible for the raster-based approach. Based on 194 validation conifer seedlings, four accuracy metrics, and a sum ranking approach, I assessed, compared, and ranked the accuracies of the point cloud (PC_{PM}, PC_{CC}) and raster-based approaches to deduce which approach is more accurate at predicting conifer seedling height change. I found that the point cloud-based approaches performed better than the raster-based approach with PC_{PM} being the most accurate at the 60th percentile metric.

For the second objective, I separated wetland validation conifer seedlings from upland validation conifer seedlings and assessed the accuracy of the change detected based on the best approach (PC_{PM}). Even though I expected wetland conifer seedlings to perform better than upland conifer seedlings, upland conifer seedlings performed better across all accuracy statistics employed for this study.

Finally, the best approaches adopted in this study depicted the uncertainties and sources of errors that may arise when interpreting seedling height change along seismic lines. These conifer seedling height change estimates offer valuable insights into seedling growth across different site conditions and highlight the potential of ALS data in supporting restoration monitoring and conservation planning along seismic lines in the boreal forest.

This study has evaluated how the unit of analysis of ALS data products and ecosite types (upland and wetland) influence the accuracy of conifer seedling height change detected along seismic lines in the boreal forest. I found that point cloud products provided a more accurate means of detecting conifer seedling height change, despite certain errors as compared to raster products. PC_{PM} was reliably applied in the large-scale mapping of conifer seedling change along seismic lines in the study area. This highlights the potential of ALS point clouds to support efficient large-scale monitoring of regeneration along seismic lines in the boreal forest to further strengthen planning and restoration efforts.

References

- Afaq, Y., & Manocha, A. (2021). Analysis on change detection techniques for remote sensing applications: A review. In *ECOLOGICAL INFORMATICS* (Vol. 63). ELSEVIER. <https://doi.org/10.1016/j.ecoinf.2021.101310>
- Alberta Parks. (2015). Natural regions and subregions of Alberta. A framework for Alberta's Parks. Alberta Tourism. *Parks and Recreation: Edmonton, AB, Canada*.
- Aldred, A. H., & Bonnor, G. M. (1985). *Application of airborne lasers to forest surveys*. Patawa National Forestry Institut.
- An, Z., & Froese, R. E. (2023). Tree stem volume estimation from terrestrial LiDAR point cloud by unwrapping. *Canadian Journal of Forest Research*, 53(2), 60–70. <https://doi.org/10.1139/cjfr-2022-0153>
- Angelidis, I., Levin, G., Díaz-Varela, R. A., & Malinowski, R. (2017). Assessment of changes in formations of non-forest woody vegetation in southern Denmark based on airborne LiDAR. *Environmental Monitoring and Assessment*, 189(9), 437. <https://doi.org/10.1007/s10661-017-6119-8>
- Arnup, R. (2000). Minimizing soil disturbance in forestry operations: A practical field guide for resource managers and equipment operators in northeastern Ontario. *The Lake Abitibi Model Forest, Cochrane, Ont*.
- Arp, H., Griesbach, J., & Burns, J. (1982). MAPPING IN TROPICAL FORESTS - A NEW APPROACH USING THE LASER APR. *ASPRS Directory of the Mapping Sciences : 1989 Members, Sustaining Members, Products and Services.*, 48(1), 91–100.
- Arumäe, T., Lang, M., & Laarmann, D. (2020). Thinning- and tree-growth-caused changes in canopy cover and stand height and their estimation using low-density bitemporal airborne

- lidar measurements – a case study in hemi-boreal forests. *European Journal of Remote Sensing*, 53(1), 113–123. <https://doi.org/10.1080/22797254.2020.1734969>
- Beckingham, J. D., & Archibald, J. H. (1996). *Field guide to ecosites of Northern Alberta*. Northern Forestry Centre.
- Blaschke, T. (2005). Towards a framework for change detection based on image objects. *Göttinger Geographische Abhandlungen*, 113, 1–9.
- Blaschke, T., Hay, G. J., Kelly, M., Lang, S., Hofmann, P., Addink, E., Queiroz Feitosa, R., van der Meer, F., van der Werff, H., van Coillie, F., & Tiede, D. (2014). Geographic Object-Based Image Analysis – Towards a new paradigm. *ISPRS Journal of Photogrammetry and Remote Sensing*, 87, 180–191. <https://doi.org/10.1016/j.isprsjprs.2013.09.014>
- Bliss, L. C., & Wein, R. W. (1972). Plant community responses to disturbances in the western Canadian Arctic. *Canadian Journal of Botany*, 50(5), 1097–1109. <https://doi.org/10.1139/b72-136>
- Boehm, H.-D. V., Liesenberg, V., & Limin, S. H. (2013). Multi-Temporal Airborne LiDAR-Survey and Field Measurements of Tropical Peat Swamp Forest to Monitor Changes. *IEEE Journal of Selected Topics in Applied Earth Observations and Remote Sensing*, 6(3), 1524–1530. <https://doi.org/10.1109/JSTARS.2013.2258895>
- Braverman, M., & Quinton, W. L. (2016). Hydrological impacts of seismic lines in the wetland-dominated zone of thawing, discontinuous permafrost, Northwest Territories, Canada. *Hydrological Processes*, 30(15), 2617–2627. <https://doi.org/10.1002/hyp.10695>
- Cade, B. S., & Noon, B. R. (2003). A gentle introduction to quantile regression for ecologists. *Frontiers in Ecology and the Environment*, 1(8), 412–420. [https://doi.org/10.1890/1540-9295\(2003\)001%255B0412:AGITQR%255D2.0.CO;2](https://doi.org/10.1890/1540-9295(2003)001%255B0412:AGITQR%255D2.0.CO;2)

- Cao, L., Zhang, Z., Yun, T., Wang, G., Ruan, H., & She, G. (2019). Estimating Tree Volume Distributions in Subtropical Forests Using Airborne LiDAR Data. *Remote Sensing*, *11*(1), 97. <https://doi.org/10.3390/rs11010097>
- Castilla, G., Filiatrault, M., McDermid, G. J., & Gartrell, M. (2020). Estimating Individual Conifer Seedling Height Using Drone-Based Image Point Clouds. *Forests*, *11*(9), 924. <https://doi.org/10.3390/f11090924>
- Chasmer, L., Lima, E. M., Mahoney, C., Hopkinson, C., Montgomery, J., & Cobbaert, D. (2021). Shrub changes with proximity to anthropogenic disturbance in boreal wetlands determined using bi-temporal airborne lidar in the Oil Sands Region, Alberta Canada. *Science of The Total Environment*, *780*, 146638. <https://doi.org/10.1016/j.scitotenv.2021.146638>
- Chen, G., Hay, G. J., Carvalho, L. M. T., & Wulder, M. A. (2012). Object-based change detection. *International Journal of Remote Sensing*, *33*(14), 4434–4457. <https://doi.org/10.1080/01431161.2011.648285>
- Chen, S., McDermid, G. J., Castilla, G., & Linke, J. (2017). Measuring Vegetation Height in Linear Disturbances in the Boreal Forest with UAV Photogrammetry. *Remote Sensing*, *9*(12), 1257. <https://doi.org/10.3390/rs9121257>
- Christensen, T. R., Johansson, T., Åkerman, H. J., Mastepanov, M., Malmer, N., Friberg, T., Crill, P., & Svensson, B. H. (2004). Thawing sub-arctic permafrost: Effects on vegetation and methane emissions. *Geophysical Research Letters*, *31*(4). <https://doi.org/10.1029/2003GL018680>
- Cichowski, D., & Dzus, E. (2010). *Status of the Woodland Caribou (Rangifer tarandus caribou) in Alberta: Update 2010*. Alberta Sustainable Resource Development.

- Dabros, A. (2009). *Effects of simulated climate change on post-disturbance «Populus tremuloides-Picea mariana» ecosystems in northwestern Quebec.*
- Dabros, A., James Hammond, H. E., Pinzon, J., Pinno, B., & Langor, D. (2017). Edge influence of low-impact seismic lines for oil exploration on upland forest vegetation in northern Alberta (Canada). *Forest Ecology and Management*, 400, 278–288. <https://doi.org/10.1016/j.foreco.2017.06.030>
- Dabros, A., Pyper, M., & Castilla, G. (2018). Seismic lines in the boreal and arctic ecosystems of North America: Environmental impacts, challenges, and opportunities. *Environmental Reviews*, 26(2), 214–229. <https://doi.org/10.1139/er-2017-0080>
- D’Adamo, T. A., Phillips, T. G., & McAree, P. R. (2018). Registration of three-dimensional scanning LiDAR sensors: An evaluation of model-based and model-free methods. *Journal of Field Robotics*, 35(7), 1182–1200. <https://doi.org/10.1002/rob.21811>
- Davidson, S. J., Goud, E. M., Franklin, C., Nielsen, S. E., & Strack, M. (2020). Seismic Line Disturbance Alters Soil Physical and Chemical Properties Across Boreal Forest and Peatland Soils. *Frontiers in Earth Science*, 8. <https://doi.org/10.3389/feart.2020.00281>
- Davies, M. A., Davidson, S. J., Deane, P. J., Filicetti, A., Ketcheson, S., Korsah, P., Kleinke, K., Nielsen, S. E., Schmidt, M. A., Tabassum, N., Waddington, J. M., Weiland, L., Wilkinson, S., & Strack, M. (2025). A data compilation and synthesis of the impacts of seismic surveys on surface soil properties in boreal Alberta, Canada. *Canadian Journal of Forest Research*, 55, 1–18. <https://doi.org/10.1139/cjfr-2024-0240>
- Dickie, M., Serrouya, R., DeMars, C., Cranston, J., & Boutin, S. (2017). Evaluating functional recovery of habitat for threatened woodland caribou. *Ecosphere*, 8(9), e01936. <https://doi.org/10.1002/ecs2.1936>

- Dolan, K. A., Hurtt, G. C., Chambers, J. Q., Dubayah, R. O., Frohling, S., & Masek, J. G. (2011). Using ICESat's Geoscience Laser Altimeter System (GLAS) to assess large-scale forest disturbance caused by hurricane Katrina. *Remote Sensing of Environment*, 115(1), 86–96. <https://doi.org/10.1016/j.rse.2010.08.007>
- Dong, P., & Chen, Q. (2018). *LiDAR Remote Sensing and Applications* (1st ed., Vol. 1). CRC Press.
- Ehlers, M., Sofina, N., Filippovska, Y., & Kada, M. (2014). Automated techniques for change detection using combined edge segment texture analysis, GIS, and 3D information. *Global Urban Monitoring and Assessment: Through Earth Observation*.
- Environment and Climate Change Canada. (2020). *Amended recovery strategy for the Woodland Caribou (Rangifer tarandus caribou), Boreal population, in Canada*. Government of Canada = Gouvernement du Canada.
- Fatemi, N. (2019). Questions of Concern in Drawing Up a Remote Sensing Change Detection Plan. *Journal of the Indian Society of Remote Sensing*, 47(9), 1455–1469. <https://doi.org/10.1007/s12524-019-00997-5>
- Ferraz, A., Saatchi, S., Bormann, K. J., & Painter, T. H. (2018). FUSION OF MULTIPLE LOW-RESOLUTION NASA AIRBORNE SNOW OBSERVATORY (ASO) LIDAR DATA FOR FOREST VEGETATION STRUCTURE CHARACTERIZATION. In *IGARSS 2018—2018 IEEE INTERNATIONAL GEOSCIENCE AND REMOTE SENSING SYMPOSIUM* (pp. 7532–7535). IEEE.
- Filicetti, A. T., & Nielsen, S. E. (2020). Tree regeneration on industrial linear disturbances in treed peatlands is hastened by wildfire and delayed by loss of microtopography. *Canadian Journal of Forest Research*, 50(9), 936–945. <https://doi.org/10.1139/cjfr-2019-0451>

- Finnegan, L., Pigeon, K. E., Cranston, J., Hebblewhite, M., Musiani, M., Neufeld, L., Schmiegelow, F., Duval, J., & Stenhouse, G. B. (2018). Natural regeneration on seismic lines influences movement behaviour of wolves and grizzly bears. *PLOS ONE*, *13*(4), e0195480. <https://doi.org/10.1371/journal.pone.0195480>
- Finnegan, L., Pigeon, K. E., & MacNearney, D. (2019). Predicting patterns of vegetation recovery on seismic lines: Informing restoration based on understory species composition and growth. *Forest Ecology and Management*, *446*, 175–192. <https://doi.org/10.1016/j.foreco.2019.05.026>
- Fisher, J. T., Witkowski, E. T. F., Erasmus, B. F. N., Mograbi, P. J., Asner, G. P., van Aardt, J. A. N., Wessels, K. J., & Mathieu, R. (2015). What lies beneath: Detecting sub-canopy changes in savanna woodlands using a three-dimensional classification method. In *APPLIED VEGETATION SCIENCE* (Vol. 18, Issue 3, pp. 528–540). WILEY. <https://doi.org/10.1111/avsc.12160>
- Frew, M. S., Evans, D. L., Londo, H. A., Cooke, W. H., & Irby, D. (2016). Measuring Douglas-Fir Crown Growth with Multitemporal LiDAR. In *FOREST SCIENCE* (Vol. 62, Issue 2, pp. 200–212). OXFORD UNIV PRESS INC. <https://doi.org/10.5849/forsci.14-062>
- Girardeau-Montaut, D., Roux, M., Marc, R., & Thibault, G. (2005). Change Detection on Points Cloud Data acquired with a Ground Laser Scanner. *International Archives of Photogrammetry. Remote Sensing*, *36*, 3/W19-30–25.
- Government of Alberta. (2017). *Restoration and Establishment Framework*. Prepared for Alberta Environment and Parks, Land and Environment Planning Branch.

- Hall, O., & Hay, G. J. (2003). A Multiscale Object-Specific Approach to Digital Change Detection. *International Journal of Applied Earth Observation and Geoinformation*, 4(4), 311–327. [https://doi.org/10.1016/S0303-2434\(03\)00010-2](https://doi.org/10.1016/S0303-2434(03)00010-2)
- Hanssen, F., Barton, D. N., Venter, Z. S., Nowell, M. S., & Cimburova, Z. (2021). Utilizing LiDAR data to map tree canopy for urban ecosystem extent and condition accounts in Oslo. In *ECOLOGICAL INDICATORS* (Vol. 130). ELSEVIER. <https://doi.org/10.1016/j.ecolind.2021.108007>
- Harper, K. A., Gray, L., & Dazé Querry, N. (2021). Spatial patterns of vegetation structure and structural diversity across edges between forested wetlands and upland forest in Atlantic Canada. *Canadian Journal of Forest Research*, 51(9), 1189–1198.
- Harris, L. I., Olefeldt, D., Pelletier, N., Blodau, C., Knorr, K.-H., Talbot, J., Heffernan, L., & Turetsky, M. (2023). Permafrost thaw causes large carbon loss in boreal peatlands while changes to peat quality are limited. *Global Change Biology*, 29(19), 5720–5735. <https://doi.org/10.1111/gcb.16894>
- Hodgson, M. E., & Bresnahan, P. (2004). Accuracy of Airborne Lidar-Derived Elevation. *Photogrammetric Engineering & Remote Sensing*, 70(3), 331–339. <https://doi.org/10.14358/PERS.70.3.331>
- Huang, J., Wan, Y., & Shen, S. (2009). An Object-Based Approach for Forest-Cover Change Detection using Multi-Temporal High-Resolution Remote Sensing Data. *2009 International Conference on Environmental Science and Information Application Technology*, 1, 481–484. <https://doi.org/10.1109/ESIAT.2009.163>
- Hussain, M., Chen, D., Cheng, A., Wei, H., & Stanley, D. (2013). Change detection from remotely sensed images: From pixel-based to object-based approaches. *ISPRS Journal of*

Photogrammetry and Remote Sensing, 80, 91–106.
<https://doi.org/10.1016/j.isprsjprs.2013.03.006>

Jones, E. A., Chasmer, L. E., Devito, K. J., & Hopkinson, C. D. (2024). Shortening fire return interval predisposes west-central Canadian boreal peatlands to more rapid vegetation growth and transition to forest cover. *Global Change Biology*, 30(2), e17185.
<https://doi.org/10.1111/gcb.17185>

Kershaw, J. A., Jr., Ducey, M. J., Beers, T. W., & Husch, B. (2016). *Forest Mensuration*. John Wiley & Sons, Incorporated. <http://ebookcentral.proquest.com/lib/ucalgary-ebooks/detail.action?docID=4731589>

Khosravipour, A., Skidmore, A. K., Isenburg, M., Wang, T., & Hussin, Y. A. (2014). Generating pit-free canopy height models from airborne lidar. *Photogrammetric Engineering & Remote Sensing*, 80(9), 863–872.

Koch, B., Kattenborn, T., Straub, C., & Vauhkonen, J. (2013). Segmentation of Forest to Tree Objects. In M. Maltamo, E. Næsset, & J. Vauhkonen (Eds.), *Forestry Applications of Airborne Laser Scanning: Concepts and Case Studies* (pp. 89–112). Springer Netherlands.
https://doi.org/10.1007/978-94-017-8663-8_5

Koenker, R. (2005). *Quantile regression* (Vol. 38). Cambridge university press.

Kurz, W. A., Shaw, C. H., Boisvenue, C., Stinson, G., Metsaranta, J., Leckie, D., Dyk, A., Smyth, C., & Neilson, E. T. (2013). Carbon in Canada's boreal forest—A synthesis. *Environmental Reviews*, 21(4), 260–292. <https://doi.org/10.1139/er-2013-0041>

Latham, A. D. M., Latham, M. C., Boyce, M. S., & Boutin, S. (2011). Movement responses by wolves to industrial linear features and their effect on woodland caribou in northeastern Alberta. *Ecological Applications*, 21(8), 2854–2865. <https://doi.org/10.1890/11-0666.1>

- Lim, K., Treitz, P., Wulder, M., St-Onge, B., & Flood, M. (2003). LiDAR remote sensing of forest structure. *Progress in Physical Geography: Earth and Environment*, 27(1), 88–106. <https://doi.org/10.1191/0309133303pp360ra>
- Linke, J., McDermid, G. J., Laskin, D. N., McLane, A. J., Pape, A., Cranston, J., Hall-Beyer, M., & Franklin, S. E. (2009). A Disturbance-Inventory Framework for Flexible and Reliable Landscape Monitoring. *Photogrammetric Engineering & Remote Sensing*, 75(8), 981–995. <https://doi.org/10.14358/PERS.75.8.981>
- Linke, J., McDermid, G. J., Shellian, C., Nielsen, S. E., Sutheimer, C., Ketcheson, S., & Bayne, E. (2022). *BERA Field Protocols: Site Assessment and Inventory for Linear Human Footprint Features in Alberta, Canada*.
- Loisel, J., Yu, Z., Beilman, D. W., Camill, P., Alm, J., Amesbury, M. J., Anderson, D., Andersson, S., Bochicchio, C., Barber, K., Belyea, L. R., Bunbury, J., Chambers, F. M., Charman, D. J., De Vleeschouwer, F., Fiałkiewicz-Kozieł, B., Finkelstein, S. A., Gałka, M., Garneau, M., ... Zhou, W. (2014). A database and synthesis of northern peatland soil properties and Holocene carbon and nitrogen accumulation. *The Holocene*, 24(9), 1028–1042. <https://doi.org/10.1177/0959683614538073>
- Lovell, J. L., Jupp, D. L. B., Newnham, G. J., Coops, N. C., & Culvenor, D. S. (2005). Simulation study for finding optimal lidar acquisition parameters for forest height retrieval. *Forest Ecology and Management*, 214(1), 398–412. <https://doi.org/10.1016/j.foreco.2004.07.077>
- Lu, D., Mausel, P., Brondízio, E., & Moran, E. (2004). Change detection techniques. *International Journal of Remote Sensing*, 25(12), 2365–2401. <https://doi.org/10.1080/0143116031000139863>

- Maclean, G. A., & Krabill, W. B. (1986). Gross-Merchantable Timber Volume Estimation Using an Airborne Lidar System. *Canadian Journal of Remote Sensing*, 12(1), 7–18. <https://doi.org/10.1080/07038992.1986.10855092>
- Madsen, B., Treier, U. A., Zlinszky, A., Lucieer, A., & Normand, S. (2020). Detecting shrub encroachment in seminatural grasslands using UAS LiDAR. In *ECOLOGY AND EVOLUTION* (Vol. 10, Issue 11, pp. 4876–4902). WILEY. <https://doi.org/10.1002/ece3.6240>
- Magnussen, S., Næsset, E., Gobakken, T., & Frazer, G. (2012). A fine-scale model for area-based predictions of tree-size-related attributes derived from LiDAR canopy heights. *Scandinavian Journal of Forest Research*, 27(3), 312–322. <https://doi.org/10.1080/02827581.2011.624116>
- Maltamo, M., Næsset, E., & Vauhkonen, J. (Eds.). (2014). *Forestry Applications of Airborne Laser Scanning: Concepts and Case Studies* (Vol. 27). Springer Netherlands. <https://doi.org/10.1007/978-94-017-8663-8>
- Marinelli, D., Coops, N. C., Bolton, D. K., & Bruzzone, L. (2022). Forest Change Detection in Lidar Data Based on Polar Change Vector Analysis. In *IEEE GEOSCIENCE AND REMOTE SENSING LETTERS* (Vol. 19). IEEE-INST ELECTRICAL ELECTRONICS ENGINEERS INC. <https://doi.org/10.1109/LGRS.2020.3022282>
- Marinelli, D., Paris, C., & Bruzzone, L. (2019). An Approach to Tree Detection Based on the Fusion of Multitemporal LiDAR Data. *IEEE Geoscience and Remote Sensing Letters*, 16(11), 1771–1775. <https://doi.org/10.1109/LGRS.2019.2908314>

- McGaughey, R. J., Carson, W. W., Reutebuch, S. E., & Andersen, H.-E. (2004). Direct measurement of individual tree characteristics from LIDAR data. *Proceedings of the Annual ASPRS Conference, 23*.
- McManamon, P. F. (2019). *LiDAR Technologies and Systems*. SPIE.
- Mielcarek, M., Kurpiewska, S., Guderski, K., Dobrowolska, D., Zin, E., Kuberski, Ł., Erfanifard, Y., & Stereńczak, K. (2025). Remote Sensing of Forest Gap Dynamics in the Białowieża Forest: Comparison of Multitemporal Airborne Laser Scanning and High-Resolution Aerial Imagery Point Clouds. *Remote Sensing, 17*(7), 1149. <https://doi.org/10.3390/rs17071149>
- Mitasova, H., Mitas, L., & Harmon, R. S. (2005). Simultaneous spline approximation and topographic analysis for lidar elevation data in open-source GIS. *IEEE Geoscience and Remote Sensing Letters, 2*(4), 375–379. <https://doi.org/10.1109/LGRS.2005.848533>
- Natural Regions Committee. (2006). *Natural regions and subregions of Alberta: Natural Regions Committee*. Government of Alberta.
- Nurminen, K., Karjalainen, M., Yu, X., Hyypä, J., & Honkavaara, E. (2013). Performance of dense digital surface models based on image matching in the estimation of plot-level forest variables. *ISPRS Journal of Photogrammetry and Remote Sensing, 83*, 104–115. <https://doi.org/10.1016/j.isprsjprs.2013.06.005>
- Page, D. (2025, March 27). *The evolution of seismic lines in Alberta and an overview of 2D, 3D, and 4D programs with their different line types*. BERA lunch-hour seminar 2024/25, Boreal Ecosystems Recovery and Assessment.

- Pasher, J., Seed, E., & Duffe, J. (2013). Development of boreal ecosystem anthropogenic disturbance layers for Canada based on 2008 to 2010 Landsat imagery. *Canadian Journal of Remote Sensing*, *39*(1), 42–58. <https://doi.org/10.5589/m13-007>
- Peng, X., Zhao, A., Chen, Y., Chen, Q., & Liu, H. (2021). Tree Height Measurements in Degraded Tropical Forests Based on UAV-LiDAR Data of Different Point Cloud Densities: A Case Study on *Dacrydium pierrei* in China. *Forests*, *12*(3), 328. <https://doi.org/10.3390/f12030328>
- Poorazimy, M., Ronoud, G., Yu, X., Luoma, V., Hyyppä, J., Saarinen, N., Kankare, V., & Vastaranta, M. (2022). Feasibility of Bi-Temporal Airborne Laser Scanning Data in Detecting Species-Specific Individual Tree Crown Growth of Boreal Forests. *Remote Sensing*, *14*(19). <https://doi.org/10.3390/rs14194845>
- Przewoźna, P., Hawryło, P., Zięba-Kulawik, K., Ingot, A., Mączka, K., Wężyk, P., & Matczak, P. (2021). Use of Bi-Temporal ALS Point Clouds for Tree Removal Detection on Private Property in Racibórz, Poland. *Remote Sensing*, *13*(4). <https://doi.org/10.3390/rs13040767>
- Qin, R., Tian, J., & Reinartz, P. (2016). 3D change detection—Approaches and applications. In *ISPRS JOURNAL OF PHOTOGRAMMETRY AND REMOTE SENSING* (Vol. 122, pp. 41–56). ELSEVIER. <https://doi.org/10.1016/j.isprsjprs.2016.09.013>
- Queiroz, G. L., McDermid, G. J., Rahman, M. M., & Linke, J. (2020). The Forest Line Mapper: A Semi-Automated Tool for Mapping Linear Disturbances in Forests. *Remote Sensing*, *12*(24), 4176. <https://doi.org/10.3390/rs12244176>
- Quinton, W. I., Hayashi, M., & Chasmer, L. e. (2011). Permafrost-thaw-induced land-cover change in the Canadian subarctic: Implications for water resources. *Hydrological Processes*, *25*(1), 152–158. <https://doi.org/10.1002/hyp.7894>

- R Core Team. (2019). *R* (Version 3.6.2) [Computer software].
<https://www.rdocumentation.org/packages/stats/versions/3.6.2/topics/wilcox.test>
- Ray, J. (2014). *Defining habitat restoration of boreal caribou: Discussion paper* [Program results;research]. <https://www.canada.ca/en/environment-climate-change/services/species-risk-public-registry/related-information/defining-habitat-restoration-boreal-caribou.html>
- Revel, R. D., Dougherty, T. D., & Downing, D. J. (1984). *Forest growth & revegetation along seismic lines*. University of Calgary Press.
- Shellian, C. A., Linke, J., McDermid, G. J., Cody, M., & Nielsen, S. E. (2024). Silviculture treatments hasten seedling growth on seismic disturbances in boreal treed fens. *Restoration Ecology*, 32(3), e14086. <https://doi.org/10.1111/rec.14086>
- Singh, A. (1989). Review Article Digital change detection techniques using remotely-sensed data. *International Journal of Remote Sensing*, 10(6), 989–1003. <https://doi.org/10.1080/01431168908903939>
- Song, Y., Imanishi, J., Sasaki, T., Ioki, K., & Morimoto, Y. (2016). Estimation of broad-leaved canopy growth in the urban forested area using multi-temporal airborne LiDAR datasets. *Urban Forestry & Urban Greening*, 16, 142–149. <https://doi.org/10.1016/j.ufug.2016.02.007>
- Spadavecchia, C., Belcore, E., Piras, M., & Kobal, M. (2022). An Automatic Individual Tree 3D Change Detection Method for Allometric Parameters Estimation in Mixed Uneven-Aged Forest Stands from ALS Data. *Remote Sensing*, 14(18), 4666. <https://doi.org/10.3390/rs14184666>

- Sparks, A. M., Corrao, M. V., & Smith, A. M. (2022). Cross-comparison of individual tree detection methods using low and high pulse density airborne laser scanning data. *Remote Sensing*, *14*(14), 3480.
- Stepper, C., Straub, C., & Pretzsch, H. (2015). Assessing height changes in a highly structured forest using regularly acquired aerial image data. *Forestry: An International Journal of Forest Research*, *88*(3), 304–316. <https://doi.org/10.1093/forestry/cpu050>
- Strack, M., Hayne, S., Lovitt, J., McDermid, G. J., Rahman, M. M., Saraswati, S., & Xu, B. (2019). Petroleum exploration increases methane emissions from northern peatlands. *Nature Communications*, *10*(1), 2804. <https://doi.org/10.1038/s41467-019-10762-4>
- Su, Y., Guo, Q., Collins, B. M., Fry, D. L., Hu, T., & Kelly, M. (2016). Forest fuel treatment detection using multi-temporal airborne lidar data and high-resolution aerial imagery: A case study in the Sierra Nevada Mountains, California. *International Journal of Remote Sensing*, *37*(14), 3322–3345. <https://doi.org/10.1080/01431161.2016.1196842>
- Sutheimer, C. M., Filicetti, A. T., Viliani, L., & Nielsen, S. E. (2024). Regeneration lags and growth trajectories influence passive seismic line recovery in western North American boreal forests. *Restoration Ecology*, *33*(3), e14353. <https://doi.org/10.1111/rec.14353>
- Szostak, M., & Pająk, M. (2023). LiDAR Point Clouds Usage for Mapping the Vegetation Cover of the “Fryderyk” Mine Repository. *Remote Sensing*, *15*(1), 201. <https://doi.org/10.3390/rs15010201>
- Tewkesbury, A. P., Comber, A. J., Tate, N. J., Lamb, A., & Fisher, P. F. (2015). A critical synthesis of remotely sensed optical image change detection techniques. In *REMOTE SENSING OF ENVIRONMENT* (Vol. 160, pp. 1–14). ELSEVIER SCIENCE INC. <https://doi.org/10.1016/j.rse.2015.01.006>

- Timoney, K., & Lee, P. (2001). Environmental management in resource-rich Alberta, Canada: First world jurisdiction, third world analogue? *Journal of Environmental Management*, 63(4), 387–405. <https://doi.org/10.1006/jema.2001.0487>
- Townshend, J. R. G., Justice, C. O., Gurney, C., & McManus, J. (1992). The impact of misregistration on change detection. *IEEE Transactions on Geoscience and Remote Sensing*, 30(5), 1054–1060. <https://doi.org/10.1109/36.175340>
- Tymińska-Czabańska, L., Hawryło, P., Janiec, P., & Socha, J. (2022). Tree height, growth rate and stand density determined by ALS drive probability of Scots pine mortality. *Ecological Indicators*, 145, 109643. <https://doi.org/10.1016/j.ecolind.2022.109643>
- United Nations Environment Programme. (2022). *Global Peatlands Assessment: The State of the World's Peatlands - Evidence for Action toward the Conservation, Restoration, and Sustainable Management of Peatlands*. <https://doi.org/10.59117/20.500.11822/41222>
- van Rensen, C. K., Nielsen, S. E., White, B., Vinge, T., & Lieffers, V. J. (2015). Natural regeneration of forest vegetation on legacy seismic lines in boreal habitats in Alberta's oil sands region. *Biological Conservation*, 184, 127–135. <https://doi.org/10.1016/j.biocon.2015.01.020>
- Vepakomma, U., St-Onge, B., & Kneeshaw, D. (2008). Spatially explicit characterization of boreal forest gap dynamics using multi-temporal lidar data. *Remote Sensing of Environment, Earth Observations for Terrestrial Biodiversity and Ecosystems Special Issue*, 112(5), 2326–2340. <https://doi.org/10.1016/j.rse.2007.10.001>
- Wang, C., & Glenn, N. F. (2009). Estimation of fire severity using pre- and post-fire LiDAR data in sagebrush steppe rangelands. *International Journal of Wildland Fire*, 18(7), 848–856. <https://doi.org/10.1071/WF08173>

- Wang, X., Liu, S., Du, P., Liang, H., Xia, J., & Li, Y. (2018). Object-Based Change Detection in Urban Areas from High Spatial Resolution Images Based on Multiple Features and Ensemble Learning. *Remote Sensing*, *10*(2), 276. <https://doi.org/10.3390/rs10020276>
- Weiland, L., Ketcheson, S., Strack, M., & McDermid, G. J. (2024). The Influence of Seismic Lines on Local Hydrology and Snow Accumulation in the Boreal Region of Northern Alberta. *Hydrological Processes*, *38*(12), e70032. <https://doi.org/10.1002/hyp.70032>
- White, J. C., Coops, N. C., Wulder, M. A., Vastaranta, M., Hilker, T., & Tompalski, P. (2016). Remote Sensing Technologies for Enhancing Forest Inventories: A Review. *Canadian Journal of Remote Sensing*, *42*(5), 619–641. <https://doi.org/10.1080/07038992.2016.1207484>
- Wilcoxon, F. (1992). Individual comparisons by ranking methods. In *Breakthroughs in statistics: Methodology and distribution* (pp. 196–202). Springer.
- Wolf, P. R., Dewitt, B. A., & Wilkinson, B. E. (2014). *Elements of Photogrammetry with Application in GIS*. McGraw-Hill.
- Yu, X., Hyypä, J., Kaartinen, H., & Maltamo, M. (2004). Automatic detection of harvested trees and determination of forest growth using airborne laser scanning. *Remote Sensing of Environment*, *90*(4), 451–462. <https://doi.org/10.1016/j.rse.2004.02.001>
- Yu, Z., Qi, J., Zhao, X., & Huang, H. (2024). Evaluating the reliability of bi-temporal canopy height model generated from airborne laser scanning for monitoring forest growth in boreal forest region. *International Journal of Digital Earth*, *17*(1), 2345725.
- Zhao, K., Suarez, J. C., Garcia, M., Hu, T., Wang, C., & Londo, A. (2018). Utility of multitemporal lidar for forest and carbon monitoring: Tree growth, biomass dynamics, and carbon flux.

In *REMOTE SENSING OF ENVIRONMENT* (Vol. 204, pp. 883–897). ELSEVIER SCIENCE INC. <https://doi.org/10.1016/j.rse.2017.09.007>

Zhou, X., Wang, W., Di, L., Lu, L., & Guo, L. (2020). Estimation of Tree Height by Combining Low Density Airborne LiDAR Data and Images Using the 3D Tree Model: A Case Study in a Subtropical Forest in China. *Forests*, *11*(12), 1252. <https://doi.org/10.3390/f11121252>

Zieba-Kulawik, K., & Wezyk, P. (2022). Monitoring 3D Changes in Urban Forests Using Landscape Metrics Analyses Based on Multi-Temporal Remote Sensing Data. In *LAND* (Vol. 11, Issue 6). MDPI. <https://doi.org/10.3390/land11060883>

APPENDIX A: Relative Shift Between Bitemporal Point Cloud

Table A 1 X, Y and Z Coordinates at the static point between 2017 and 2022 and their corresponding shifts (X shift, Y shift, Z shift). SP = Static Point

SPID	X_Cord (2017)	Y_Cord (2017)	Z_Cord (2017)	X_Cord (2022)	Y_Cord (2022)	Z_Cord (2022)	X_Shift (m)	Y_Shift (m)	Z_Shift (m)
SP01	493093.	613612	699.427	493093.	613612	699.440	-	0.10758	-
	875706	9.78830	9785	911382	9.68071	0024	0.03567		0.01202
	000020	000013		000020	999959		6		
	728	1130		240	6477				
SP02	495159.	613440	715.004	495159.	613440	715.090	-	-	-0.086
	444543	6.71085	0283	481513	6.81706	0269	0.03697	0.10622	
	000019	000038		999984	999987		1		
	621	1470		600	3638				
SP03	491213.	613595	707.294	491212.	613595	707.320	0.17476	-	-0.026
	059593	5.03732	0063	884827	5.37734	0073	6	0.34002	
	999991	000011		999980	000012				
	193	9507		189	2786				
SP04	496002.	613448	729.054	496002.	613448	729.070	0.12265	-	-
	956745	6.04153	0161	834091	6.36684	0073	4	0.32531	0.01599
	999981	999965		999975	999987				
	649	6379		499	4830				

SP05	489309.	613591	700.265	489309.	613591	700.429	0.05219	0.17499	-0.164
	576561	1.37418	9912	524369	1.54918	9927	2		
	999972	999988		999999	000008				
	910	5857		180	9109				
Absolute Mean Shifts							0.085	0.212	0.061

APPENDIX B: Accuracy Statistics for all ALS-Detected Change Results for All Point Cloud Point Metrics and Raster Threshold Metrics

Table B 1 Accuracy Statistics for Point Cloud Point Metrics in Detecting Seedling Height Change Across Study Site

Metrics	N	RMSE	Mean_Bias	MAE	MEDAE	Rank Sum	Rank
p40_pm_change	194	33.9977	14.5257	18.3051	10.2	15	2
p50_pm_change	194	34.8065	12.5927	19.7432	11.15	19	4
p60_pm_change	194	31.9157	9.8541	19.2716	11.55	13	1
p70_pm_change	194	33.3367	7.6252	20.6860	11.95	18	3
p80_pm_change	194	44.7970	6.0984	25.4128	13.9	22	5
p90_pm_change	194	60.8704	4.3644	31.5201	15.9	22	5
p99_pm_change	194	71.7136	4.9067	38.3623	18.25	26	7

Table B 2 Accuracy Statistics for Percentile Threshold Set in Detecting Raster Seedling Height Change Across Study Site

Cutoff Thresholds	N	RMSE	Mean_Bias	MAE	MEDAE	Rank Sum	Rank
change_40p_cm	194	54.4122	17.0357	27.8285	11.4995	7	1
change_50p_cm	194	112.4524	15.9134	39.8621	14.2015	11	3
change_60p_cm	194	96.9909	12.0051	39.7475	14.8526	9	2
change_70p_cm	194	171.8813	23.4983	54.7079	14.9986	18	5
change_80p_cm	194	195.6661	10.5555	65.9651	15.4506	17	4
change_90p_cm	194	186.3888	19.3271	66.1027	15.4506	22	6

APPENDIX C: Change Results for All Seedlings Across the Three Approaches

Table C 1 Seedling Height Change for All Three Approaches, Field Measurements and Predicted PC_{PM} Change

Uniq ueID	Be lt_ ID	Sd _S p	Ecosi te_Ty pe	2017_F ield_He ight	2022_F ield_He ight	Field _Cha nge	PC_C C_Cha nge	PC_P M_Ch ange	Raster _Cha nge	Predicted_ PCPM_Ch ange
440_ B1_1 156	44 0_ B1	Sb	Upla nd	20	41	21	16	13.4	9.997 56	22.586466 17
440_ B1_1 157	44 0_ B1	Sb	Upla nd	85	93	8	10	2.5	3.100 59	14.755221 39
440_ B1_1 537	44 0_ B1	Pj	Upla nd	14	40	26	16	15.8	16.29 64	24.310776 94
440_ B1_1 541	44 0_ B1	Sb	Upla nd	23	42	19	63	4.6	5.200 2	16.263993 32
440_ B1_1 550	44 0_ B1	Pj	Upla nd	18	38	20	8	15.6	15.89 97	24.167084 38
440_ B1_1 552	44 0_ B1	Sb	Upla nd	35	182	147	5	3.9	5.999 76	15.761069 34
440_ B1_1 556	44 0_ B1	Sb	Upla nd	57	74	17	124	2.2	98.30 32	14.539682 54
440_ B1_1 559	44 0_ B1	Sb	Upla nd	15	24	9	63	4.9	5.200 2	16.479532 16
440_ B1_1 566	44 0_ B1	Sb	Upla nd	11	23	12	15	10.8	9.899 9	20.718462 82
440_ B1_1 568	44 0_ B1	Sb	Upla nd	31	48	17	9	9.1	9.399 41	19.497076 02
440_ B1_1 569	44 0_ B1	Sb	Upla nd	37	62	25	25	4.7	14.90 48	16.335839 6
440_ B1_1 595	44 0_ B1	Sb	Upla nd	19	34	15	17	16.9	14.00 15	25.101086 05

440_B1_1620	44_0_B1	Sb	Upland	35	49	14	16	15.3	18.7988	23.95154553
440_B1_317	44_0_B1	Sb	Upland	12	29	17	9	13.8	13.0981	22.87385129
440_B1_322	44_0_B1	Sb	Upland	14	42	28	13	17.8	14.6973	25.74770259
440_B1_392	44_0_B1	Sb	Upland	43	66	23	18	16.8	8.89893	25.02923977
440_B1_394	44_0_B1	Sb	Upland	37	74	37	6	17.9	17.6025	25.81954887
440_B1_443	44_0_B1	Sb	Upland	37	65	28	16	20.4	15.6982	27.61570593
440_B1_445	44_0_B1	Pj	Upland	38	72	34	0	17.9	12.0972	25.81954887
440_B1_448	44_0_B1	Pj	Upland	31	55	24	17	17	16.4001	25.17293233
440_B1_449	44_0_B1	Sb	Upland	19	40	21	32	20.3	30.4016	27.54385965
440_B1_480	44_0_B1	Sb	Upland	20	40	20	33	9.8	12.4023	20
440_B1_485	44_0_B1	Sb	Upland	40	70	30	17	18.1	13.8977	25.96324144
440_B1_487	44_0_B1	Sb	Upland	27	47	20	11	12.8	12.5977	22.15538847
440_B1_519	44_0_B1	Sb	Upland	38	66	28	19	17.2	14.3005	25.3166249
440_B1_532	44_0_B1	Sb	Upland	16	52	36	15	18.3	8.30078	26.106934
440_B1_533	44_0_B1	Sb	Upland	17	51	34	26	19	26.3	26.60985798

440_B1_571	44_0_B1	Sb	Upland	30	54	24	8	15.1	11.4014	23.80785297
440_B1_575	44_0_B1	Pj	Upland	35	62	27	23	14.9	-221.802	23.6641604
440_B1_623	44_0_B1	Sb	Upland	25	50	25	28	18.5	23.999	26.25062657
440_B1_639	44_0_B1	Sb	Upland	27	43	16	115	18.2	9.60083	26.03508772
443_B1_1004	44_3_B1	Lt	Wetland	38	72	34	0	5.3	7.19604	16.76691729
443_B1_1008	44_3_B1	Sb	Wetland	17	51	34	16	15.7	10.7971	24.23893066
443_B1_1010	44_3_B1	Sb	Wetland	27	44	17	19	6.6	17.9016	17.70091896
443_B1_1012	44_3_B1	Sb	Wetland	30	43	13	13	11.6	6.89697	21.29323308
443_B1_1024	44_3_B1	Sb	Wetland	26	44	18	11	5.6	10.9985	16.98245614
443_B1_1040	44_3_B1	Sb	Wetland	32	66	34	15	3.9	3.49731	15.76106934
443_B1_1061	44_3_B1	Sb	Wetland	23	55	32	37	20.8	10.7971	27.90309106
443_B1_1080	44_3_B1	Sb	Wetland	32	47	15	3	7.9	9.00269	18.63492063
443_B1_1086	44_3_B1	Sb	Wetland	39	50	11	7	13.4	18.9026	22.58646617
443_B1_1091	44_3_B1	Lt	Wetland	16	45	29	28	11.1	9.99756	20.93400167
443_B1_1360	44_3_B1	Sb	Wetland	20	44	24	19	9.8	6.19507	20

443_B1_26	44_3_B1	Sb	Wetland	22	31	9	8	7.8	15.3015	18.56307435
443_B1_32	44_3_B1	Sb	Wetland	34	52	18	29	4.7	15.7959	16.3358396
443_B1_44	44_3_B1	Lt	Wetland	34	57	23	15	9.7	18.7988	19.92815372
443_B1_45	44_3_B1	Sb	Wetland	20	50	30	10	11.6	-4.10156	21.29323308
443_B1_46	44_3_B1	Sb	Wetland	55	76	21	31	16.5	4.89502	24.81370092
443_B1_47	44_3_B1	Sb	Wetland	29	64	35	21	12	9.39941	21.58061821
443_B1_60	44_3_B1	Sb	Wetland	26	50	24	19	7.9	5.79834	18.63492063
443_B1_61	44_3_B1	Sb	Wetland	22	57	35	13	4.6	6.29883	16.26399332
443_B1_67	44_3_B1	Sb	Wetland	31	60	29	10	10.4	5.10254	20.43107769
443_B2_1017	44_3_B2	Lt	Wetland	66	114	48	6	28.6	15.8997	33.50710109
443_B2_1028	44_3_B2	Lt	Wetland	170	350	180	92	152.9	-17.4988	122.8120301
443_B2_1030	44_3_B2	Sb	Wetland	81	118	37	18	14.5	13.8	23.37677527
443_B2_1032	44_3_B2	Lt	Wetland	117	245	128	66	129.9	-26.001	106.2873851
443_B2_1033	44_3_B2	Sb	Wetland	191	295	104	93	186.8	-14.9963	147.1679198
443_B2_1037	44_3_B2	Lt	Wetland	133	260	127	170	11.3	13.9038	21.07769424

443_B2_1_056	44_3_B2	Sb	Wetland	124	218	94	12	80.9	34.3018	71.08270677
443_B2_1_058	44_3_B2	Lt	Wetland	156	315	159	93	109.6	-14.9963	91.70258981
443_B2_1_073	44_3_B2	Sb	Wetland	159	215	56	14	64.1	45.5994	59.01253133
443_B2_1_092	44_3_B2	Lt	Wetland	52	95	43	74	71.7	87.5977	64.47284879
443_B2_1_094	44_3_B2	Lt	Wetland	66	88	22	27	22.6	12.2986	29.19632414
443_B2_1_099	44_3_B2	Lt	Wetland	167	365	198	39	139.4	-39.3982	113.112782
443_B2_1_305	44_3_B2	Sb	Wetland	26	54	28	2	7.7	67.8955	18.49122807
443_B2_1_308	44_3_B2	Sb	Wetland	65	83	18	22	19	18.2983	26.60985798
443_B2_1_309	44_3_B2	Sb	Wetland	178	310	132	48	135.8	16.3025	110.5263158
443_B2_1_317	44_3_B2	Lt	Wetland	106	180	74	2	16	67.8955	24.45446951
443_B2_1_334	44_3_B2	Lt	Wetland	230	410	180	27	161.5	2.99683	128.9908104
443_B2_1_339	44_3_B2	Sb	Wetland	170	295	125	15	-14.5	-24.6033	2.541353383
443_B2_1_344	44_3_B2	Sb	Wetland	100	183	83	34	30.1	42.3035	34.58479532
443_B2_1_346	44_3_B2	Lt	Wetland	53	106	53	66	20.7	14.801	27.83124478
443_B2_1_352	44_3_B2	Lt	Wetland	189	295	106	95	129.5	1.09863	106

443_B2_1364	44_3_B2	Sb	Wetland	36	60	24	56	14.9	29.6021	23.6641604
443_B2_1375	44_3_B2	Sb	Wetland	91	145	54	13	43.5	64.801	44.21219716
443_B2_1381	44_3_B2	Lt	Wetland	100	155	55	61	25.2	59.3018	31.06432749
443_B2_15	44_3_B2	Sb	Wetland	56	106	50	-4	16.2	7.59888	24.59816207
443_B2_1641	44_3_B2	Sb	Wetland	18	48	30	8	26.8	25	32.213868
443_B2_19	44_3_B2	Lt	Wetland	119	182	63	3	41.3	20.3979	42.63157895
443_B2_22	44_3_B2	Sb	Wetland	29	71	42	32	21.1	27.8992	28.11862991
443_B2_23	44_3_B2	Lt	Wetland	230	380	150	139	10.9	10.4004	20.79030911
443_B2_35	44_3_B2	Sb	Wetland	140	232	92	80	23.7	39.801	29.98663325
443_B2_36	44_3_B2	Lt	Wetland	141	235	94	17	30	30.896	34.51294904
443_B2_38	44_3_B2	Lt	Wetland	82	163	81	18	32.4	17.6025	36.23725982
443_B2_40	44_3_B2	Lt	Wetland	82	136	54	26	13.6	26.3	22.73015873
443_B2_69	44_3_B2	Lt	Wetland	51	96	45	57	18.9	43.5974	26.5380117
445_B1_1268	44_5_B1	Sb	Upland	50	65	15	11	11.7	8.20312	21.36507937
445_B1_1707	44_5_B1	Lt	Upland	33	73	40	-1	3.1	1.39771	15.18629908

445_B1_1715	44_5_B1	Sb	Upland	11	22	11	4	12.4	5.9021	21.86800334
445_B1_1738	44_5_B1	Lt	Upland	56	79	23	-8	12.1	11.7004	21.65246449
445_B1_1750	44_5_B1	Sb	Upland	13	34	21	11	13	18.2007	22.29908104
445_B1_1754	44_5_B1	Lt	Upland	29	66	37	8	18	16.1011	25.89139515
445_B1_1761	44_5_B1	Sb	Upland	17	32	15	13	11.7	9.8999	21.36507937
445_B1_1767	44_5_B1	Lt	Upland	50	121	71	23	19.2	15.8997	26.75355054
445_B1_1769	44_5_B1	Lt	Upland	46	86	40	5	10.1	7.20215	20.21553885
445_B1_1773	44_5_B1	Sb	Upland	16	32	16	11	15.2	18.2007	23.87969925
445_B1_1774	44_5_B1	Lt	Upland	40	97	57	4	8.3	5.9021	18.92230576
445_B1_1801	44_5_B1	Lt	Upland	18	34	16	17	13.2	16.4001	22.4427736
445_B1_1812	44_5_B1	Sb	Upland	46	64	18	13	6.9	13.2996	17.91645781
445_B1_1818	44_5_B1	Lt	Upland	21	41	20	21	19.2	17.7002	26.75355054
445_B1_1821	44_5_B1	Lt	Upland	36	67	31	-3	5.1	5.49927	16.62322473
445_B1_1831	44_5_B1	Lt	Upland	41	84	43	-2	6.7	-5.50537	17.77276525
445_B1_1853	44_5_B1	Sb	Upland	16	33	17	28	13.2	15.3992	22.4427736

445_B1_1 856	44_5_B1	Lt	Upland	38	82	44	3	17.1	23.90 14	25.244778 61
445_B1_1 857	44_5_B1	Lt	Upland	28	52	24	4	6.4	7.598 88	17.557226 4
445_B1_1 858	44_5_B1	Lt	Upland	31	54	23	11	2.8	- 5.902 1	14.970760 23
445_B1_1 862	44_5_B1	Lt	Upland	28	52	24	3	21.9	23.90 14	28.693400 17
445_B1_1 879	44_5_B1	Lt	Upland	21	48	27	20	21.4	23.99 9	28.334168 76
445_B1_1 900	44_5_B1	Lt	Upland	12	25	13	-8	9.3	3.601 07	19.640768 59
445_B1_3 54	44_5_B1	Lt	Upland	70	99	29	11	3.4	- 5.902 1	15.401837 93
445_B1_3 76	44_5_B1	Lt	Upland	61	119	58	-1	3.5	1.397 71	15.473684 21
445_B1_3 98	44_5_B1	Lt	Upland	15	34	19	9	20.4	29.99 88	27.615705 93
445_B1_3 99	44_5_B1	Lt	Upland	29	68	39	11	12.4	24.09 67	21.868003 34
445_B1_4 05	44_5_B1	Sb	Upland	12	26	14	27	26.7	9.802 25	32.142021 72
445_B1_4 12	44_5_B1	Lt	Upland	8	20	12	22	12.3	7.299 8	21.796157 06
445_B1_4 20	44_5_B1	Sb	Upland	57	87	30	-2	1.4	- 5.505 37	13.964912 28
445_B1_4 25	44_5_B1	Sb	Upland	74	97	23	11	17.4	8.203 12	25.460317 46
445_B1_4 40	44_5_B1	Lt	Upland	51	95	44	-10	15.9	16.10 11	24.382623 22

445_B2_1 131	44_5_B2	Sb	Upland	13	35	22	21	18.3	22.39 99	26.106934
445_B2_1 611	44_5_B2	Sb	Upland	32	61	29	11	15.2	14.00 15	23.879699 25
445_B2_1 629	44_5_B2	Sb	Upland	14	31	17	0	9.3	11.79 81	19.640768 59
445_B2_1 632	44_5_B2	Lt	Upland	15	27	12	8	10.7	9.503 17	20.646616 54
445_B2_1 635	44_5_B2	Sb	Upland	18	40	22	0	12.1	10.60 18	21.652464 49
445_B2_1 636	44_5_B2	Lt	Upland	11	32	21	7	16.4	71.29 52	24.741854 64
445_B2_1 638	44_5_B2	Sb	Upland	17	32	15	27	16.8	23.40 09	25.029239 77
445_B2_1 642	44_5_B2	Lt	Upland	19	35	16	18	13.2	15.69 82	22.442773 6
445_B2_1 644	44_5_B2	Sb	Upland	13	30	17	0	8.4	7.397 46	18.994152 05
445_B2_1 645	44_5_B2	Sb	Upland	26	47	21	0	9.2	- 6.195 07	19.568922 31
445_B2_1 646	44_5_B2	Sb	Upland	9	26	17	5	7.2	11.60 28	18.131996 66
445_B2_1 651	44_5_B2	Sb	Upland	19	55	36	24	18.6	20.00 12	26.322472 85
445_B2_1 653	44_5_B2	Sb	Upland	8	35	27	7	12.8	12.79 91	22.155388 47
445_B2_1 654	44_5_B2	Sb	Upland	8	24	16	7	8	8.001 71	18.706766 92
445_B2_1 659	44_5_B2	Lt	Upland	8	26	18	27	23.6	23.80 37	29.914786 97

445_B2_1 719	44_5_B2	Sb	Upland	13	28	15	9	11.6	10.90 09	21.293233 08
445_B2_1 722	44_5_B2	Sb	Upland	12	39	27	0	19.9	23.30 32	27.256474 52
445_B2_1 724	44_5_B2	Sb	Upland	11	26	15	16	17.5	17.40 11	25.532163 74
445_B2_1 725	44_5_B2	Sb	Upland	8	27	19	71	14.6	15.80 2	23.448621 55
445_B2_1 728	44_5_B2	Lt	Upland	8	37	29	15	12.5	10.60 18	21.939849 62
445_B2_1 757	44_5_B2	Sb	Upland	11	27	16	17	16.4	17.49 88	24.741854 64
445_B2_1 824	44_5_B2	Sb	Upland	8	23	15	27	24.4	23.40 09	30.489557 23
448_B1_1 114	44_8_B1	Sb	Upland	12	21	9	22	21.1	75.79 96	28.118629 91
448_B1_1 620	44_8_B1	Sb	Upland	25	45	20	18	14.5	17.40 11	23.376775 27
448_B1_1 626	44_8_B1	Sb	Upland	10	28	18	23	17.6	27.30 1	25.604010 03
448_B1_1 647	44_8_B1	Sb	Upland	12	21	9	12	13.9	16.80 3	22.945697 58
448_B1_1 676	44_8_B1	Sb	Upland	15	37	22	7	-2.3	1.898 19	11.306599 83
448_B1_1 770	44_8_B1	Sb	Upland	10	28	18	8	13.8	8.697 51	22.873851 29
448_B1_1 789	44_8_B1	Sb	Upland	16	28	12	12	12.1	11.90 19	21.652464 49
448_B1_1 799	44_8_B1	Sb	Upland	27	54	27	4	-7	- 6.005 86	7.9298245 61

448_B1_1869	44_8_B1	Lt	Upland	24	38	14	12	9.3	14.8987	19.64076859
448_B1_494	44_8_B1	Sb	Upland	10	22	12	17	17.6	21.4966	25.60401003
448_B1_524	44_8_B1	Sb	Upland	27	50	23	1	7	-1.70288	17.98830409
448_B1_540	44_8_B1	Sb	Upland	30	57	27	12	16.3	14.8987	24.67000835
448_B2_1243	44_8_B2	Sb	Upland	10	26	16	24	13.2	24.7986	22.4427736
448_B2_1652	44_8_B2	Sb	Upland	15	30	15	19	16.8	14.3005	25.02923977
448_B2_1795	44_8_B2	Sb	Upland	19	33	14	21	11.6	16.803	21.29323308
448_B2_1803	44_8_B2	Sb	Upland	24	44	20	22	16.7	16.8945	24.95739348
448_B2_1807	44_8_B2	Sb	Upland	9	25	16	13	14.1	13.0005	23.08939014
448_B2_1808	44_8_B2	Sb	Upland	20	43	23	-2	18.2	7.59888	26.03508772
448_B2_1828	44_8_B2	Sb	Upland	25	41	16	27	29.4	32.2021	34.08187135
448_B2_1837	44_8_B2	Sb	Upland	20	44	24	0	14.3	7.69653	23.23308271
448_B2_1859	44_8_B2	Sb	Upland	42	63	21	19	17.3	14.3005	25.38847118
448_B2_1863	44_8_B2	Sb	Upland	17	33	16	17	15.3	13.2019	23.95154553
448_B2_1870	44_8_B2	Sb	Upland	12	29	17	21	17.5	18.3044	25.53216374

453_B1_3_12	45_3_B1	Sb	Upland	39	63	24	0	14.2	9.198	23.16123642
453_B1_3_14	45_3_B1	Sb	Upland	99	155	56	37	17.1	150.995	25.24477861
453_B1_3_15	45_3_B1	Sb	Upland	110	150	40	60	5.1	377.698	16.62322473
453_B1_3_17	45_3_B1	Sb	Upland	23	34	11	10	9.7	13.4033	19.92815372
453_B1_3_69	45_3_B1	Sb	Upland	75	113	38	0	37.7	30.7007	40.04511278
453_B2_1_247	45_3_B2	Sb	Upland	31	55	24	12	17.3	7.50122	25.38847118
453_B2_1_261	45_3_B2	Pj	Upland	23	39	16	12	15.7	32.0007	24.23893066
453_B2_1_604	45_3_B2	Sb	Upland	33	56	23	46	20.9	23.0957	27.97493734
453_B2_1_63	45_3_B2	Sb	Upland	35	53	18	15	18.2	13.4033	26.03508772
453_B2_1_648	45_3_B2	Sb	Upland	10	24	14	0	21.7	18.6035	28.5497076
453_B2_1_649	45_3_B2	Sb	Upland	24	45	21	17	14.6	11.0962	23.44862155
453_B2_1_698	45_3_B2	Sb	Upland	50	74	24	0	42.6	56.2988	43.56558062
453_B2_1_743	45_3_B2	Sb	Upland	64	107	43	3	16.2	14.1052	24.59816207
453_B2_1_823	45_3_B2	Sb	Upland	48	70	22	23	12.5	15.3992	21.93984962
453_B2_1_838	45_3_B2	Sb	Upland	68	118	50	73	16	3.302	24.45446951

453_B2_1_840	45_3_B2	Sb	Upland	52	102	50	67	-211.4	12.2009	-138.9239766
453_B2_1_849	45_3_B2	Sb	Upland	27	42	15	3	12.1	29.9988	21.65246449
453_B2_1_855	45_3_B2	Sb	Upland	20	34	14	18	16	16.2964	24.45446951
453_B2_1_866	45_3_B2	Sb	Upland	22	34	12	18	20.8	19.5007	27.90309106
453_B2_1_868	45_3_B2	Sb	Upland	11	26	15	16	17.1	19.7021	25.24477861
453_B2_1_871	45_3_B2	Sb	Upland	17	30	13	14	16.3	14.5996	24.67000835
453_B2_1_875	45_3_B2	Sb	Upland	62	89	27	23	13.2	15.3992	22.4427736
453_B2_1_877	45_3_B2	Sb	Upland	27	43	16	21	16.6	11.3037	24.8855472
453_B2_1_882	45_3_B2	Sb	Upland	75	109	34	17	12.2	18.4998	21.72431078
453_B2_2_02	45_3_B2	Sb	Upland	58	87	29	43	77.4	26.8982	68.56808688
453_B2_2_89	45_3_B2	Sb	Upland	94	167	73	65	111	150	92.70843776
453_B2_3_02	45_3_B2	Sb	Upland	21	33	12	3	13.8	29.9988	22.87385129
453_B2_3_03	45_3_B2	Sb	Upland	64	94	30	22	17	17.1997	25.17293233
453_B2_3_61	45_3_B2	Sb	Upland	43	61	18	17	16.7	19.6045	24.95739348
453_B2_3_63	45_3_B2	Sb	Upland	125	176	51	8	14.4	3.20435	23.30492899

453_B2_67	45_3_B2	Sb	Upland	66	92	26	-17	12.9	-5.49927	22.22723475
453_B2_72	45_3_B2	Sb	Upland	14	28	14	11	17	14.801	25.17293233

APPENDIX D: Quantile Regression and Test of Difference

Table D 1 Quantile regression Model Table for the Point Cloud Point Metric Approach

Term	Estimate	Conf.low	Conf.high	tau
(Intercept)	15.6172539	11.4043630	17.3435808	0.5
PC PM Change	0.5467801	0.2653858	0.8541172	0.5

Table D 2 Quantile regression Model Table for the Point Cloud Cloud Compare Approach

Term	Estimate	Conf.low	Conf.high	tau
(Intercept)	18.4333333	13.55712640	23.0170617	0.5
PC CC Change	0.3666667	-0.03664532	0.6676485	0.5

Table D 3 Quantile regression Model Table for the Raster-Based Approach

Term	Estimate	Conf.low	Conf.high	tau
(Intercept)	22.91908964	21.23746986	26.7825402	0.5
Raster Change	0.04522373	-0.09111886	0.1968366	0.5

Table D 4 W Statistic and p values of best approach and other approaches based on the paired Wilcoxon signed rank test

Comparison	V_Statistic	P_Value	Alternative
PC _{PM} vs PC _{CC}	10441	0.1047	greater
PC _{PM} vs Raster	11378	0.007104	greater

Table D 5 W Statistic and p values of wetland against upland ecosite type based on an independent Wilcoxon rank-sum test

Comparison	W_Statistic	P_Value	Alternative
Wetland vs Upland	2368.5	5.681e-05	greater